Multi-Scale Techniques for Masonry Structures

M. L. De Bellis
V. Ciampi
S. Oller
D. Addessi

Multi-Scale Techniques for Masonry Structures

M. L. De Bellis
V. Ciampi
S. Oller
D. Addessi

Contents

Chapter 1

Introduction

1.1 Study of masonry panels response

The study of the quasi-static response of masonry structures undergoing seismic like loading conditions is of great interest in civil engineering.
In fact in the last few decades, it has been shown there is an increasing interest in the preservation and restoration of historical and artistic building heritage. Moreover the construction of new masonry buildings is still in demand.
Despite masonry being a very ancient building material, a comprehensive understanding of the resulting structural behavior has been neglected over a long period of time, being the design based only on practical rules,even nowadays it is still defective.
The fundamental reason of such statement of fact is that it is really a difficult task to satisfactorily reproduce the mechanical behavior of masonry materials, even if only periodic brickwork is considered. In fact, such a behavior is characterized by the inner complexity related to the heterogeneity of the constituents and to the anisotropy of the response caused both by the initial arrangement of bricks and mortar joints and by the onset and the evolution of damaging phenomena.
Indeed, strongly non-linear behavior and the appearance and growth of cracks characterize the masonry response even under low levels of lateral loading conditions.
A proper understanding of the dominant evolution mechanisms, ranging from cracking up to complete failure, would be highly recommended in order to reproduce and predict the global behavior.

The advances in numerical methods have given a significant contribution to the aforementioned purpose and many examples of numerical models, obtained starting from different standpoints, are currently available in literature to approach the study of the response of masonry structures.
An out-and-out dichotomy between two antithetic approaches has been determined in the framework of the finite elements method: on the one hand, the so-called *discrete approach* and, on the other hand, the *continuum approach*.
The former approach is based on the common idea that the failure of joints is decisive in the non-linear overall response of masonry and a separate modeling of single constituents (bricks and mortar joints) as discrete elements is effective in capturing the actual behavior. The first attempt in this direction is by Page (1978) and it consists in the adoption of an interface model in order to simulate the behavior of joints.
Another example of a discrete model is by Baggio and Trovalusci (1993), who model mortar joints by means of a series of non-linear shear and normal springs, while the bricks are considered as rigid bodies. Again in Lofti and Shing (1994) interface elements are used for joints which take into account the dilatancy and softening behavior.
Also the works by Loureno and Rots (1997), Nappi and Tin-Loi (2001) and Giambanco et al. (2001) place themselves in the same discrete approach.

1

Unfortunately the inner limit of *discrete approach* is related to the high computational costs required to separately discretize interface elements and blocks.

The *continuum approach*, instead, is based on a diametrically opposite idea: the macro-modeling of masonry as a homogeneous material.
The composite material is replaced by an equivalent homogeneous medium and the constitutive model is accountable for the response of the real structure. It is clear that a proper definition of the constitutive law is a key point of the approach and different choices have been taken in order to fulfill this requirement. In fact it is possible to distinguish between the laws based on phenomenological or micro-mechanical approaches.
In the first approach the identification of the characterizing law parameters is based on experimental results.
Several contributions are included in the phenomenological models as the works by Romano and Sacco (1984), Giaquinta and Giusti (1985), Del Piero (1989) that consider masonry as elastic material not resistant to tension.
In the non-linear framework, instead, the contributions by Papa and Nappi (1997) and Berto et al. (2002) are noteworthy as for isotropic or anisotropic damage models and as for plasticity model the work by Loureno et al. (1997) is important.

Another possibility is the definition of suitable constitutive laws obtained by modeling the micro-structure of a representative sample of masonry in detail, taking into account the heterogeneities and the respective arrangement of constituents.
The response of such a structure is then homogenized by formulating different hypotheses: these are the micro-mechanically based continuum approaches.
The First attempts in this direction place themselves in the linear range both for in-plane and out of plane hypotheses (see Pande and Middleton (1989), Anthoine (1995), Zucchini and Loureno (2002), Cecchi and Sab (2002)).
In several other contributions, instead, the non-linear behavior of constituents is taken into account. The work by De Buhan and De Felice (1997) is focused on the assessment of ultimate strength of brick masonry. Moreover damage models are often considered as in Maier et al. (1991), Luciano and Sacco (1995), Luciano and Sacco (1997a), Pietruszczak and Niu (1992), Calderini and Lagomarsino (2006).
Massart et al. (2001) have proposed a 2D anisotropic damage model in a multi-plane framework.
In Zucchini and Loureno (2004) an iterative coupled algorithm is developed in order to implement the non-linear homogenization formulation considering damaging effects; in Zucchini and Loureno (2007) an extension to the damage and plasticity is carried out in the case of masonry under compression, while in Zucchini and Loureno (2009) the previous model is used to study the behavior of shear walls.
In Berto et al. (2004) the shear behavior of masonry panel is investigated by adopting an isotropic damage model to simulate the behavior of mortar joints in the micro-model while an orthotropic damage model is used in the macro-model calibrated on the basis of the micro one.
Another important choice in the *continuum approach* is related to the continuum adopted at the macro-level. For example Besdo (1985), Masiani et al. (1995) and Sulem and Muhlhaus (1997) have considered the importance of taking into account the blocks rotations, thus they have adopted micro-polar continuum instead of classical Cauchy continuum.
The idea of adopting a micro-polar continuum instead of a Cauchy continuum has been expressed and motivated, in another context,the works by De Borst (1991) and Mhlhaus (1989). It has been claimed, in fact, that this choice is very effective in cases of material showing softening behavior. In fact the intrinsic regularization properties of such a continuum is due to the natural introduction of a characteristic length.
Several authors have considered a Cosserat medium in the description of masonry behavior starting from Trovalusci and Masiani (1996), to Casolo (2006), Brasile et al. (2007a), Brasile et al. (2007b) and Stefanou et al. (2008). A more recent contribution is the work by Salerno and De Felice (2009) that aims to investigate the capability of Cauchy and Cosserat continua in modeling the linear behavior of periodic brickwork compared to the response of a rigid block system.

In the work by Trovalusci and Masiani (2005) a multi-scale procedure is adopted in order to describe the non-linear behavior of block masonry structures. A lattice model is used to represent the micro-level and macroscopic constitutive equations are obtained for an equivalent continuum macro-model.

The crucial point of the *continuum approach*, that is often troublesome, is the requirement of analytical expressions for the homogenized constitutive laws. This is a difficult task especially because the definition of closed-form macroscopic constitutive equations requires strong simplifications. It is very difficult to opportunely take into account, in the evolving irreversible damaging processes, the microstructural interaction effects between constituents that considerably affect the global response.

A very promising strategy to overcome the aforementioned problem seems to be the application of *computational homogenization techniques* also called *global-local analysis*.

Substantially classical (analytical or semi-analytical) homogenization methods for the representation of heterogeneous materials have been complemented by multi-scale computational approaches: the objective is to apply such a multi-scale approach for structural analyses.

The basic ideas have been presented in papers by Suquet (1985), Guedes and Kikuchi (1990), Ghosh et al. (1995) and Ghosh et al. (1996).

The goal of a such modeling procedure is that it does not lead to closed-form overall constitutive equations, but it enables the computation of the stress-strain relationship at every point of interest at the macro-level by detailed modeling of the microstructure attributed to that point.

Also the works by Smit et al. (1998), Miehe et al. (1999), Forest and Sab (1998), Kouznetsova et al. (2001), Kouznetsova (2002), Kouznetsova et al. (2004), Ghosh et al. (2001), Feyel (2001) and Massart et al. (2007) place themselves in the framework of *computational homogenization techniques*.

The problem is split into two scales: a macro-scale, where an equivalent homogeneous continuum is considered, whose formulation is completely stated except for the constitutive law, and a micro-scale, in which all constituents are modeled taking into account geometrical arrangement, size and constitutive laws of different constituents. On the micro-scale structure a properly defined boundary value problem, driven by a macro-level strain measure, is solved and averaged stresses are recovered and passed back to the macro-level.

The noticeable advantages of such an approach are that:

1. no closed form constitutive laws are required at the macro-level;

2. detailed descriptions of micro-level response are enabled: it is possible to take into account different non-linear behaviors of the constituents and the macro-level is directly affected by the possible evolution of the microstructure;

3. any modeling techniques at the micro-level are appropriate as finite element method, the Voronoi cell method and Fast Fourier Transforms.

The work by Zalamea (2001) is an example of computational homogenization, using finite element method, in which, at both levels, classical Cauchy continua are adopted: in this case the response at a (macroscopic) material point depends only on the first gradient of the displacement field. This is the so-called *first order computational homogenization*. In Kouznetsova (2002) this approach is presented and its inner disadvantages are outlined.

The existing first-order micro-macro computational approaches, in fact, can account for the volume fraction, distribution and morphology of the constituents, but cannot consider the absolute size of the microstructure and consequently fail to account for geometrical size effects.

Another problem originates from the inner hypothesis of uniformity of the macroscopic (stress-strain) fields attributed to each micro-level representative structure. This uniformity assumption relies on the concept of separation of scales and it is not appropriate in critical regions of high gradients, where the macroscopic fields can vary rapidly.

Starting from the two aforementioned considerations, in the work by Kouznetsova (2002) a novel second-order computational homogenization procedure has been proposed. On the microstructural level, the micro-macro kinematical coupling is introduced as a second-order Taylor series expansion of the macro

displacement field, and the microstructural displacement variation is gathered in a fluctuation term. Another attempt in the same direction is owing to Larsson and Diebels (2007).

A further possibility in order to overcome the intrinsic limits of first order computational homogenization is the coupling between a Cosserat medium at the macro-level and a Cauchy one at the micro-level.

In the framework of a Cosserat based homogenization technique, starting from a micro-model, the work by Forest and Sab (1998) has been very important. They have adopted a standard Cauchy continuum as for the micro-model description, while a Cosserat continuum at the macro-level. The homogenization rules have been obtained by properly coupling the different variables at both scales in case of linear behavior and considering a square and unit length micro-structure.

In Feyel (2001) an extension to the multi-scale computational homogenization of the aforementioned approach has been applied to fiber composite structures in the context of inelastic analysis.

The idea of extending the multi-scale computational homogenization to the study of masonry structures has been firstly developed by Massart (2003): a modified first order computational homogenization technique has been adopted, the macroscopic damage localization has been treated by embedding localization bands in the macroscopic description by means of the use of an approximate composite model. The finite size of the damaged zone has been taken into account, leading to a physically realistic prediction of the energy dissipation.

On the basis of the existing literature advances, it seems to be very interesting the extension of the multi-scale computational homogenization, based on coupling a Cosserat continuum at the macro-level with a Cauchy continuum at the micro-level, to the study of the response of masonry panels subjected to seismic like loading conditions.

This choice enables two-fold advantages:

- the adoption of the multi-scale computational homogenization, with the use of an imbricated finite element technique (the micro-level problem is nested into the macro-level one), guarantees a detailed description of the micro-level phenomena that have fundamental influence on the macroscopic response. Real-time developed non-linear effects are captured at the lower level and passed at the macro-level, thus the analysis includes them in a natural way;

- the use of a Cosserat continuum at the macro-level, as aforementioned, allows the introduction of a material length scale so that the overall response of the composite material is spontaneously bound to the absolute size of the constituents. The effect of considering a Cosserat continuum at the macro-level, in fact, is to enrich the displacement, strain and stress descriptions and, thus, to pass additional information to the micro-level: apart from the standard Cauchy three deformation modes (two axial and one shear symmetric deformation), three additional deformation modes are considered (a skew-symmetric shear and two bending deformations). This means that, at least for shear and bending behaviors, with this formulation is possible to account for size effects (directly related to the *RVE* dimensions) as well as to regularize the response in case of localization phenomena.

1.2   Objectives

The aim of this work is, hence, to adopt the *computational homogenization techniques* to obtain the global response of masonry structures.

Since the experimental global response curves, obtained in typical shear tests on masonry panels, show stiffness and resistance degradation, damage is the fundamental ingredients which must be taken into account in such problems.

Moreover, as it is well known, due to the aforementioned softening behavior, regularization techniques are required in order to avoid spurious mesh dependencies when a numerical solution is sought in the framework of finite element method.

The first step of this work is the adoption of the standard first order computational homogenization, where Cauchy continuum is used both at the macro and micro-level. This approach is well known in literature and several authors applied it to different engineering problems. An example of the adoption

of regularization techniques in the context of multi-scale approaches is found in Massart (2003).

Hence a regularization based on the imposition of the macroscopical length scale at the micro-level, in the framework of the fracture energy regularization, is proposed.

However, as previously stated, many authors have pointed out the inner limits of first order computational homogenization. Such a formulation, in fact, may be adopted only if

1)the microstructure is very small with respect to the characteristic size at the macro-scale;

2)the absolute size of the constituents does not affect the mechanical properties of the homogenized medium and in presence of low macroscopic gradients of stresses and strains.

As a consequence no localization phenomena typically exhibited by masonry can be analyzed.

For masonry structures, instead, microstructural typical sizes are comparable with the macro-structural sizes; shape, size and arrangement of the constituents strongly affect the mechanical global response and high deformation gradients typically appear.

An *enriched formulation* is then proposed in order to overcome these problems, based on the adoption of a Cosserat medium at the macro-level and a Cauchy medium at the micro-level. The theoretical and computational schemes remain the same as before but for the fact that the two media present different variables. In particular in the Cosserat medium additional strain and stress variables appear, with respect to the Cauchy continuum, as a consequence of the independent rotational degree of freedom assigned to every material point. Thus, a more sophisticated kinematic map, containing higher order polynomial expansions, is needed to state proper bridging conditions between the two levels.

The innovative contribution of this work concerns the adoption of an enhanced multi-scale *computational homogenization technique* for studying the masonry response, together with the employment of damage models for the constituents description.

Thus, by exploiting the inner regularization properties of the Cosserat continuum at the macro-level and by adopting a classical fracture energy regularization at the micro-level, localization phenomena, typically exhibited by masonry structures, are analyzed. Since this material shows a typical strain softening behavior, an *ad hoc* regularization technique has been developed at both levels in order to obtain objective numerical responses. To the knowledge of the author, no previous examples of Cosserat-Cauchy *computational homogenization techniques*, taking into account localization effects, have been presented.

A possible objection to the use of a fully-coupled multi-scale technique could be related to the high computational efforts required, but here the use of parallel computing brings them down. In this context, these procedures strike a good balance between the achievement of detailed information at the scale of the constituents and the requirement of holding the computational costs down.

1.3 Outline

The work is organized as follows:

- Chapter 2 is focused on the State of the Art. A brief review of the most widely used computational approaches to simulate the masonry structural response is outlined. A short description of computational homogenization as the adopted strategy, together with the motivations of such a choice end the chapter.

- Chapter 3 is devoted to a review of the typical mechanical behavior of masonry, starting from the behavior of single constituents, moving to the response of masonry material and finally to the masonry structures characterization.

- in Chapter 4 the well known first order homogenization technique is described. The basic hypotheses and key concepts are revisited, the bridging conditions between micro and macro levels

are explained. The parallel numerical implementation of the method adopting the finite element method is outlined.

Some numerical examples show the capabilities and, at the same time, the intrinsic limits of the method.

Damage behavior is accounted for by adopting isotropic damage models for each of the constituents (bricks and mortar) at the lower scale.

- in Chapter 5 the proposed Cosserat-Cauchy homogenization is presented as an effective tool to solve properly the problem of studying masonry non-linear behavior. The conceptual scheme presented in Chapter 4 is substantially repeated with the debated differences introduced by coupling the two different continua.

  The parallel numerical implementation of the method adopting the finite element method is outlined.

  Theoretical and experimental tests in linear and non-linear ranges are performed in order to investigate the capabilities of the method. Damage behavior is accounted for by adopting isotropic damage models for each of the constituents (bricks and mortar) at the lower scale.

- Chapter 6 presents conclusions and further developments.

Chapter 2

State of the Art

Brickwork masonry is a composite material constituted by the periodic repetition of two materials (bricks and mortar joints) characterized by different mechanical properties. The heterogeneity in the composition along with the arrangement of the constituents (bond pattern, thickness of the mortar joints) lead to a composite that is strongly anisotropic both in linear and in non-linear ranges. The overall behavior is therefore prominently affected by the relative arrangement of the constituents and by their constitutive laws. That is why the description of masonry structures mechanical behavior is a very difficult task in engineering and effective computational methods are hardly defined.

Several approaches have been proposed to deal with the aforementioned task.

Until the last few years there was a rigid dichotomy between the two most widespread approaches, i.e. *discrete approach* and *continuum approach*, based on diametrically opposite hypotheses. In the framework of *continuum approach* the development of the homogenization strategies has been a very important basis for further developments, The fundamental goal of the homogenization theory is, in fact, to derive macroscopic overall characteristics of heterogeneous media from the behavior of the constituent materials.

A first attempt in this branch of research has been *The rule of the mixtures* (Trusdell and Toupin (1960)) that is a widespread technique to reproduce composite materials (such as masonry) behavior. The composite material is considered to be homogeneous and the single components participate in the overall response proportionally to their respective volume portion. Two formulations have been developed: the first one is called in series because all the components undergo the same deformation ratio (Ortiz and Popov (1982)); the latter is called *in series and in parallel* (Oller et al. (1995)).

Other efforts in extrapolating homogenized measures of stresses and strains for the composite material detailed description have been the *effective medium approximation* (Eshelby (1958); Hashin (1962); Mori and K. (1973)) and the *self consistent approach* (Hill (1965); Christensen (1979)). In the former the heterogeneous medium is described by means of inclusions of one material into an infinite matrix of another material and mechanical parameters of the equivalent homogenized medium are properly extrapolated, while the latter approach can be defined as an extension of the first.

More recently the *unit cell methods* have been established by including two important classes of methods: the *Average methods* (Suquet (1982)) and the *Asymptotical methods*(Sanchez-Palencia (1980); Bensoussan et al. (1978); Fish et al. (1999)).

The basic hypothesis of the *Average methods* (also known as *heuristic method*) is that the macroscopic variables of the problem (stresses and strains) are computed by evaluating the mean value of the respective microscopical ones.

The *Hill-Mandel method* (Hill (1967); Mandel (1972)) is used to obtain an elastic constitutive law for the composite material and the homogenization law is indeed a weighted average of the microscopical constitutive law, using the strain concentration tensor as the weight factor.

The *Asymptotical methods* enable the derivation of heterogeneous medium response in both the macro

and micro scales on the basis of an asymptotic expansion of displacement and stress fields on the *natural length parameter*, which is the ratio of a characteristic size of the heterogeneities and a measure of the macrostructure. The applicability of such an approach is doubtful in non-linear applications.

Also Pande and Middleton (1989) have applied approximate homogenization techniques to identify apparent elastic modulus of masonry.

Anthoine (1997, 1995); Pegon and Anthoine (1997) have given an important contribution to the advances and the applications of the homogenization techniques. These works have been useful in order to overcome the inner limits restricting the effectiveness of the previous available homogenization technique. Such limits have been resumed by Anthoine as follows:

1. The homogenization procedure was performed in several steps, head joints and bed joints being introduced successively. Such a methodology thus introduced two sources of error: first, the result was generally dependent on the order of the successive steps, as shown by Geymonat et al. (1987); second, the geometrical arrangement was not fully taken into account in the sense that different bond patterns (running bond and stack bond for example) could lead to exactly the same result.

2. The homogenization procedure itself was sometimes approximate Pietruszczak and Niu (1992);

3. The geometry of the arrangement was often simplified, mortar joints being treated as interfaces or ellipsoidal inclusions Pietruszczak and Niu (1992);

4. Finally, the thickness of masonry was never taken into account because masonry was considered either as infinitely thin (in Maier et al. (1991); Pande and Middleton (1989)), or as infinitely thick (in Pietruszczak and Niu (1992); Pande and Middleton (1989)).

In the works Anthoine (1997, 1995); Pegon and Anthoine (1997), the study is focused on the quasi-static behavior of masonry walls. The masonry is treated as a periodic composite continuum.

The work of Anthoine (1995) is focused on the identification of the in-plane elastic characteristic of masonry walls performed in one step. The basic hypothesis is to consider a two-dimensional periodic media undergoing plane stress (and it is also considered an extension to the three-dimensional periodic media having only two directions of periodicity) for which mechanical properties of the media can be considered just on a small domain called *cell*.

A subsequent study in Pegon and Anthoine (1997) is an extension of the previous one for the solution of problems involving in-plane macroscopic non-linear behavior of masonry.

Two different two-dimensional models are considered: plane stress and generalized plane strain (GPS) defined in Saada (1974).

The latter one shows more realistic response for the masonry behavior.

The homogenization theory is specialized for a parallelogram cell and for a continuum damage model for bricks and mortar joints. The damage model proposed in Mazars (1986) is chosen for describing the masonry components. Regularizing the constitutive model via the fracture energy is useful in order to prevent mesh size dependency but for the mesh orientation dependency a non local regularization is necessary. A non-local formulation in case of softening is necessary to avoid the mesh size dependency.

Also other authors have given their contribution in the study of elastic behavior of masonry using homogenization techniques (Cecchi and Di Marco (2000); Cecchi and Sab (2002); Cecchi and Rizzi (2001); Pietruszczak and Niu (1992)).

In Zucchini and Loureno (2002) the identification of the elastic moduli of masonry is carried out while in the more recent Zucchini and Loureno (2007) the study of masonry under compression, using a novel non-linear homogenization tool that includes the possibility of tensile and compressive progressive damage, both in the unit and mortar is executed. convergence difficulties.

The common idea of the aforementioned homogenization approaches is that the material properties of the

equivalent homogeneous medium are extrapolated *una tantum* from the microstructure and they remain constant during the calculations, i.e. they do not account for the geometrical and physical changes of the microstructure, moreover they are not suitable for large deformations nor complex loading paths.

This is why new approaches have been developed in the last few years with the aim of defining computational models in which different scales of observation of the same physical phenomenon interact, exchanging information in *real time*. This is the basic idea of *computational homogenization techniques* in which the macro-scale is continuously linked to the micro-scale via a boundary value problem to be solved at every time step. No closed form constitutive laws are required, being extracted numerically from the micro-structure. The first contributions was given by Luciano and Sacco (1997a, 1998) in the linear framework. Other authors as Zalamea (2001); Kouznetsova (2002); Feyel (2001); Massart (2003); Miehe et al. (1999) have applied the *computational homogenization techniques* recently, both in linear and non linear range, and using standard Cauchy continuum theory for micro and macro levels as Zalamea (2001) or enhanced continua for the macro scale as second order fully expansion (as Kouznetsova (2002)) or Cosserat continuum (as Forest and Sab (1998); Feyel (2001)). All those works share the choice of a finite element discretization of the macro-continuum which is locally coupled at each Gauss point with a finite element discretization of the attached micro-structure .

Zalamea applies the first order computational homogenization technique as general tool for dealing with composite materials structural problems, respecting the hypothesis of periodic medium and adopting plastic and damage laws. The limitations of first order homogenization techniques are well emphasized in Kouznetsova (2002): such a formulation may be adopted only if the microstructure is very small with respect to the characteristic size at the macro-scale; if the absolute size of the constituents does not affect the mechanical properties of the homogenized medium and in presence of low macroscopic gradients of stresses and strains. As a consequence no localization phenomena, typically exhibited by masonry, can be analyzed in the framework of first order homogenization techniques.

In the work of Kouznetsova (2002) a new computational homogenization technique is developed for the multi-scale modeling of non-linear deformation processes in evolving multi-phase materials. With the aim of overcoming the inner limits of the standard homogenization techniques, based on the first order theories, she presents an innovative second order computational homogenization scheme. The study is not focused on a specific material characterized by a specific constitutive law, but rather provides a general tool to solve a wide set of practical problems involving multi-phase materials.

The study of the micro-level is just the same (preserving the imposition of the periodic boundary conditions) as the standard homogenization techniques, in accordance with the classical continuum mechanics; on the contrary the changes are introduced at the global level.

The higher order model is obtained using a second order Taylor series expansion of the gradient of the macroscopic deformation tensor. The choice of a classical Cauchy continuum formulation for the micro-level is due to the fact that in the scientific literature the treatment of the single-phase materials constitutive laws using an higher order continuum approach is not enough developed while for the classical local formulation constitutive equations and experimental procedure are widely used.

Another relevant contribution to the enhanced homogenization techniques is the work of Massart (2003). The adopted approach is founded on a first order homogenization procedure opportunely enriched to deal with the localization phenomena of quasi-brittle materials.

Of primary importance is the definition of the main working hypotheses at the microscopic level, where the response of the single constituents are directly obtained. At this lower level, hence, plane stress conditions are considered; the complex phenomena of damage growth are taken into account via an implicit gradient damage model; it is assumed that the microscopical structure is periodic and the localization problem is handled introducing a finite measure of the localization bands in the macroscopic level so as to realistically predict the energy dissipation.

The damage models selected for the microscopic constituents level (bricks and mortar joints) are isotropic and the overall anisotropic structural behavior is recovered in natural way by the interaction between the parts (as recognized in Dhanasekar et al. (1982), in the extensive experimental campaigns on clay brick masonry specimens).

A Drucker-Prager type criterion has been used to reflect the quasi-brittle and frictional nature of mortar,

featuring a low tensile strength and a high sensitivity to shear stress states. The brick material has been modeled with a maximum principal stress criterion or a modified von Mises criterion.

A properly conceived criterion, based on the acoustic tensor, is defined in order to establish when to introduce the localization band in the computation.

Feyel (2001) developed a computational homogenization technique known as FE^2 (or also *imbricated finite element*), on the basis of a previous work of Forest and Sab (1998), by coupling a Cosserat medium at the macro level with a Cauchy one at the micro level. Among different generalized continua (as for example Second grade material used by Kouznetsova or micromorfic materials) the Cosserat continuum has been chosen in different multi-scale applications. The translational displacement field, the only one in the Cauchy continuum, is enriched with a micro-rotation field accounting for the independent rotation of a rigid tryad attached to the micro-structure of the material.

This simple assumption engenders, as matter of course, the loss of symmetry of the strain tensor and the appearance of the curvature tensor. In a natural way it is, thus, possible to account for size effects and other non-local effects, in fact by coupling a Cosserat medium at the macro-level and a Cauchy one at the micro, the absolute size of the micro-level representative volume becomes decisive in order to extract the micro-level response that is no long dependent only by volume fractions and spatial relative distributions of the constituents. The need of a generalized continua is undeniable, according to Forest (1999) and Besdo and Dorau (1988) when the absolute size of the *RVE* (Representative volume element), defined at the micro-level, is comparable with the wavelength of stress and strain variations induced in the structure.

The most difficult part of the procedure is the choice of properly conceived transformation rules i.e. the definition of bridging laws in order to pass information between the two levels characterized by different numbers of variables. The kinematic map (the linking conditions between macro and micro displacement and strain fields) is obtained by postulating that the actual Cauchy displacement field of the *RVE* at the micro-level is perfectly fitted by the Cosserat displacement vector at the macro-level corresponding to the macroscopic point directly linked to the *RVE*. A key concept driving the aforementioned homogenization method is the assumption of periodicity conditions as for the microstructure.

Hereafter the approach adopted in the present thesis is presented. The study of masonry structures response, in case of seismic like loading conditions, is handled by means of computational homogenization techniques.

The classical first order homogenization is the starting point of the actual investigation. The main goals of such a method are:

1) the possibility of the method to deal with complex micro-structures;

2) the uselessness of closed-form macroscopic constitutive laws, as the mechanical response arises in a natural way from the micro-level study;

3) the accuracy of both levels response.

One of the basic hypotheses of the first order approach is the *principle of separation of scales* that is hardly fulfilled when masonry structures are taken into account, in fact, in such structures, typical sizes are comparable with the macro-structural ones; shape, size and arrangement of the constituents strongly affect the mechanical global response and high deformation gradients typically appear.

An enriched formulation, based on a generalized continuum is thus required.

The investigation, in the second stage, deals with a computational homogenization technique, which adopts a Cosserat medium, at the macro level, and a Cauchy model, at the micro level.

The heterogeneous masonry material is replaced by an equivalent homogeneous Cosserat medium at the macro-level where explicit constitutive laws are not available. In the framework of a global displacement method, the evaluation of the stresses and of the tangent constitutive matrix at the macro-scale is performed by solving a properly formulated Boundary Value Problem (BVP) at the micro-level on the Representative Volume Element (*RVE*) which contains all the constitutive information in detail. At the micro-level only isotropic damage models for the constituents are adopted, the global anisotropic behavior being recovered by means of the interaction between constituents themselves.

Chapter 3

Mechanical behavior of masonry: a brief review

Masonry can be regarded as a composite material made up of bricks and mortar joints. Those constituents show very different mechanical features that strongly influence the structural overall behavior. The response is marked by a pronounced anisotropy that is dependent not only by the loading extent but also by his direction: it is possible to assert that masonry is a material exhibiting distinct directional properties due to mortar joints, which act as planes of weakness (see Zucchini and Loureno (2009)).

In the sequel a brief review of typical masonry behavior is outlined. First of all bricks and mortar fundamental properties are recalled together with local failure characteristics. Subsequently, macroscopic properties are reviewed in order to underline the strong dependency of masonry response on the orientation of the applied loads. Finally large panels behavior is considered.

3.1 Masonry constituents

Several experimental campaigns have been carried out on masonry specimens in the last few decades with the aim of characterizing the main properties of masonry and its constituents and interesting results have been provided. Simple experimental tests on small scale masonry specimens provide information as for the masonry in its entirety as for the constituents individually, it is important to underline, in fact, as asserted by van der Pluijm (1999) and remarked by Massart (2003), that the properties of mortar are considerably influenced by the presence of bricks because of water absorbtion, therefore tests performed on prisms consisting solely of mortar are not representative of the effective behavior.

Standard uniaxial tensile-compressive tests on masonry specimens shows distinctive features (In Figure 3.1 a sample of $\sigma - \varepsilon$ diagram is given):

- both constituents show tensile strengths prominently lower than the compressive ones;

- bricks display compressive strength f_{bc} and Young modulus E considerably higher than mortar;

- bricks exhibit nearly linear responses followed by brittle failures;

- mortar joints show a strongly non linear behavior and a remarkable ductility;

- masonry shows a typical non linear behavior characterized by a compressive strength more or less in the middle if compared with the constituents. The linear branch ends when cracks appear and damaging mechanisms start to catching on. Tensile strength is generally $2 \div 7\%$ of the compression strength.
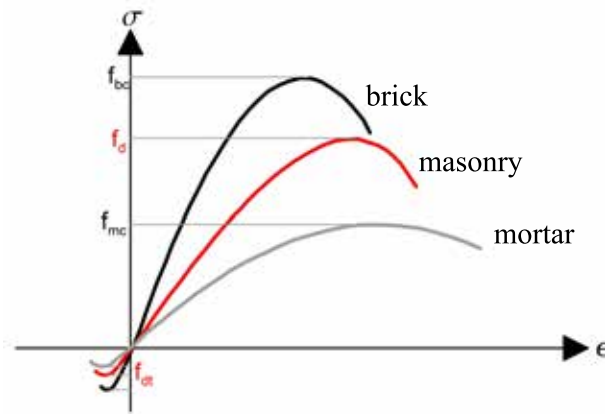
11

Figure 3.1: Dependency of masonry compression strength on bricks and mortar features.

In table 3.1 indicative values of mechanical parameters for bricks and mortar joints are shown, they have been obtained as a result of several experimental tests:

Material	Compression strength $f_c[MPa]$	Tensile strength $f_t[MPa]$	Young modulus $E[MPa]$	Poisson coefficient ν
mortar	$3 - 30$	$0.2 - 0.8$	$(8 - 20)10^3$	$0.1 - 0.35$
brick	$6 - 80$	$1.5 - 9$	$(15 - 25)10^3$	$0.1 - 0.25$

Table 3.1: Mechanical parameters table

A large experimental scatter is observed and it is noticeable that the bricks and mortar mechanical parameters strongly depend both on natural material features and on the manufacturing system. As for mortar in particular, the strength depends on binder and his dosage. Different constituents assembly (stacking of the bricks) together with quantity and quality of binder lead to a wide range of masonry typologies. Even if bricks and mortar joints can be accounted as sufficiently homogeneous and isotropic constituents, the global behavior depends on their respective arrangements and on their interactions. This is essentially the reason why masonry can be considered as a structure and not as a material. In particular the interaction between mortar and bricks is influenced by several mechanical and physic-chemical factors that can be summarized as follows:

- Bricks:

    - compression and tensile strength for uniaxial and multiaxial tests;

    - Young modulus, ductility and creep;

    - superficial roughness;

    - water absorption features;

    - Chemical agent resistance;

    - volume variation due to damp, temperature and chemical reactions;

    - weight, shape, hole distribution (in artificial elements).

- Mortar:

    - compression strength for multiaxial tests;

  – Young modulus, ductility and creep;

  – adhesion;

  – workability and plasticity .

- Method of construction:

  – geometry and arrangement of bricks;

  – thickness of mortar joint compared with brick dimensions;

  – lack of uniformity of mortar joint thickness.

Figures 3.2 show the influence of mortar typologies (for example aerial and hydraulic) on masonry behavior.
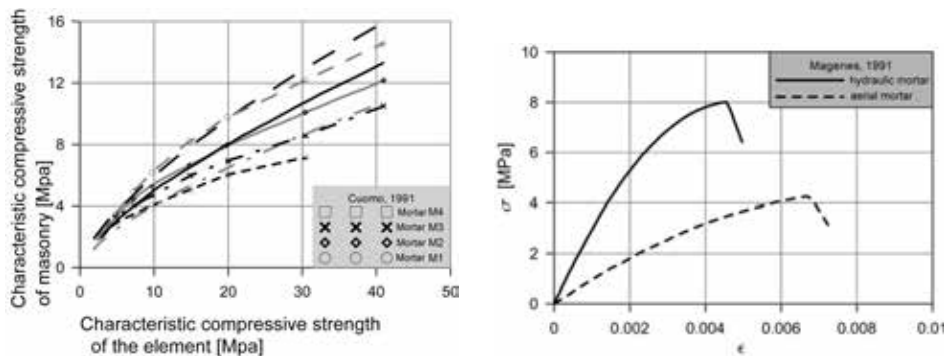

Figure 3.2: Dependency of masonry compression strength on mortar typologies (left);Dependency of masonry constitutive law $\sigma - \varepsilon$ on mortar typologies(right).

A very important feature of the masonry constituents response is the characteristic *softening* behavior (see Fig. 3.3). Steep slopes and subsequent nearly linear branches are a consequence of material damaging. At the macroscopic scale vertical or diagonal cracks appear due to the overtaking of the strength threshold.
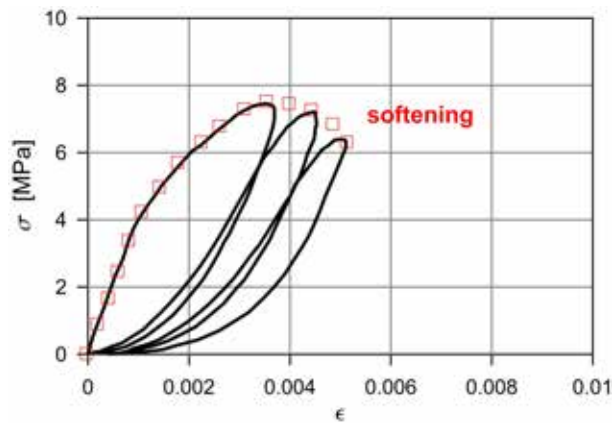

Figure 3.3: Typical softening behavior emerging from loading-unloading cycles on masonry.

Classically quasi-brittle materials, as clay bricks, mortar, concrete and rock, exhibit typical softening behavior, i.e. drop in mechanical strength corresponding to increase of imposed deformation on the experimental specimen. In particular it has been noticed that softening behavior is related to material heterogeneities due to the presence of different constituents as well as to pre-existing defects. In fact in the

mortar, micro-cracks appear due to autogenous shrinkage and to the presence of aggregates; also bricks show micro-damaging phenomena. The presence of aforementioned defects together with the internal variability of strength and stiffness are the main causes of cracking growth during the experimental tests. At the beginning the cracks develop only if load levels increase, thus the process is still stable, but when the peak load is reached the phenomenon quickly increases and macro-cracks appear. An unstable phase starts and the test can be carried on only if the load decreases (displacement driven tests). Typically the cracks are restricted to a very narrow zone, while the remaining part of the apparatus is unloaded. Shear tests show that the softening behavior results in the degradation of the cohesion in the Coulomb friction model. As for compression tests it appears that boundary conditions and specimen dimensions strongly affect the response.

3.2 Masonry material

A macroscopic characterization of masonry is very important in order to understand the role played by the respective arrangement of bricks and mortar in the definition of the overall structural behavior.

The interface between bricks and mortar joints is a very important zone because it is liable for the non-linear behavior of the mortar. It is possible to identify two different interface crack types: Mode I (tensile failure) and Mode II (shear failure). van der Pluijm (1999) executed a few of deformation controlled tests on masonry specimens containing only one mortar joint in order to characterize the aforementioned failure modes.

3.2.1 Mode I- Tensile failure

This failure mode is characterized by tension softening curves with an exponential trend. The measured fracture energy G_f^I varies between 0.005 and 0.015 $[Nmm/mm^2]$ and the strength between 0.3 and 0.9 $[N/mm^2]$. For the current case the fracture energy is defined as the energy amount required to engender a unit area of crack along the interface. More precisely it has been noticed that the effective area of the specimen is smaller than its dimensions and it is centered in the internal zone of the specimen and the test is governed by the failure of the interface between bricks and mortar. In the Figure 3.4 the experimental apparatus for the test and resulting curves are shown.
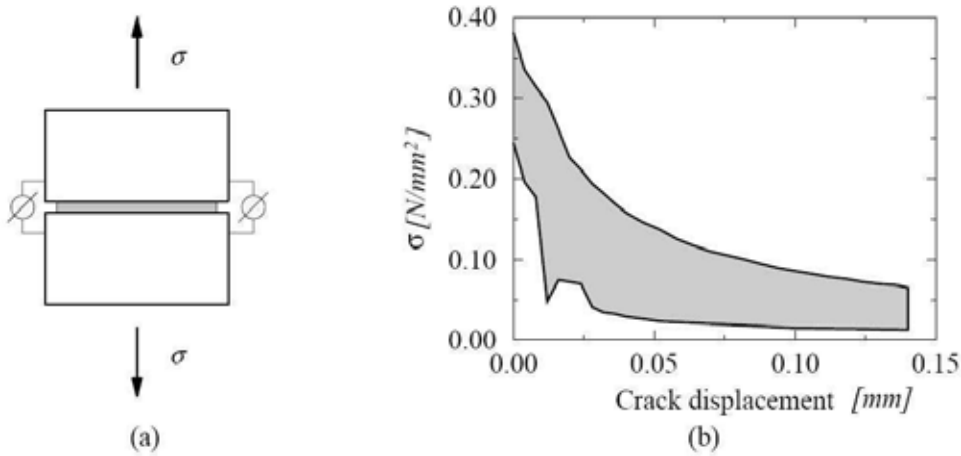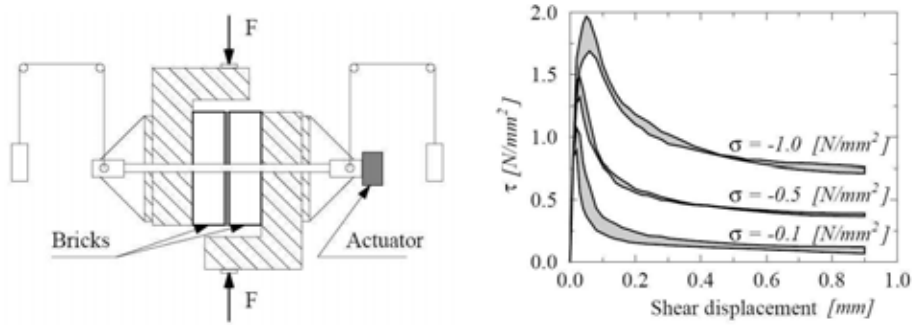

Figure 3.4: (a) Experimental apparatus (b) Curves σ-δ

3.2.2 Mode II- Shear failure

The experimental apparatus (see Figure 3.5(a)) designed for this test allows to apply a constant confining pressure (together with shear forces) and three different levels have been considered: 0.1, 0.5 e 1 $[N/mm^2]$. Figure 3.5(b) shows the curves τ-δ corresponding to the different aforementioned confining pressure levels and it appears that the peak shear strength increases in direct proportion with the confining pressure.

Uniaxial and multi-axial tests point out the main effects of the stacking of the bricks on the failure scenarios.
Starting with uniaxial behavior, it is considered a typical stack bond masonry undergoing loading condition orthogonal or parallel to bed joints.

Figure 3.5: (a) Experimental apparatus (b) Curves τ-δ.

3.2.3   Uniaxial compressive behavior

Traditionally the only parameter considered to characterize the masonry structural properties was the compressive strength orthogonal to bed joints. The related experimental test is usually performed on prisms of stacking bond masonry (see Fig. 3.6).
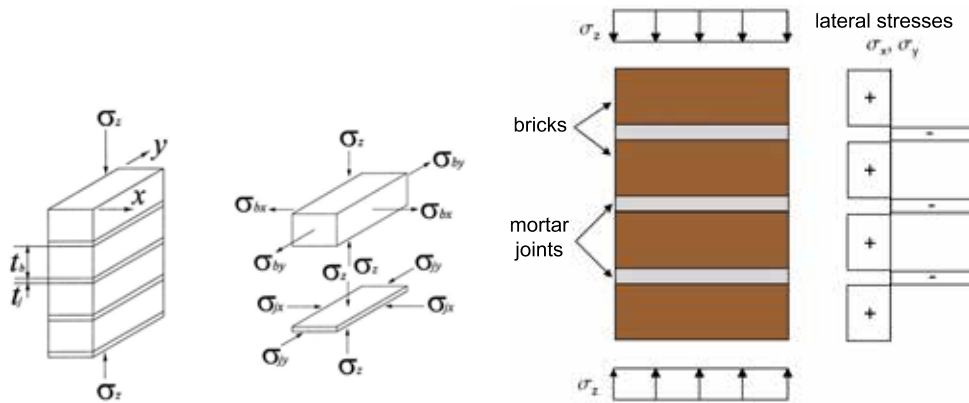

Figure 3.6: Stresses in a masonry prism undergoing compression loading.

The confining pressure, transmitted by bricks, engenders a triaxial compression state in the mortar joints. This is the reason why masonry can undertake loading conditions exceeding the uniaxial compressive strength of mortar. It is underlined that vertical cracks development is related to tensile stresses orthogonal to the compressive loading direction. The different deformation behavior of mortar and bricks, in fact, causes this indirect stress state. In the Figure 3.7 the σ-δ curve is shown corresponding to different values of mortar strength. The behavior becomes more brittle when the mortar strength increases.

As for the uniaxial compression test in the same direction of bed joints the ratio between the strength along this direction and the orthogonal one is varies from 0.2 to 0.8.

3.2.4   Uniaxial tensile behavior

When the tensile load acts in the orthogonal direction with respect to the bed joints, the failure appears in the proximity of the interface between bricks and mortar. Usually the tensile strength of masonry is is ruled by the interface and only in very rare case the brick strength is less than the mortar one. A typical experimental test is described by Backes H.P. (1985): the experimental specimen is made up by four layers of bricks of running bond masonry. The top and bottom boundaries of the specimen are "*clamped*" in steel beams (see Fig.3.8).
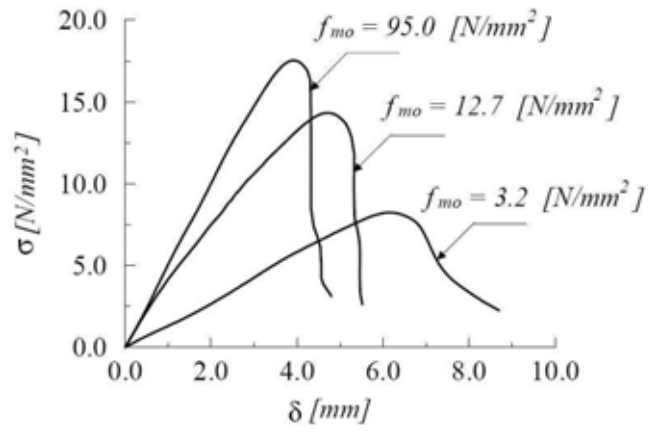
Figure 3.7: Uniaxial compression behavior for different values of compressive mortar strength f_{mo}.
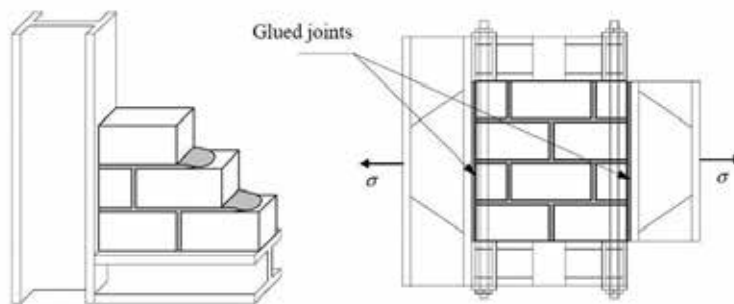

Figure 3.8: Uniaxial tensile test specimen

In Fig. 3.9 two possible responses associated with different failure patterns are shown: depending on the respective strength between joints and bricks. In the first case, for English bond,the failure zigzags occurring in the horizontal and vertical joints. The related global response curve shows a "plateau" when the critical stress is reached. As for the second case, the failure is vertical like by crossing bricks and mortar joints. In the associated global curve it is noticed a marked softening behavior that leads to the full loss of strength.
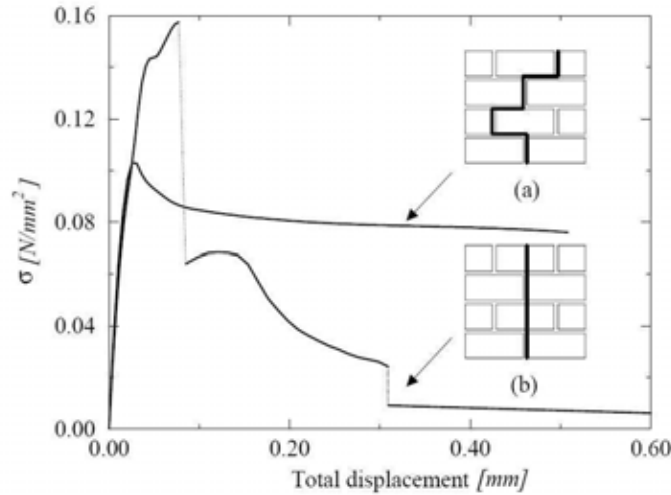

Figure 3.9: Possible responses:a)"zigzag" cracks; b) nearly vertical cracks.

3.2.5   Biaxial loading cases

Peak stress values and residual strength of masonry are strongly influenced by the different applied loading conditions, this is the reason why t is very important to take into account the response under biaxial loading case. Orthotropic behavior is very pronounced when the strength of mortar is strongly lower than the bricks ones; on the other hand, if the bricks are weaker than the mortar, the orientation of joints and the bonding have no influence on the response.

In Fig.3.10 envelopes of strength experimentally obtained by Page (1983) for biaxial loading case are shown. In Fig.3.11, instead, Macchi and Magenes (2002) collected possible failure modes by varying the loading case and the angle between bed joints orientation and load direction. Different loading conditions are considered: uniaxial traction, traction/compression, uniaxial compression and biaxial compression. The first three cases are characterized by planar stress state while as for the biaxial compression out-of-plane effects are engendered. It is clear how depending on the orientation of the principal stresses with respect to the orthotropic axes of masonry the failure patterns change strongly.
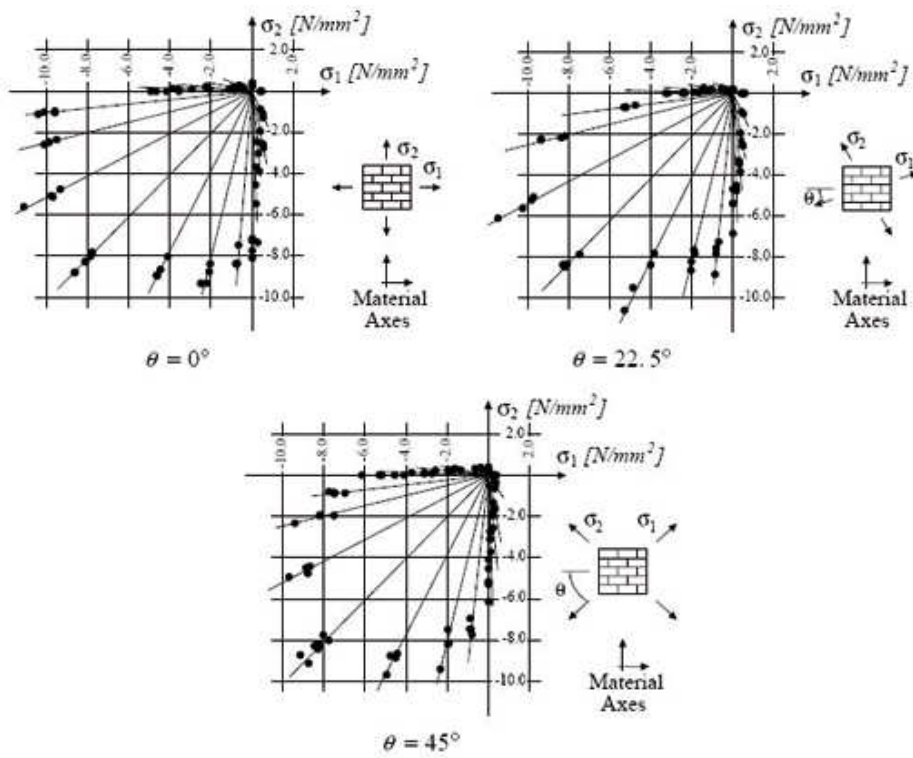
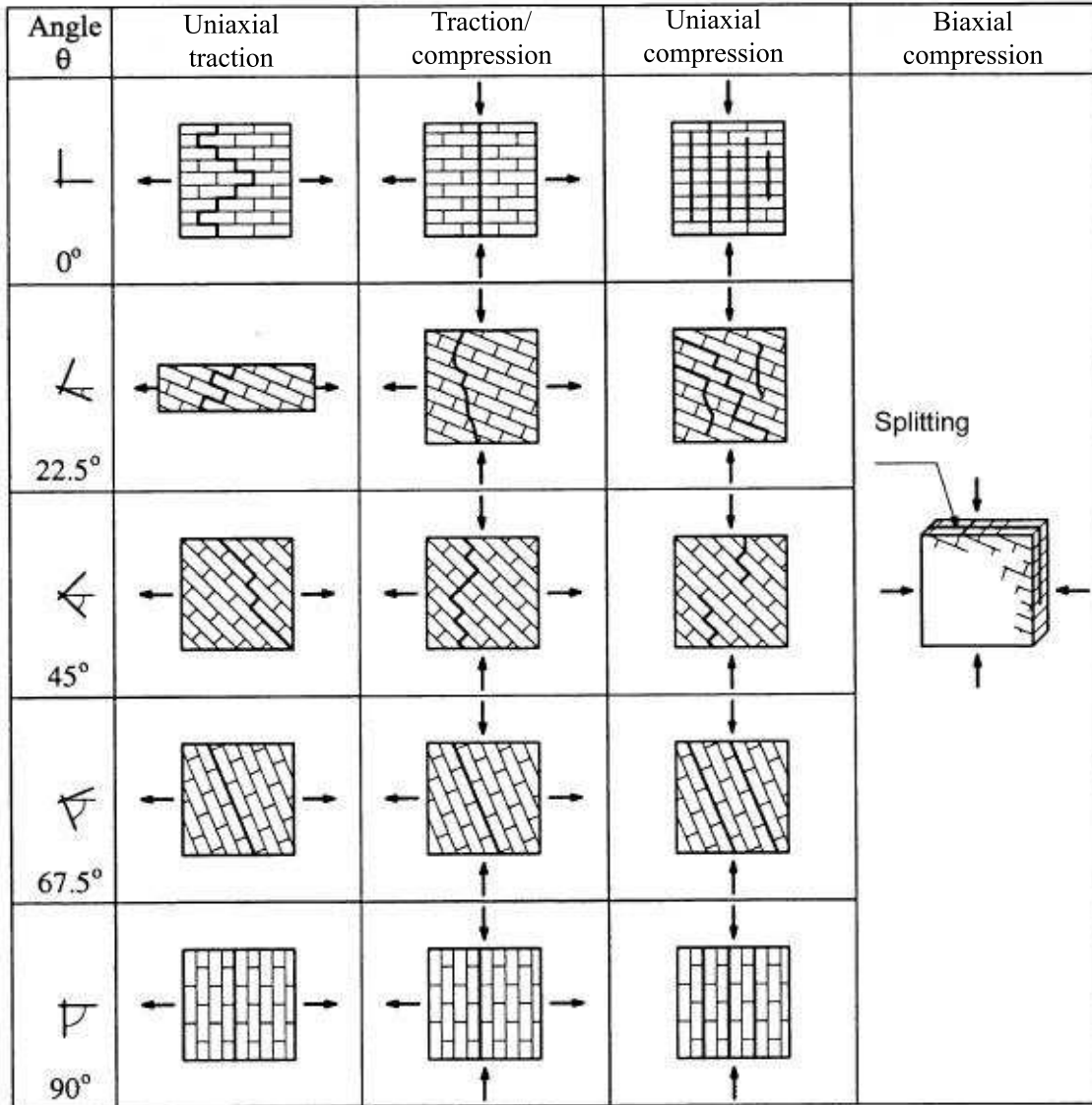Figure 3.10: Biaxial state strength envelopes obtained by Page.

Figure 3.11: Failure modes for masonry panels depending on the loading case (uniaxial or biaxial) Macchi and Magenes (2002).

3.3   Types of masonry bonds

Pattern bond refers to the pattern formed by the masonry units and mortar joints on the face of a wall. Figures 3.12 and 3.13 show the six basic pattern bonds in common use: running, 1/3 running, stack, Flemish, English and Dutch bond.

The running bond is the simplest of the six patterns, consisting of all stretchers. The running bond is used largely in cavity wall construction, brick veneer walls, and facing tile walls made with extra wide stretcher tile.

The 1/3 running bond is a variation of the running bond, having all stretchers with a 1/3 superposition. In the Flemish bond, each course consists of alternating headers and stretchers. The headers in every other course center over and under the stretchers in the courses in between. The joints between stretchers in all stretcher courses align vertically. When headers are not required for structural bonding, you can use bricks called blind headers. You can start the corners in two different ways. In the Dutch corner, a three-quarter closure starts each course. In the English corner, a 2-inch or quarter closure starts the course. The English bond consists of alternating courses of headers and stretchers. The headers center over and under the stretchers. However, the joints between stretchers in all stretcher courses do not align vertically. You can use blind headers in courses that are not structural bonding courses.

The stack bond is purely a pattern bond, with no overlapping units and all vertical joints aligning.

The Dutch bond is a variation of the English bond. It differs only in that the joints between the stretchers in the stretcher courses align vertically.
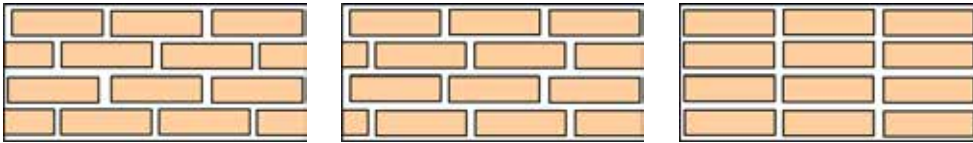

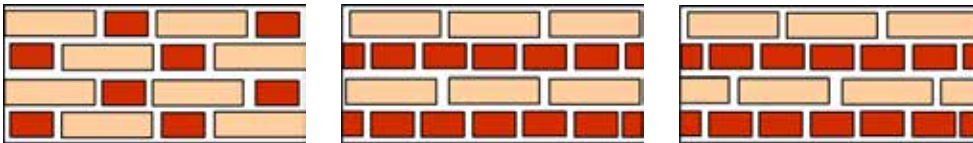Figure 3.12: Running bond (left), 1/3 running (center) and stack (right).

Figure 3.13: Flemish bond (left), English (center) and Dutch (right).

3.4   Masonry structures

Seismic vulnerability is strictly related to the response of masonry panels undergoing shearing loads. It is thus interesting to study the behavior of such masonry portions by simulating seismic loading conditions.

3.4.1   Experimental response

A particular test on a masonry panel is considered in which the specimen is subjected initially to a uniform vertical compression σ_0 and later to a shear tension on the top edge. This loading condition is typical when a panel, included into a structure, undergoes horizontal actions. Mann, W. and Mller, H., (1982) have identified three main failure mechanisms:

- cracking in the bed joints, when low values of compression stresses σ_0 hold ;

- cracking due to shear and tension, for intermediate values of σ_0;

- cracking due to masonry crushing, when σ_0 reaches values close to masonry uniaxial compression strength.

In the first case failure appears due to shear in the bed joints, the cracks follow the horizontal and vertical joints. The authors have proposed to characterize the bed joints using a Coulomb friction load and when the failure appears the following relation holds:

(3.1) $$\tau_m = c + \mu\sigma_m$$

where c is the cohesion and e μ is the friction coefficient that characterize the bed joints response, while τ_m and σ_m are the local stresses.
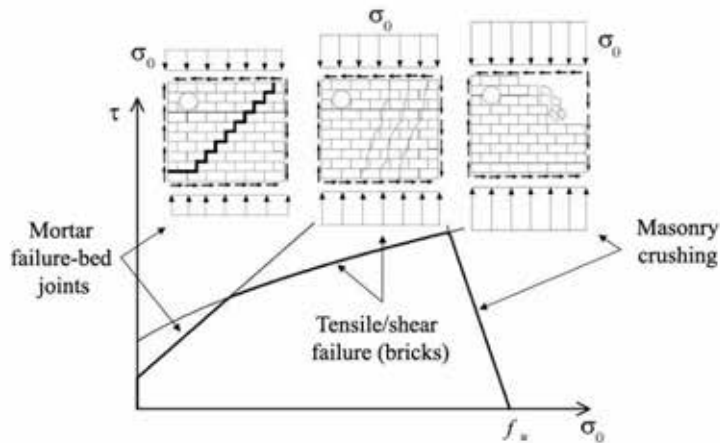

Figure 3.14: Failure envelopes for combined loading case (vertical and shearing)
.

The failure appears when the tensile principal stress in the brick reaches the tensile strength threshold (second case), or when the maximum value of vertical compression stress reaches the the compression strength threshold (third case). In Figure 3.14 the failure domain obtained by Mann, W. and Mller, H., (1982) is shown. Experimental tests hence show that different failure mechanisms are possible due to the combined actions of vertical and shear loading conditions:

- cracking and failure due to combined compressive and bending stress (Figure 3.15_a);

- cracking or failure due to shear and diagonal traction (Figure 3.15_b);

- sliding (Figure 3.16_a and 3.16_b).

The actual failure mechanism (combined compressive and bending stress or shear) depends on the ratio H/B between the longitudinal dimensions of the whole panel (when no hole are considered) or of the single portions constituting the panel (when windows or doors interrupt the continuity of the panel), it depends also on the material parameters and on the vertical load applied. Slender panels usually shown the first failure mechanism, while squat panels the second one.
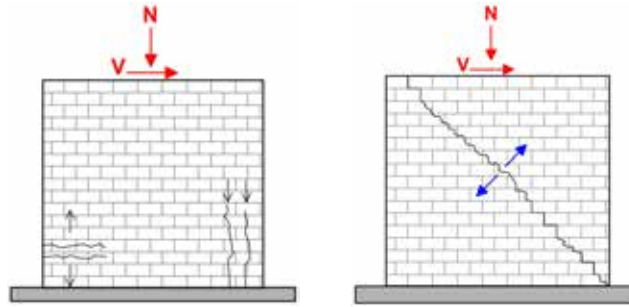
Figure 3.15: Principal failure mechanism for large dimensions panels; from left to right:(a) combined compressive and bending stress; (b) shear and diagonal traction.
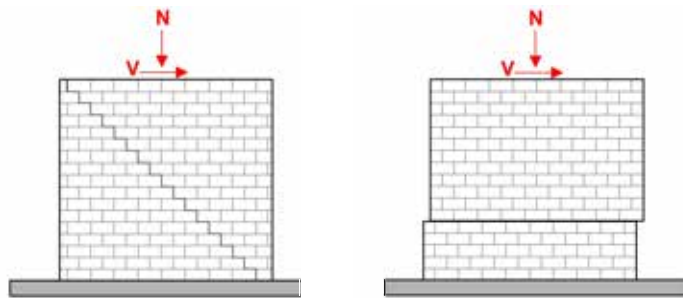
Figure 3.16: Principal failure mechanism for large dimensions panels; from left to right:(a)staircase sliding; (b) horizontal sliding.

3.4.2   Failure due to combined compressive and bending stress

In such a case, it is reasonable to suppose that an *ideal strut* appears in the panel in order to assure that the external actions are equilibrated by the stress state on the end sections. This rafter picks out the reacting part of the panel. See Figures 3.17 e 3.18.

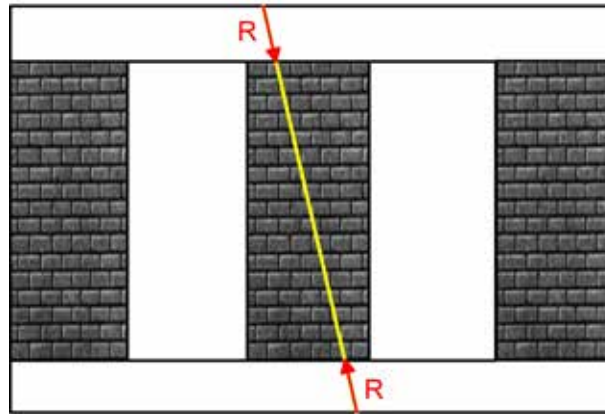Figure 3.17: Combined compressive and bending stress: diagonal strut (stress distribution).

Figure 3.18: Combined compressive and bending stress: diagonal strut (resultant).

The failure occurs when the compressed edges of the extreme sections are crushed (see Fig.3.19_a), moreover usually bending wide cracks appear and also rigid body motion ("rocking"), Fig. 3.19_b, can take place.

This kind of failure is more desirable than the shear failure because a more ductile global behavior is shown and the structure can undergo larger displacements before failure.

3.4.3   Failure due to shear

Shear failure mechanisms, due to combined shear stresses (due to horizontal loads) and normal stresses, are the most common in masonry structures in reason of standard ratios between characteristic dimensions of bricks and mortar joints). Depending on the respective strength of bricks and mortar, different cracking pattern may occur. When the mortar is very weaker with respect to bricks, only the bed joints are cracked. In the typical cracking scenario, the cracks develop starting from the middle zone of the panel along the compressed diagonal, see Figure 3.20.
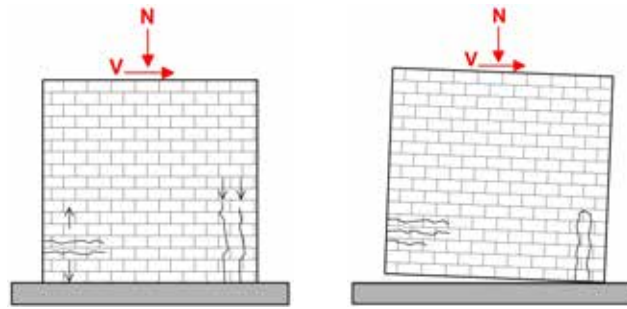
Figure 3.19: Principal failure mechanism for large dimensions panels; from left to right:(a) bending; (b) diagonal traction.
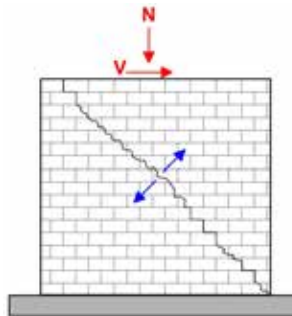

Figure 3.20: Failure mechanism due to shear driven traction : diagonal cracks in the prevalent compressive direction.

Such a failure is considered as a ultimate limit state because often it corresponds to maximum shear resistance V, when N is fixed. Anyway it is possible that the residual strength, after cracking, is considerable, depending on the the value of normal action N.

As the fracture onset appears along the prevalent direction of compression, it is supposed that the maximum tensile strength is reached. If a failure criterion limiting maximum normal tensile strength is adopted, the crisis appears when the tensile strength is overtaken into the panel. In this case the maximum value of horizontal load that the panel can be submitted to is, conventionally, the value V_t for whom diagonal cracks appear.

essendo b un coefficiente che dipende dalla distribuzione delle tensioni tangenziali lungo la sezione trasversale del pannello e che varia, in generale, sia con le caratteristiche geometriche che con lo stato tensionale.

3.4.4 Sliding in the joints

Another failure scenario due to shear appear when a portion of the panel slips with respect to the other one. Usually the cracks run along a horizontal bed joint. Usually those mechanisms are related to Mohr-Coulomb Criterion.

Chapter 4

First order computational homogenization

4.1 Introduction

This chapter is devoted to the study of the overall response of masonry panels by employing a *First order computational homogenization technique.* If regular brick patterns are considered, a portion of masonry may be regarded as a periodic composite structure, consisting of two different phases arranged respecting periodicity. At the structural scale, the overall constitutive behavior, resulting from the interaction between the different constituent materials, is *a-priori* unknown.

In order to overcome the lack of a global constitutive law, a numerical derivation is possible and the first order computational homogenization technique provides an appropriate strategy to reproduce the global behavior of a multi-phase material, characterized by a fair compromise between the detailed information need (size, volume fractions, arrangement, material properties and their evolution strongly affect the global behavior) and the requirement of keeping down computational efforts.

Adopting the multi-scale strategy, known as *Computational Homogenization*, it is possible to obtain the macroscopic constitutive response, from the microscopical description of the single phase materials, solving a proper boundary value problem (*BVP*).

The conceptual scheme of a general multi-scale technique can be explained as follows: the problem is split into two scales:

- a macro-scale, the structural one, in which an equivalent homogeneous medium is considered. This fictitious material is assumed to have the same average properties as the heterogeneous one and it does not contain explicit information about its own constitutive behavior; At this scale it is possible to globally reproduce the behavior of the actual structure;

- a micro-scale, where the different constituents are reproduced, respecting arrangement, size and material properties. It corresponds to a detailed description of a representative portion of the composite material.

Therefore, whenever a constitutive information is required at the macro-level, i.e. a relation between macro-deformation vs macro-tension, it is necessary to go down to the micro-level, via a *localization rule*. At the micro-level, on the other hand, all information are available and can be extrapolated, by means of a *homogenization process*, and go onto the upper scale.

The Figure 4.1 shows a very simple but effective scheme of such a technique, summarizing the concepts of localization and homogenization as the two required links between scales.

Suquet (1985) established the fundamental steps towards formulating a homogenization scheme: first of all it is necessary to define a proper portion of microstructure, able to statistically represent the
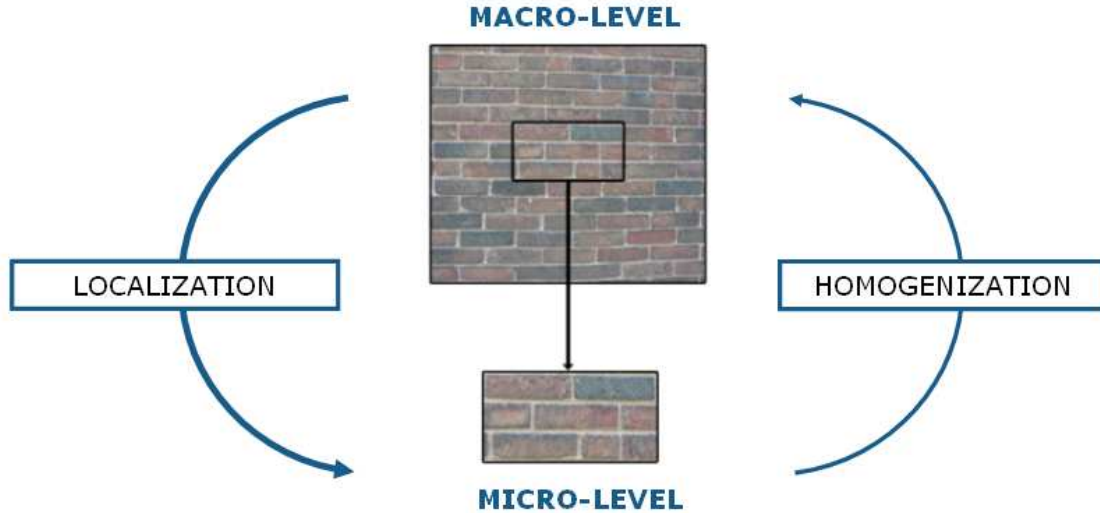
Figure 4.1: First order computational homogenization theoretical scheme.

properties of the composite material, constituted by a realistic topological arrangement of the different material phases. This portion is named *RVE* (*Representative Volume Element*) and it defines the basic cell at the micro-level; it is also necessary to establish the boundary conditions to be imposed on the *RVE* and furthermore proper relations between macro and micro-level stresses have to be defined and, finally, a numerical relation between the macroscopical input (strains) and output (stresses) data has to be obtained.

The homogenization theory, presented in this chapter for the solution of the quasi-static problem of masonry panels, is based on classical the first-order approaches proposed and adopted by many authors (Smit et al. (1998); Miehe et al. (1999); Zalamea (2001); Kouznetsova (2002)).
The formulation is based on the principle of the *local periodicity* (Sanchez-Palencia (1987)), in the sense that the microstructure repeats itself in a narrow zone near a macroscopic point, while if not close together macro-level points are considered, the related *RVEs* may be different among them.
It is worth mentioning that this two scale model is justified when there is a substantial difference between the two length scales involved in the problem. This property is referred to as *Principle of separation of scales* and an exhaustive illustration of this concept can be found in Zaoui (2002).
Five length scales in ascending order for both levels are defined, as follows:

1. μ_0 is the lower length bound, under which continuum mechanics is not valid anymore;

2. μ is the characteristic size of heterogeneities ;

3. l is the characteristic size of the *RVE*;

4. λ is the fluctuation length of the prescribed mechanical loading over the structure;

5. L is the characteristic size of the structure.

Between the aforementioned length scales, particular relations must arise. First of all the size of the *RVE* must be much smaller than the one of the structure (i.e. $l \ll L$).
Moreover the characteristic size of the heterogeneities must be much smaller than the size of the *RVE* (i.e. $\mu \ll l$); in order to guarantee that continuum mechanics remain valid at the scale of the *RVE*, it has to arise that $\mu_0 \ll \mu$. The last relation links the fluctuation length of the prescribed mechanical loading

over the structure and the size of the *RVE* (i.e. $l \ll \lambda$), so that the use of the classical integral and differential tools of structural analysis remains valid.

Typical materials that fit well the *Principle of separation of scales* are, for example, metal alloys, metals having a polycrystalline structure with grains or, finally, metal matrix composites (see Kouznetsova (2002)).

As for masonry, instead, the ratio between macroscopic and microscopic characteristic sizes is in the range of 10-100 (see Massart (2003)) and the application of the computational homogenization requires particular attention.

A *strain driven formulation* is chosen, therefore, the homogenized strain vector **E** is evaluated at the macro-level for all the local points of the equivalent homogeneous continuum. At this level the direct evaluation of related stresses **Σ** is not possible, due to the lack of macro-level closed form constitutive laws. This is the reason why a proper formulated *BVP* at the micro-level has to be solved. To this end **E** is used as input data for the imposition of local boundary conditions on the *RVE*, using a properly conceived *kinematic map*.

The quasi-static boundary value problem on the *RVE* is solved and the homogenized stress tensor **Σ**, as volume average of the local computed stress field, is calculated.

The obtained value is sent back to the macrostructure.

In the Figure 4.2 the first order computational homogenization scheme is summarized. Let's imagine to consider a macro-level point (shown in the figure) where a strain measure is available (**E**); the kinematic map may be visualized as an arrow, as a bridge condition, through which the macro-level measure is passed to the *RVE*. The equilibrium problem at this level, where the problem is well posed (also the constitutive laws are know $\sigma = f(\varepsilon)$), is solved. The last step, in order to complete the scale-transition scheme, is the definition of the averaged stresses **Σ** sent back to the macro-level.

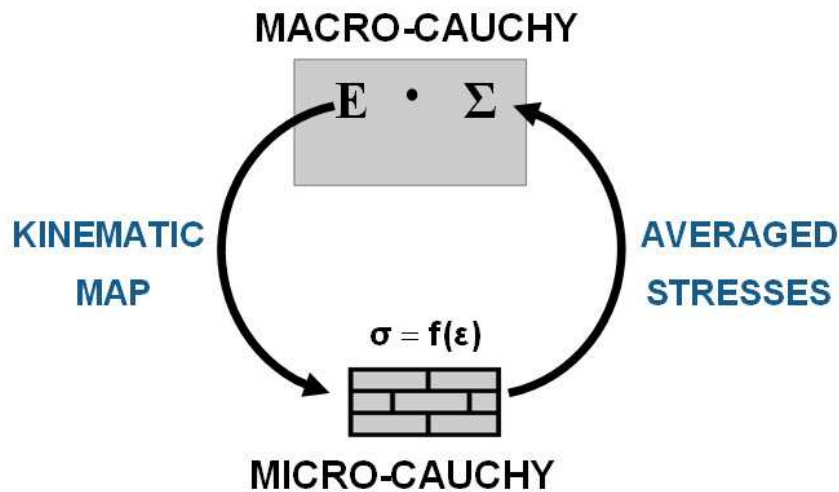Figure 4.2: First order computational homogenization working scheme.

Choice of the RVE

A very important task in the proper formulation of a computational homogenization procedure is the convenient choice of the *RVE*. Several definitions of such a representative volume are available, formulated by many authors.

Jiang et al. (2001) write: "mathematically, *RVE* is an infinite length scale limit, relative to the micro-

scale in which the material appears uniform and the continuum concept may be applied".

Drugan and Willis (1996) established that an *RVE* has to be a statistically representative sample of the microstructure, i.e. it has to include virtually a sampling of all possible microstructural configurations that occur in the composite. More precisely, by making mention of the original definition, "an *RVE* is the smallest material volume element of the composite for which the usual spatially constant *overall modulus* macroscopic constitutive representation is a sufficiently accurate model to represent average constitutive response".

In the case of non-regular and non-uniform microstructure, this definition leads to a considerably large *RVE*, because it has to be large enough to represent the microstructure without introducing non-existing properties.

Another important definition is the one of Hill (1963) according to whom the *RVE* is "a sample that is structurally entirely typical of the whole mixture on average and contains a sufficient number of inclusions for the apparent overall moduli to be effectively independent of the surface values of traction and displacement, so long as these values are macroscopically uniform".

Practically speaking, the *RVE* is well defined if it reflects the material microstructure and if the responses, under uniform displacement and traction boundary conditions, coincide. If a microstructural cell does not contain sufficient microstructural information, its overall response under uniform displacements and traction boundary conditions will differ and the first condition define an approximation by excess of the effective moduli, while the other by defect so, as explained in Terada et al. (2000), there is a dependency of the macroscopic field variables on the selected size of unit cells before reaching the convergence.

A rigorous procedure to extract an *RVE*, adopted for example by Jiang et al. (2001) in a parametric study on elastic anti-plane responses of unidirectional fiber-matrix composites, is to consider increasing *windows of observation* of heterogeneous material, to which apply different types of boundary conditions: displacement- and traction-controlled, periodic boundary conditions, and mixed boundary conditions. The overall properties tend to converge to steady values, as the *windows of observation* increase.

In the case of masonry structures, Anthoine (1995) has suggested the simplest acceptable basic cell, made up of one brick surrounded by half mortar joint. The introduction of two independent vectors (named *periodicity vectors*), namely $\mathbf{v}_1$ and $\mathbf{v}_2$ is necessary to consider different bond patterns, in Figure 4.3, in fact, the respective orientation of the aforementioned vectors is shown as for stack bond (on the left) and running bond (on the right). The concept of *periodicity vectors* will be extensively discussed in Section 4.4.4.
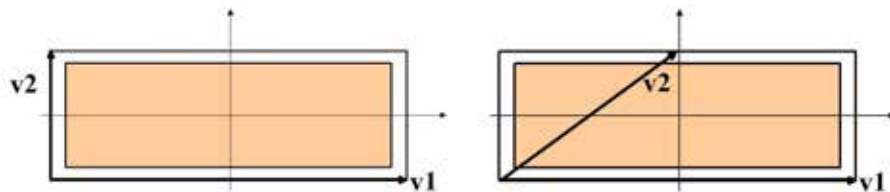

Figure 4.3: Unit cell proposed by Anthoine (1995) provided with *periodicity vectors* as for stack bond (left) and running bond (right).

In the present work different types of *RVE* have been considered, depending on the arrangement of masonry. Therefore for stack or running bonds one brick surrounded by half mortar joint it is considered (also Massart (2003) adopted the same). It should be mentioned that the aforementioned choice of the *RVE* in the case of running bond is valid only in the first order computational homogenization framework and it will be shown in the sequel (5.6.3) that in the enhanced first order homogenization technique a different choice is needed.

As for more complex bond patterns (Dutch bond, Flemish bond, etc..), rectangular or square *RVE*, containing the minimum periodic arrangement, have been used. The Figures 4.4 and 4.5 show the

adopted *RVEs* depending on the type of masonry bond (as suggested by Anthoine (1995)).
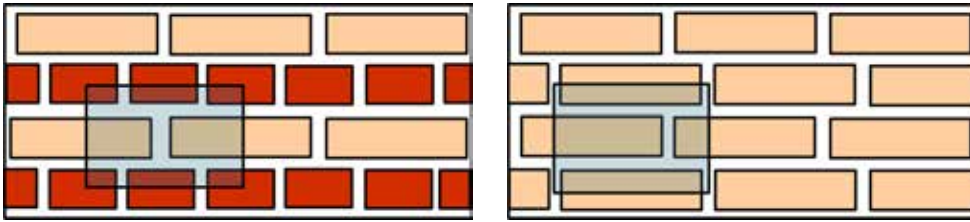

Figure 4.4: *RVE* as for English bond (left) and 1/3 running bond (right).
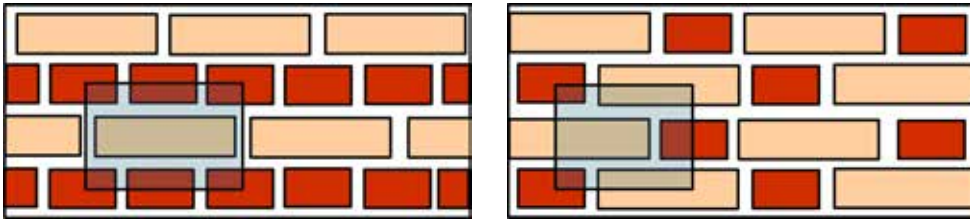

Figure 4.5: *RVE* as for Dutch bond (left) and Flemish bond (right).

In the sequel, capital and lower case letters are used to label the macro and micro scale variables, respectively.

4.2   Statement of the *two scale* problem

Conceptually in the scale transition procedure, every material point P of the equivalent homogenized domain Ω at the macro-level is linked to an underlying domain ω at the micro-level (the aforementioned *RVE*), obtained by ideally enlarging the narrow zone around the point P. In Figure 4.6 a schematic representation is shown.
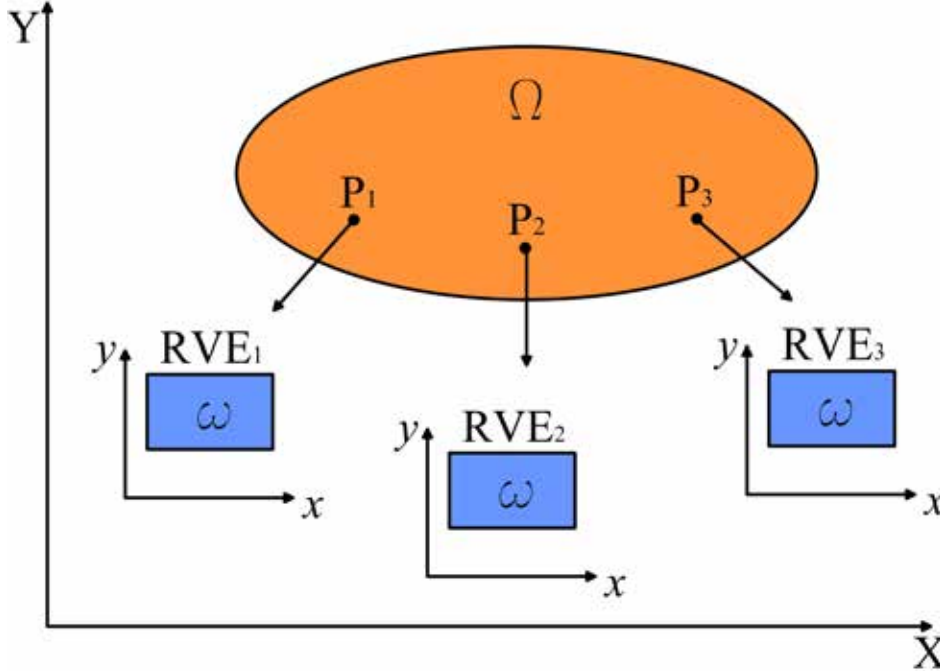

Figure 4.6: Scale transition procedure.

It is supposed that such a domain is periodically repeated in its neighborhood (*local periodicity*) and undergoes periodic deformations, while *RVEs*, corresponding to macroscopic points not lying close in the domain Ω, may be different.

In order to describe the first order computational homogenization technique, it is necessary to establish again the fundamental ingredients required: at the macro-level the heterogenous material, i.e. the actual composite structure, is replaced by an equivalent homogeneous medium, whose closed form constitutive laws are unknown. Therefore, at this scale the structural response is obtained by solving a continuum problem that preserves all the characteristics of a standard Cauchy problem (definition of strains and stresses, balance equations, congruence equations) except for the constitutive laws. Thus, in the framework of a *strain driven formulation*, the derivation of macro stresses on the basis of respective strains is possible by formulating and solving a nested problem. In fact the strain measure, available at the macro-level, is sent to the *RVE* as input information of a properly defined *BVP*. As said before, the *RVE* is a representative portion of continuum medium thus it can be studied as a standard problem in quasi-static continuum solid mechanics. Equilibrium, congruence equations and also constitutive laws are available at this level. The information obtained from the *RVE* in terms of stresses distributions have to be homogenized and send back to the macro level.

In the sequel the macro and micro level problems are outlined together with the bridging conditions between the macro-level material point and the related underlying *RVE*.

All the derivations are obtained fora 2D geometry for small displacements and small deformations and are expressed in incremental form in order to define variables suitable in a non-linear framework.

4.3 Statement of the Macro-level problem

In the framework of first order homogenization, the Macro-level continuum problem is a standard Cauchy continuum problem (classical continuum mechanics). In the sequel the description of strain and deformation, on one hand, and forces and stresses, on the other hand, is briefly recalled together with the equilibrium and kinematic equations. As aforementioned no constitutive laws are explicitly considered at this level.

4.3.1 Compatibility equations

At the macroscopic level the 2D domain Ω of the equivalent homogenized material is considered.
As well known, every material point is characterized by two translational degrees of freedom $\mathbf{U} = [U, V]^T$; the incremental form of the compatibility equations is established hereafter:

$$(4.1) \qquad \dot{\mathbf{E}} = \underline{\mathbf{D}}\dot{\mathbf{U}} \quad \text{in} \quad \Omega$$

where $\dot{\mathbf{E}}$ is the increment, in the infinitesimal time increment dt, of the strain vector (called *Homogenized strain vector*), $\underline{\mathbf{D}}$ is the compatibility operator and $\dot{\mathbf{U}}$ is the increment of the displacement vector.
In the expanded form the equations are:

$$(4.2) \qquad \left\{ \begin{array}{c} \dot{E_{XX}} \\ \dot{E_{YY}} \\ \dot{E_{XY}}; \end{array} \right\} = \left[\begin{array}{cc} \frac{\partial}{\partial X} & 0 \\ 0 & \frac{\partial}{\partial Y} \\ \frac{\partial}{\partial Y} & \frac{\partial}{\partial X} \end{array} \right] \left\{ \begin{array}{c} \dot{U} \\ \dot{V} \end{array} \right\};$$

If $\partial\Omega = \partial\Omega_U \cup \partial\Omega_T$ is the boundary contour of the domain Ω, divided into the contour on which only the displacements are prescribed $\partial\Omega_U$ and the other on which only tractions are prescribed $\partial\Omega_T$, the Dirichlet boundary condition are defined as follows:

$$(4.3) \qquad \dot{\mathbf{U}} = \dot{\overline{\mathbf{U}}} \quad \text{on} \quad \partial\Omega_U$$

.

4.3.2 Forces and stresses

The static local equilibrium in the incremental form of the Cauchy stress tensor $\dot{\boldsymbol{\Sigma}}$ is:

$$(4.4) \qquad \underline{\mathbf{D}}^T\dot{\boldsymbol{\Sigma}} + \dot{\mathbf{B}} = \mathbf{0} \quad \text{in} \quad \Omega;$$

where the increment of the body forces $\dot{\mathbf{B}}$ in the Ω domain are taken into account.
The vector of the increment of the stress components is :

$$(4.5) \qquad \dot{\boldsymbol{\Sigma}} = \left\{ \begin{array}{c} \dot{\Sigma_X} \\ \dot{\Sigma_Y} \\ \dot{\Sigma_{XY}} \end{array} \right\}$$

The incremental form of the traction boundary condition, resulting from the Cauchy's theorem, are defined as follows:

$$(4.6) \qquad \underline{\mathbf{N}}\dot{\boldsymbol{\Sigma}} = \dot{\mathbf{T}} \quad \text{on} \quad \partial\Omega_T$$

where $\underline{\mathbf{N}}$ is the matrix containing the unit vectors normal to the traction boundary contour $\partial\Omega_T$ and $\dot{\mathbf{T}}$ is the vector of the increment of surface forces defined on the same contour.

4.3.3   Constitutive relations

As for the constitutive laws at the macro level, the lack of closed form global relationships between strains and stresses requires the construction of a numerically based strategy, with the aim of properly extracting from the micro-level the required information at the macro-level.

In a displacement-based framework, the values of the dependent variables (i.e. $\dot{\boldsymbol{\Sigma}}$) are obtained by averaging the related measures at the micro-scale (See 4.5) and also the homogenized tangent constitutive tensor $\underline{\mathbf{C}}$ is obtained from the RVE. The incremental constitutive relation linking homogenized stresses and strains by means of the homogenized constitutive tensor holds as:

$$(4.7) \qquad\qquad\qquad \dot{\boldsymbol{\Sigma}} = \underline{\mathbf{C}} \quad \dot{\mathbf{E}}$$

4.4   Statement of the Micro-level problem

At the micro-level a nested BVP has to be solved on the RVE that receives a macroscopic measure as input variable and returns an averaged output variable to the upper level. In the following sections, Congruence and Equilibrium equations are defined on the RVE (ω). At this level the constitutive laws, characterizing different constituents, are supposed to be known. Particulary attention is needed for the definition of a BVP for which periodic boundary conditions are considered.

4.4.1   Compatibility equations

At this level, the domain ω of the RVE is taken into account.
The incremental form of the symmetric strain vector, is:

$$(4.8) \qquad\qquad\qquad \dot{\mathbf{e}} = \underline{\mathbf{d}}\dot{\mathbf{u}} \quad \text{in} \quad \omega$$

where $\underline{\mathbf{d}}$ is the compatibility operator and $\dot{\mathbf{u}}$ is the increment of the displacement vector.
In the expanded form the compatibility equations are:

$$(4.9) \qquad\qquad \left\{ \begin{array}{c} \dot{\epsilon_x} \\ \dot{\epsilon_y} \\ \dot{\epsilon_{xy}} \end{array} \right\} = \left[\begin{array}{cc} \frac{\partial}{\partial x} & 0 \\ 0 & \frac{\partial}{\partial y} \\ \frac{\partial}{\partial y} & \frac{\partial}{\partial x} \end{array} \right] \left\{ \begin{array}{c} \dot{u} \\ \dot{v} \end{array} \right\}.$$

4.4.2   Forces and stresses

Assuming that the RVE is much smaller than the characteristic length at the macro-scale, the body forces $\mathbf{b}$ are supposed to be negligible and only interaction forces, generated by different constituent materials, are taken into account, thus the static local equilibrium in the incremental form is:

$$(4.10) \qquad\qquad\qquad \underline{\mathbf{d}}^T\dot{\boldsymbol{\sigma}} = \mathbf{0} \quad \text{in} \quad \omega;$$

where the vector of the increments of the stress components is:

$$(4.11) \qquad\qquad\qquad \dot{\boldsymbol{\sigma}} = \left\{ \begin{array}{c} \dot{\sigma_x} \\ \dot{\sigma_y} \\ \dot{\sigma_{xy}} \end{array} \right\}.$$

The admissible stress field which satisfies the previous equilibrium equation, is referred to as a *self equilibrated stress field* (Cristescu et al. (2004)).

4.4.3 Constitutive relations

Each material constituent, i.e. blocks and mortar joints, is described by to its respective constitutive law. In abridged form, mathematical expressions for generic time and history dependent constitutive relations, specified for a single material phase i, are:

$$(4.12) \qquad \boldsymbol{\sigma}^i(t) = \boldsymbol{F}^i\{\mathbf{e}^i(\tau), \tau \in [0, t]\}$$

where it has been supposed that the free variable is the the strain vector $\mathbf{e}$.

The incremental form of the constitutive relation between homogenized stresses and strains is:

$$(4.13) \qquad \dot{\boldsymbol{\sigma}} = \underline{\mathbf{c}}\dot{\mathbf{e}}$$

In the sequel for bricks and mortar the same constitutive law, but with different material parameters, has been chosen, i.e. a scalar isotropic damage law. The details of the model and the related implementation are reported in Appendix A.

4.4.4 Boundary value problem

The problem definition at the micro-level has to be completed by properly defining the *RVE* boundary conditions, i.e., from the load (strain) defined at each point of the macroscopic level (e.g. at integration points of a finite element mesh of the structure), it is necessary to establish which boundary conditions must be applied to the corresponding RVE.
Special conditions are required in order to effectively formulate the scale transition procedure.
As previously said, a macroscopical strain measure $\mathbf{E}$ is the macro-level information passed to the *RVE*. A specific approach has to be used in order to include this information into an appropriately devised *BVP* on the *RVE* (kinematic map).
In the referred literature different types of boundary conditions are proposed as for example in Kouznetsova (2002).

Three types of *BVP* are typically used:

- prescribed displacements;

- prescribed traction;

- periodicity conditions.

Several authors have extensively discussed about the possible different boundary conditions to be imposed on the *RVE* with the aim to obtain the best estimation of the overall properties. Terada et al. (2000), van der Sluis et al. (2000) have pointed out that the uniform displacement boundary conditions lead to an overestimation of the elastic properties of the composite material, while uniform tractions lead to an underestimation.
In the case of the first order (Cauchy-Cauchy) computational homogenization, the periodic boundary conditions strike a good balance and provide the best response. In the Fig.4.7 a very meaningful trend is shown: it appears that, for the limited extent of the first order computational homogenization, when the microstructural cell size increases, the homogenized properties tend to the effective value for all three types of boundary conditions, however with the periodic boundary conditions the effective value is reached before (using a smaller cell size).
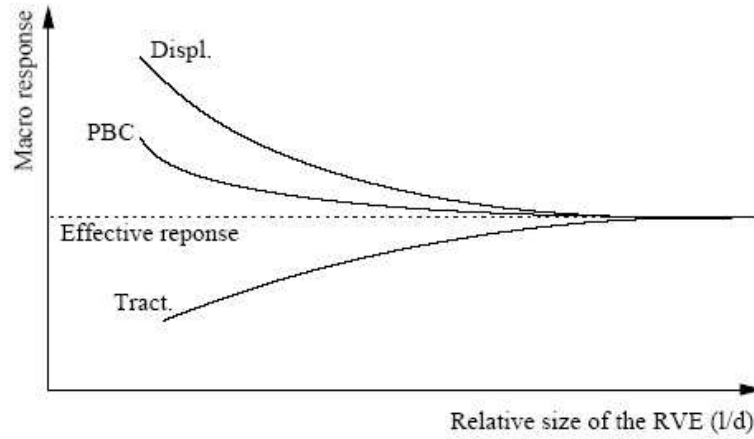
Figure 4.7: Apparent properties obtained using different boundary conditions when the microstructural cell size increases.

In the present work the periodic boundary conditions have, thus, been chosen also by reason of the characteristic periodic arrangement of regular masonry. The fundamental advantage assured by a periodic medium is that a relatively simple *RVE* is able to represent all the heterogeneities and it repeats itself in the continuum domain, generating a regular arrangement.

Due to the repetition of the cell in all directions before and after application of the load, periodic deformations and anti-periodic tractions are applied at each corresponding pair of nodes lying on opposite faces of the RVE boundary (see Figure 4.8).
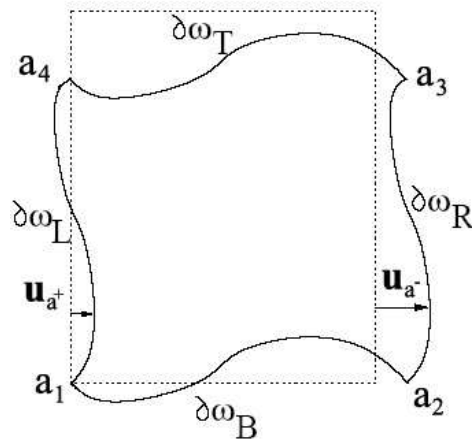

Figure 4.8: Possible deformed shape of a rectangular *RVE* undergoing periodic boundary conditions (Anthoine (1995)).

This is equivalent to impose that:

(4.14)
$$\mathbf{u}_{a+} - \mathbf{u}_{a-} = \underline{\mathbf{E}}\left(\mathbf{x}_{a+} - \mathbf{x}_{a-}\right) = \underline{\mathbf{E}}\,\triangle\mathbf{x}_a$$

where $a+$ and $a-$ is a generic couple of periodic points (represented in Figure 4.8) and $\underline{\mathbf{E}}$ is the macro-level strain tensor. The imposed displacement field is, thus, *strain periodic* (Anthoine (1995)) and the

displacements on two opposite sides must be equal up to a rigid displacement.

As for the anti-periodic tractions:

$$\mathbf{f}_{a+} = -\mathbf{f}_{a-};$$ (4.15)

Without loss of generality the *strain periodic* displacement field may be written in the following form:

$$\mathbf{u}(\mathbf{x}) = \underline{\mathbf{E}}\,\mathbf{x} + \mathbf{u}^p(\mathbf{x});$$ (4.16)

where $\underline{\mathbf{E}}$ is the macroscopic strain tensor, $\mathbf{x}$ is the position vector in the *RVE* and $\mathbf{u}^p(\mathbf{x})$ is a periodic micro-level fluctuation field (vanishing in the corner points of the *RVE*).
The displacement field, solution of the *RVE*, is thus obtained as the superposition of two different fields, the first one, $\underline{\mathbf{E}}\,\mathbf{x}$ driven by the macro-level (i.e. the kinematic map imposed on the contour) and the second one, $\mathbf{u}^p(\mathbf{x})$ that is a local solution field respecting the periodicity between couples of periodic edges.

4.5 Homogenization procedure

A fundamental definition is the *mean value* of an integrable scalar, vector or tensor field $\mathbf{f}$ given on a generic domain Ω_*:

$$\mathbf{F} = \frac{1}{\Omega_*} \int_{\Omega_*} \mathbf{f}(\mathbf{x}) d\Omega_*;$$ (4.17)

where $\mathbf{x}$ is the position vector in a local frame attached to the domain Ω_*.
This assumption is very important, as a macroscopic property can be defined as the volume average of that property over the whole *RVE*. In the sequel the compact notation $\langle \mathbf{f}(\mathbf{x}) \rangle_{\Omega_*}$ will be adopted for the *mean value*.

The homogenized deformation tensor $\underline{\mathbf{E}}$, also called *macroscopic strain tensor* corresponds to an averaged deformation value over the *RVE*, in fact:

$$\langle \underline{\mathbf{e}}(\mathbf{x}) \rangle_\omega = \langle \nabla \mathbf{u} \rangle_\omega = \langle \nabla(\underline{\mathbf{E}}\mathbf{x} + \mathbf{u}^p(\mathbf{x})) \rangle_\omega = \underline{\mathbf{E}} + \langle \nabla(\mathbf{u}^p(\mathbf{x})) \rangle_\omega = \underline{\mathbf{E}}$$ (4.18)

where $\underline{\mathbf{e}}$ is the deformation tensor at the micro scale, $\nabla \mathbf{u}$ is the symmetric part of the displacement gradient of a point with respect to the micro-scale (corresponding to $\underline{\mathbf{E}}\,\mathbf{x} + \mathbf{u}^p(\mathbf{x})$) using the equation 4.16) and ω is the global volume of the *RVE*; the second term in *RHS* (Right Hand Side) is equal to zero because the periodic displacement fluctuation field produces zero mean strain.

The remaining half part of the macro-micro bridging conditions has to be built. The *RVE* receives the homogenized strain tensor and it must evaluate and send back the homogenized stress tensor. Similarly to the 4.18, the macroscopic stress tensor is obtained :

$$\underline{\boldsymbol{\Sigma}} = \langle \underline{\boldsymbol{\sigma}}(\mathbf{x}) \rangle_\omega;$$ (4.19)

As Pegon and Anthoine (1997) underline, the *Hill's Lemma* (in this case specialized for periodic boundary conditions) assures that the averaging procedure is valid in an energetic sense, it reads:

if $\underline{\mathbf{e}}$ is a kinematically admissible strain field corresponding to $\underline{\mathbf{E}}$ and $\boldsymbol{\sigma}$ is an admissible self-equilibrated stress field tensor ($\underline{\mathbf{d}}^T \boldsymbol{\sigma} = \mathbf{0}$) and either the stress field, or the strain field satisfies the periodic boundary conditions, then the mean value of the product $\boldsymbol{\sigma} \, \underline{\mathbf{e}}$ is equal to the product of the means values:

$$\langle \boldsymbol{\sigma} \, \underline{\mathbf{e}} \rangle_\omega = \langle \boldsymbol{\sigma} \rangle_\omega \, \langle \underline{\mathbf{e}} \rangle_\omega; \tag{4.20}$$

Up to now, no hypothesis has been made on a possible link between stresses and strains. If they are coupled through a constitutive law, the lemma ensures the equality between the average of the microscopic work $\boldsymbol{\sigma} \, \underline{\mathbf{e}}$ and the macroscopic work $\langle \boldsymbol{\sigma} \rangle_\omega \, \langle \underline{\mathbf{e}} \rangle_\omega$. This result is commonly called Hill-Mandel condition or macro-homogeneity condition.

Set of governing equation at the two levels: summarizing table

To sum up, the analytical problems are stated by defining two sets of governing equations, both at the micro and macro-level, as shown in the following summarizing table:

Macro-level		Micro-level	
$\underline{\mathbf{D}}^T \dot{\boldsymbol{\Sigma}} + \dot{\mathbf{B}} = \mathbf{0}$	in Ω;	$\underline{\mathbf{d}}^T \dot{\boldsymbol{\sigma}} = \mathbf{0}$	in ω;
$\dot{\boldsymbol{\Sigma}} = \underline{\mathbf{C}} \quad \dot{\mathbf{E}}$	in Ω;	$\dot{\boldsymbol{\sigma}} = \underline{\mathbf{c}} \quad \dot{\boldsymbol{\epsilon}}$	in ω;
$\dot{\mathbf{U}} = \dot{\bar{\mathbf{U}}}$	on $\partial\Omega_U$	$\mathbf{u}(\mathbf{x}) = \underline{\mathbf{E}} \cdot \mathbf{x} + \mathbf{u}^p(\mathbf{x})$	on $\partial\omega_U$;
$\underline{\mathbf{N}}\dot{\boldsymbol{\Sigma}} = \dot{\mathbf{T}}$	on $\partial\Omega_T$		

Table 4.1: Summarizing table

4.6   FE solution algorithm

In the table 4.1 the two set of equilibrium equations arising at macro and micro-level are defined. The micro-level problem is nested into the macro one.
As it is well known, several modeling techniques are available, all of them suitable for the computational homogenization method discretization:

1. Voronoi method (Ghosh et al. (1995, 1996));

2. Fast fourier Transform(Moulinec and Suquet (1998));

3. Finite Element Method (FEM) (Terada and Kikuchi (2001); Feyel (2001); Kouznetsova (2002); Massart (2003); Forest and Sab (1998)).

In this work the FEM has been used to discretize the problem.
Both domains (the *equivalent homogenized medium* at the macro-level and the *RVE* at the micro-level) are discretized and the discrete form of the governing equations is obtained, as usual, by applying the *Weighted Residual Method* to the weak form of equilibrium equations (Bathe (1995); Crisfield (1997a,b); Hinton and Owen (1977); Hughes (2000); Mori (1986); Reddy (2005, 2004); Zienkiewicz and Taylor (1989, 2000)).
There is a one-to-one correspondence between each integration point at the macro-level and the related

RVE, where the nested *BVP* is solved.

It is important to focus the attention on two crucial points of the adopted FE procedure: the solution of the BVP at the micro-level, together with the proper implementation of periodic boundary conditions, and the derivation of the consistent tangent stiffness at the macro-level (that has to be properly extracted from the micro-level, because no constitutive information are available at the macro-level).

4.6.1 Discrete problem at the micro-level

In order to impose the periodic boundary conditions on the *RVE* the method proposed by Pegon and Anthoine (1997) is adopted.

The periodic boundary conditions that the *RVE* must satisfy, as above mentioned, hold as:

$$(4.21) \qquad \mathbf{u}_{a+} - \mathbf{u}_{a-} = \mathbf{E} \triangle \mathbf{x}_a$$

for the displacement field. It means that the displacements of periodic nodes $a+$ and $a-$, lying on the external edges of the *RVE*, are forced to be linked respecting the relation 4.21. In other words, the respective displacements between periodic nodes are imposed to be equal to macro-level driven displacements containing the kinematic map.

As for the antiperiodic tractions, the following relation turns out to be fulfilled for every pair of periodic nodes on the contour and it results in a natural way as solution of the imposed equilibrium problem:

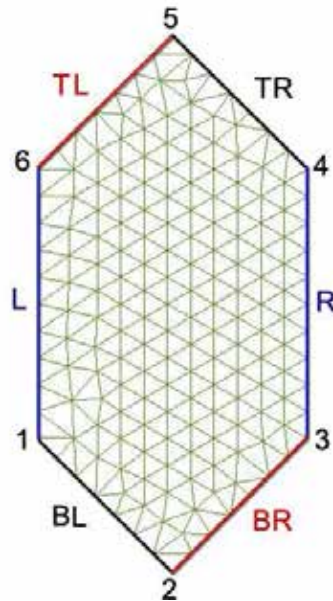$$(4.22) \qquad \mathbf{f}_{a+} = -\mathbf{f}_{a-};$$

.

Figure 4.9: drawn lagrange.

In the Figure 4.9 a possible sample of hexagonal *RVE* has been divided into *N-elem* elements; *N-couple* (L-R; BR-TL; BL-TB) is the number of correspondent couples of periodic nodes lying on the external contour and *N-vert* (1-2-3-4-5-6) is the number of vertexes in the *RVE*-mesh. The periodic boundary

conditions have to be imposed between those linked nodes.

In the selected strategy, the imposition of the aforementioned boundary conditions is obtained by considering a global equilibrium system augmented by Lagrangian multipliers.
This solution leads in general to some inconveniences such as the increased number of the system equations and the enlarged band width of the stiffness matrix. Moreover the last disadvantage (that usually limits the effectiveness of the method) is the existence of zero-terms on the main diagonal of the system matrix, but it is overcome by defining two identical vectors of Lagrangian multipliers $\mathbf{\Lambda}1$ e $\mathbf{\Lambda}2$ (as suggested by Pegon and Anthoine (1997)) that represent combination of the equilibrated forces in the respective periodical nodes on the *RVE* contour.
Just a brief recall to the Lagrangian Multipliers method is outlined. For an exhaustive explanation refer to Bertsekas (1996); Kazufumi and Kunisch (2004).
For the following part refer to the "Wolfram Mathworld" website.
Lagrange multipliers can be used to find the extremes of a multivariate function $f(x_1, x_2, ..., x_n)$ subject to the constraint $g(x_1, x_2, ..., x_n) = 0$, where f and g are functions with continuous first partial derivatives on the open set containing the curve $g(x_1, x_2, ..., x_n) = 0$, and $\nabla g = 0$ at any point on the curve (where ∇ is the gradient).
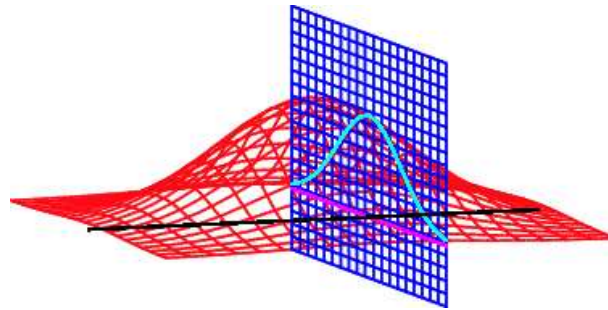

Figure 4.10: drawn lagrange.

For an extremum of f to exist on g , the gradient of f must line up with the gradient of g. In the illustration above (Figure 4.10), f is shown in red, g in blue, and the intersection of f and g is indicated in light blue. The gradient is a horizontal vector (i.e., it has no z -component) that shows the direction that the function increases; for g it is perpendicular to the curve, which is a straight line in this case. There is a red arrow representing the direction of the gradient of both f and g at the optimal point. If the two gradients are in the same direction, then one is a multiple $(-\lambda)$ of the other, so

(4.23) $\nabla f = -\lambda \nabla g;$

The two vectors are equal, so all of their components are as well, giving

(4.24) $\dfrac{\partial f}{\partial x_k} + \lambda \dfrac{\partial g}{\partial x_k} = 0;$

for all k=1, ...,n , where the constant (λ) is called the Lagrange multiplier.
The extremum is then found by solving the $n+1$ equations in $n+1$ unknowns, which is done without inverting g, which is why Lagrange multipliers can be so useful.
For multiple constraints, $g_1 = 0$, $g_2 = 0$, ...

(4.25) $\nabla f + \lambda_1 \nabla g_1 + \lambda_2 \nabla g_2 = 0;$

Linear elastic constitutive behavior

In the case under consideration, i.e. the solution of the equilibrium problem at the micro-level under periodic boundary conditions, the function for which it is necessary to find the extremes is the total potential energy function. In this case the linear elastic range is considered and the total potential energy is expressed in the discretized form as a function of the displacement parameters:

$$(4.26) \qquad\qquad W = \frac{1}{2}\mathbf{u}^T \underline{\mathbf{K}}\mathbf{u} - \mathbf{u}^T \mathbf{f}_e;$$

where $\mathbf{u}$ is the vector collecting nodal displacements of the whole *RVE*; $\underline{\mathbf{K}}$ is the elastic stiffness matrix and $\mathbf{f}_e$ is the vector of external forces.
The aforementioned multiple constraints $g_1 = 0$, $g_2 = 0$,..., $g_n = 0$, are, in this case, the periodic boundary conditions, that have to be satisfied by the *RVE* (see relation 4.21).
Equation 4.26, via the imposition of such boundary conditions, is thus converted in the following augmented form obtained by imposing Lagrange multipliers:

$$(4.27) \qquad W^* = W + \boldsymbol{\Lambda}_1(\underline{\mathbf{k}}_p\mathbf{u} - \underline{\mathbf{E}}\,\triangle\mathbf{x}_a) + \Lambda_2(\underline{\mathbf{k}}_p\mathbf{u} - \underline{\mathbf{E}}\,\triangle\mathbf{x}_a) + \frac{1}{2}(\boldsymbol{\Lambda}_1 - \boldsymbol{\Lambda}_2)^T(\boldsymbol{\Lambda}_1 - \boldsymbol{\Lambda}_2);$$

where the boundary conditions are expressed in compact form using a matrix $\mathbf{k}_p$ that selects the adequate components of the displacement vector linked by the periodic conditions (it is a boolean matrix, in fact, it is full of zeros except for the displacement components corresponding to periodic points where there is ± 1 and its number of rows is equal to the number of periodic couples *Ncouple*); $\boldsymbol{\Lambda}_1$ and $\boldsymbol{\Lambda}_2$ are the vectors collecting Lagrange multipliers and also the square norm of the distance between $\boldsymbol{\Lambda}_1$ and $\boldsymbol{\Lambda}_2$ is introduced.

The global system obtained by minimizing the functional with respect to the three unknown vectors $(\mathbf{u}, \boldsymbol{\Lambda}_1, \boldsymbol{\Lambda}_2)$ i.e.:

$$(4.28) \qquad\qquad \frac{\partial W^*}{\partial \mathbf{u}} = \mathbf{0}; \quad \frac{\partial W^*}{\boldsymbol{\Lambda}_1} = \mathbf{0}; \quad \frac{\partial W^*}{\boldsymbol{\Lambda}_2} = \mathbf{0};$$

is expressed in matrix form as:

$$(4.29) \qquad\qquad \begin{bmatrix} \underline{\mathbf{K}} & \mathbf{k}_p^T & \mathbf{k}_p^T \\ \underline{\mathbf{k}}_p & \underline{\mathbf{I}} & -\underline{\mathbf{I}} \\ \underline{\mathbf{k}}_p & -\underline{\mathbf{I}} & \underline{\mathbf{I}} \end{bmatrix} \left\{ \begin{array}{c} \mathbf{u} \\ \boldsymbol{\Lambda}_1 \\ \boldsymbol{\Lambda}_2 \end{array} \right\} = \left\{ \begin{array}{c} \mathbf{f}_e \\ \underline{\mathbf{E}}\,\triangle\mathbf{x}_a \\ \underline{\mathbf{E}}\,\triangle\mathbf{x}_a \end{array} \right\};$$

where:

- $\underline{\mathbf{I}}$ is the identity matrix ;

- $\underline{\mathbf{E}}\,\triangle\mathbf{x}_a$ is the vector representing the imposed valor of displacement difference between periodic nodes.

The one presented in 4.29 is a symmetric, well-conditioned linear system. If *N-Nodes* is the total number of nodes of the *RVE* each equipped with *N-dof* degrees of freedom and *Ncouple* is the aforementioned number of periodic couples, the global dimensions of the augmented system are:
[(*N-Nodes* x *N-dof*)+ 2 (*Ncouple* x *N-dof*)] x [(*N-Nodes* x *N-dof*)+ 2 (*Ncouple* x *N-dof*)].

In order to better explain the construction of the aforementioned system, it is useful to consider a practical example in which the imposition of periodic boundary conditions is shown for a selected couple

of periodic points.

A very simple discretization mesh for a square *RVE* is considered, as shown in Fig.4.11.

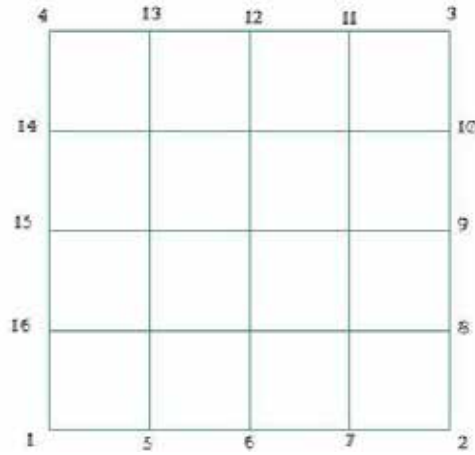Four vertices and six couples of periodic points arise from the discretization.

Figure 4.11: drawn lagrange.

The vertices are: 1 - 2 - 3 - 4, while the couples of periodic points are: 5-13; 6-12; 7-11; 16-8; 15-9; 14-10.

Consequently the expression $\mathbf{u}_{a+} - \mathbf{u}_{a-} = \underline{\mathbf{E}}\,\triangle\mathbf{x}_a$ specialized, for example, for the couple 6-12 is:

$$(4.30) \qquad \left\{ \begin{array}{c} u_6 - u_{12} \\ \\ v_6 - v_{12} \end{array} \right\} = \left\{ \begin{array}{c} E_{XX}\Delta x + \frac{1}{2}E_{XY}\Delta y \\ \\ E_{YY}\Delta y + \frac{1}{2}E_{XY}\Delta x \end{array} \right\};$$

where u and v are the displacement degrees of freedom; Δx and Δy are the spacing between periodic points in the x and y directions respectively and $[E_{XX} \quad E_{YY} \quad E_{XY}]^T$ are the components of the homogenized strain vector $\mathbf{E}$.

The fundamental deformation modes imposed to the *RVE* via aforementioned boundary conditions are shown in Figure 4.12. They consist of axial stretching in the x and y directions and symmetric shear.

It is worth recalling that the periodic boundary conditions not imply a periodic displacement field on the *RVE*, but periodic strain and associate stress fields (as it is *strain periodic*).
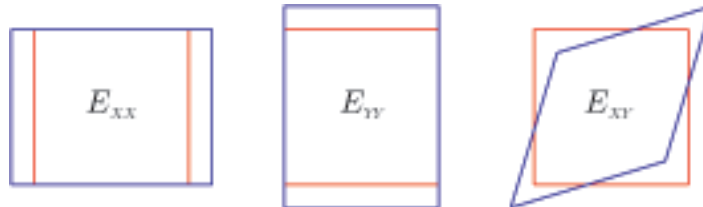

Figure 4.12: Fundamental deformation modes.

Nonlinear constitutive behavior

When a non-linear case is taken into account, the starting point is the general form of the total potential energy function (corresponding, in the elastic case, to equation 4.26) as:

$$(4.31) \qquad W = \mathbf{u}^T \mathbf{f}_i(\mathbf{u}) - \mathbf{u}^T \mathbf{f}_e;$$

where $\mathbf{f}_i(\mathbf{u})$ is the vectorial term collecting the internal forces for all the nodes of the *RVE* structure. In this work only non-linearities due to constitutive material behavior are taken into account, dealing with the infinitesimal deformation frameworks.

The expression of the functional restricted via the periodic conditions introduced, as before, using Lagrange multipliers is the same as for the elastic case (in 4.32) but for the new expression of W, hence, it results as:

$$(4.32) \qquad W^* = \mathbf{u}^T \mathbf{f}_i(\mathbf{u}) - \mathbf{u}^T \mathbf{f}_e + \mathbf{\Lambda}_1(\underline{\mathbf{k}}_p \mathbf{u} - \underline{\mathbf{E}} \triangle \mathbf{x}_a) + \mathbf{\Lambda}_2(\underline{\mathbf{k}}_p \mathbf{u} - \underline{\mathbf{E}} \triangle \mathbf{x}_a) + \frac{1}{2}(\mathbf{\Lambda}_1 - \mathbf{\Lambda}_2)^T(\mathbf{\Lambda}_1 - \mathbf{\Lambda}_2);$$

The linearization of the new system of equilibrium equations is obtained using the Newton-Raphson method (see for example Whittaker and Robinson (1967)).

Assume that at the step n the vector of imposed external actions is:

$$(4.33) \qquad {}^n\mathbf{F}_{ext} = \left\{ \begin{array}{c} {}^n\mathbf{f}_e \\ {}^n\underline{\mathbf{E}} \triangle \mathbf{x}_a \\ {}^n\underline{\mathbf{E}} \triangle \mathbf{x}_a \end{array} \right\};$$

and assume also that the convergence for the system has been achieved, this means that the residual vector provides null values:

$$(4.34) \qquad \mathbf{r}({}^n\mathbf{v}) = \mathbf{0};$$

where ${}^n\mathbf{v}$ is the vector collecting nodal displacements and Lagrange multipliers solution of the problem at step n:

$$(4.35) \qquad {}^n\mathbf{v} = \left\{ \begin{array}{c} {}^n\mathbf{u} \\ {}^n\mathbf{\Lambda}_1 \\ {}^n\mathbf{\Lambda}_2 \end{array} \right\};$$

If a new increment is imposed on the external action (step *n+1*), the next equilibrium point is reached when, for the iteration *(i+1)*, the general expression of the residual, obtained by linearizing the residual around the previous iteration solution is equal to zero:

$$(4.36) \qquad \mathbf{r}({}^{n+1}\mathbf{v}^{i+1}) \approx \mathbf{r}({}^{n+1}\mathbf{v}^i) + \frac{\partial \mathbf{r}}{\partial \mathbf{v}}\big|_{({}^{n+1}\mathbf{v}^i)} \cdot ({}^{n+1}\triangle\mathbf{v}^{i+1}) = 0;$$

where $\frac{\partial \mathbf{r}}{\partial \mathbf{v}}\big|_{({}^{n+1}\mathbf{v}^i)}$ is the Jacobian matrix which involves the computation of derivatives, the corresponding expression is:

$$(4.37) \qquad \underline{\mathbf{J}}({}^{n+1}\mathbf{v}^i) = \left[\begin{array}{ccc} \frac{\partial({}^{n+1}\mathbf{r}_1^i)}{\partial({}^{n+1}\mathbf{u}^i)} & \frac{\partial({}^{n+1}\mathbf{r}_1^i)}{\partial({}^{n+1}\mathbf{\Lambda}_1^i)} & \frac{\partial({}^{n+1}\mathbf{r}_1^i)}{\partial({}^{n+1}\mathbf{\Lambda}_2^i)} \\ \frac{\partial({}^{n+1}\mathbf{r}_2^i)}{\partial({}^{n+1}\mathbf{u}^i)} & \frac{\partial({}^{n+1}\mathbf{r}_2^i)}{\partial({}^{n+1}\mathbf{\Lambda}_1^i)} & \frac{\partial({}^{n+1}\mathbf{r}_2^i)}{\partial({}^{n+1}\mathbf{\Lambda}_2^i)} \\ \frac{\partial({}^{n+1}\mathbf{r}_3^i)}{\partial({}^{n+1}\mathbf{u}^i)} & \frac{\partial({}^{n+1}\mathbf{r}_3^i)}{\partial({}^{n+1}\mathbf{\Lambda}_1^i)} & \frac{\partial({}^{n+1}\mathbf{r}_3^i)}{\partial({}^{n+1}\mathbf{\Lambda}_2^i)} \end{array} \right];$$

The actual residual is a vector constituted by the following three sub-vectors:

(4.38)
$$^{n+1}\mathbf{r}_1^i = \mathbf{f}_i(^{n+1}\mathbf{u}^i) - ^{n+1}\mathbf{f}_e + \underline{\mathbf{k}}_p^T(^{n+1}\mathbf{\Lambda}_1{}^i) + \underline{\mathbf{k}}_p^T(^{n+1}\mathbf{\Lambda}_2{}^i);$$

(4.39)
$$^{n+1}\mathbf{r}_2^i = \underline{\mathbf{k}}_p(^{n+1}\mathbf{u}^i) - ^{n+1}\underline{\mathbf{E}}\,\triangle\mathbf{x}_a + ^{n+1}\mathbf{\Lambda}_1{}^i - ^{n+1}\mathbf{\Lambda}_2{}^i;$$

(4.40)
$$^{n+1}\mathbf{r}_3^i = \underline{\mathbf{k}}_p(^{n+1}\mathbf{u}^i) - ^{n+1}\underline{\mathbf{E}}\,\triangle\mathbf{x}_a - ^{n+1}\mathbf{\Lambda}_1{}^i + ^{n+1}\mathbf{\Lambda}_2{}^i;$$

where:

- $^{n+1}\mathbf{f}_e$ is the vector of external forces at step *n+1*: this vector is equal to zero because no external forces are directly applied to the *RVE*;

- $^{n+1}\underline{\mathbf{E}}$ is the homogenized strain tensor that the *RVE* receives from the macro-level at step *n+1*;

- $\triangle\mathbf{x}_a$ is the vector collecting the distance components between periodic points, it remains constants during the *RVE* evolution because of the infinitesimal displacements hypothesis;

- $^{n+1}\mathbf{u}^i$ is the displacement vector corresponding to previous iteration in the same step;

- $^{n+1}\mathbf{\Lambda}_1{}^i$ and $^{n+1}\mathbf{\Lambda}_2{}^i$ are the Lagrange multipliers vectors corresponding to previous iteration in the same step;

To sum up, for the iteration (*i+1*), corresponding to the step $(n + 1)$, the matrix form of the resulting global system can be written as:
(4.41)
$$\begin{bmatrix} ^{n+1}\underline{\mathbf{K}}_{tang}^i & \underline{\mathbf{k}}_p^T & \underline{\mathbf{k}}_p^T \\ \underline{\mathbf{k}}_p & I & -I \\ \underline{\mathbf{k}}_p & -\underline{\mathbf{I}} & \underline{\mathbf{I}} \end{bmatrix} \left\{ \begin{array}{c} ^{n+1}\Delta\mathbf{u}^{i+1} \\ ^{n+1}\Delta\mathbf{\Lambda}_1^{i+1} \\ ^{n+1}\Delta\mathbf{\Lambda}_2^{i+1} \end{array} \right\} = - \left\{ \begin{array}{c} \mathbf{f}_i(^{n+1}\mathbf{u}^i) - ^{n+1}\mathbf{f}_e + \underline{\mathbf{k}}_p^T(^{n+1}\mathbf{\Lambda}_1{}^i) + \underline{\mathbf{k}}_p^T(^{n+1}\mathbf{\Lambda}_2{}^i) \\ \underline{\mathbf{k}}_p(^{n+1}\mathbf{u}^i) - ^{n+1}\underline{\mathbf{E}}\,\triangle\mathbf{x}_a + ^{n+1}\mathbf{\Lambda}_1{}^i - ^{n+1}\mathbf{\Lambda}_2{}^i \\ \underline{\mathbf{k}}_p(^{n+1}\mathbf{u}^i) - ^{n+1}\underline{\mathbf{E}}\,\triangle\mathbf{x}_a - ^{n+1}\mathbf{\Lambda}_1{}^i + ^{n+1}\mathbf{\Lambda}_2{}^i \end{array} \right\};$$

where:

- $^{n+1}\mathbf{K}_{tang}^i$ is the tangent stiffness matrix of the *RVE* updated at the previous iteration ;

- $^{n+1}\Delta\mathbf{u}^{i+1}$ is the actual increment of displacement vector;

- $^{n+1}\Delta\mathbf{\Lambda}_1^{i+1}$ and $^{n+1}\Delta\mathbf{\Lambda}_2^{i+1}$ are the actual increments of Lagrange multipliers vectors;

Another possibility is to apply the *modified Newton-Raphson* method (Zienkiewicz and Taylor (2000)): the stiffness matrix is not updated at every step of the calculation, but the initial elastic constitutive tensor is preserved.

4.6.2 Discrete problem at the macro-level

A very crucial task in the two-scale finite element implementation is the proper determination of the homogenized constitutive tensor, required to construct the stiffness matrix at the macro level.

Different strategies are available, for example Kouznetsova (2002) extract a *Consistent tangent stiffness* by direct condensation of the constrained degrees of freedom, while Miehe (1996)and Zalamea (2001) adopt a numerical differentiation of the numerical macroscopic stress-strain relation. In this work the latter aforementioned approach is followed.

The basic assumption is that the homogenized constitutive tensor, due to periodic arrangement of the materials at the micro-level, is symmetric.

Lene (1986); Lene and Leguillon (1982); Guedes and Kikuchi (1990) demonstrate that it is also orthotropic.

In the elastic range, the homogenized constitutive law establishes the relations between homogenized stresses and strains:

$$\dot{\boldsymbol{\Sigma}} = \underline{\mathbf{C}} \quad \dot{\mathbf{E}}.$$

where $\underline{\mathbf{C}}$ is unknown.

It is however possible to construct the homogenized stress vector $\boldsymbol{\Sigma}$ by applying the corresponding homogenized strain vector $\mathbf{E}$ as input condition of the BVP on the RVE, i.e. using the two-scale correspondence. Hence $\underline{\mathbf{C}}$ can be extracted by applying different perturbations (infinitesimal homogenized strain vector) to the RVE as input conditions, so that the different elastic constants of the composite structure are recovered.

Considering a $2D$ problem, in plane stress or plane strains conditions, the elastic tensor can be expressed as:

$$(4.42) \qquad \underline{\mathbf{C}} = \left[\begin{array}{ccc} C_{XXXX} & C_{XXYY} & 0 \\ C_{YYXX} & C_{YYYY} & 0 \\ 0 & 0 & C_{XYXY} \end{array} \right] ;$$

its components can be obtained in the following manner: by applying successively three simple perturbation vectors to the RVE:

$$(4.43) \qquad \mathbf{E}_1 = \left\{ \begin{array}{ccc} \delta & 0 & 0 \end{array} \right\}^T ;$$

$$(4.44) \qquad \mathbf{E}_2 = \left\{ \begin{array}{ccc} 0 & \delta & 0 \end{array} \right\}^T ;$$

$$(4.45) \qquad \mathbf{E}_3 = \left\{ \begin{array}{ccc} 0 & 0 & \delta \end{array} \right\}^T ;$$

where δ is a scalar value corresponding to the perturbation intensity, the corresponding homogenized stress vectors are $\boldsymbol{\Sigma}(\mathbf{E}_1)$; $\boldsymbol{\Sigma}(\mathbf{E}_2)$ and $\boldsymbol{\Sigma}(\mathbf{E}_3)$.

Thus the components of the homogenized constitutive tensor can be obtained as:

$$(4.46) \qquad C_{XXXX} = \frac{\Sigma_{XX}(\mathbf{E}_1)}{\delta} ;$$

$$(4.47) \qquad C_{XXYY} = \frac{\Sigma_{XX}(\mathbf{E}_2)}{\delta} ;$$

$$(4.48) \qquad C_{YYYY} = \frac{\Sigma_{YY}(\mathbf{E}_2)}{\delta} ;$$

(4.49)
$$C_{YYXX} = \frac{\Sigma_{YY}(\mathbf{E}_1)}{\delta};$$

(4.50)
$$C_{XYXY} = \frac{\Sigma_{XY}(\mathbf{E}_3)}{\delta};$$

This strategy can be easily generalized in the non-linear range.

The tangent homogenized constitutive tensors are hence obtained via the same perturbation method described above.

In order to avoid an excessive amount of computational costs, the extraction of aforementioned tensor is not performed for every iteration belonging to every load step, but just at the first iteration and then it is kept equal during the same step; the modified Newton-Raphson strategy is hence used.

4.6.3 Algorithm

The F.E. program, used in the calculations, has been developed on the basis of the preexisting finite element code PLCd3 created at the *Universidad Politecnica de Catalua* in Barcelona by S. Oller, B. Luccioni, E. Car, L. Neamtu, P. Mata and X. Martinez.
The code is integrally developed in FORTRAN and it allows to solve linear and non-linear mechanical problems accounting for small or large deformations.
It is possible to carry out quasi-static and dynamic analyses taking into account constitutive or geometrical non-linearities.
Many constitutive models have been implemented and are available for the users.

The first step, in order to generate the multi-scale code, has been the duplication of the existing code: the computational homogenization technique, in fact, is based on the solution of coupled problems defined at different levels.
By adopting the Finite Element Method is, hence, necessary to define finite element meshes as for the macro-level and as for the micro-level. A Finite element program is required to solve the associated mesh.
In order to briefly explain the structure of the generated two-scale code, it is useful to define the so-called MASTER program (that is the part of the code corresponding to the macro-model) and several SLAVES programs which represent the underlying micro-structures.
The number of SLAVES is equal to the number of integration point of the MASTER. In the SLAVE program the Lagrange multipliers technique has been implemented to impose the periodic boundary conditions; at this level the constitutive equations are available and can be integrated to obtain the constitutive material response. The SLAVES are copies of the same program and by using a so called producer-consumer logic the MPI libraries allow to obtain clones of the SLAVE.
In the following subsections two alternative algorithms are presented: the first one is the so-called *Fully iterative algorithm* in which at each iteration of a load step at the macro-level corresponds a fully cycle of iterations at the micro-level, till the convergence has reached; the second one, instead, is the so-called *Consistent iterative algorithm*, characterized by the fact that at each iteration of a load step at the macro-level corresponds a single iteration at the micro-level. Two information are, thus, passe at the macro-level: the trial stress values and the stress residual.

Fully iterative algorithm

In the Flux-diagram showed in Figure 4.13 the logical operations executed by the program are explained. In order to simplify the scheme only the MASTER and one SLAVE are taken into account because all the SLAVES undertake the same operations. For the actual application the MPI library (*Message Passing Interface*) has been used.
In the following the logical sequence of the operations that the program performs is presented.

A) The MASTER proceeds to run: it reads the input files and initializes the database.

The input file contains geometrical data of the macro-structure; mesh discretization and boundary conditions (constrains and loads). The data relating to materials and constitutive laws are missing because to obtain the stress-strain macroscopical relation a passage to the sub-scale is necessary.

B) At this point the MASTER execute a loop on the SLAVES' number to send them the respective input data file name.
The input files for the SLAVES contain geometrical data of the micro-structure; mesh discretization; boundary conditions (constrains); information about the vertices and the periodic nodes couples on the contour of the cell and also data relating to materials and constitutive laws.

C) The MASTER can't construct the initial elastic stiffness matrix before receiving the constitutive tensor from the SLAVE. The perturbation is the technique chosen to extract the constitutive tensor from
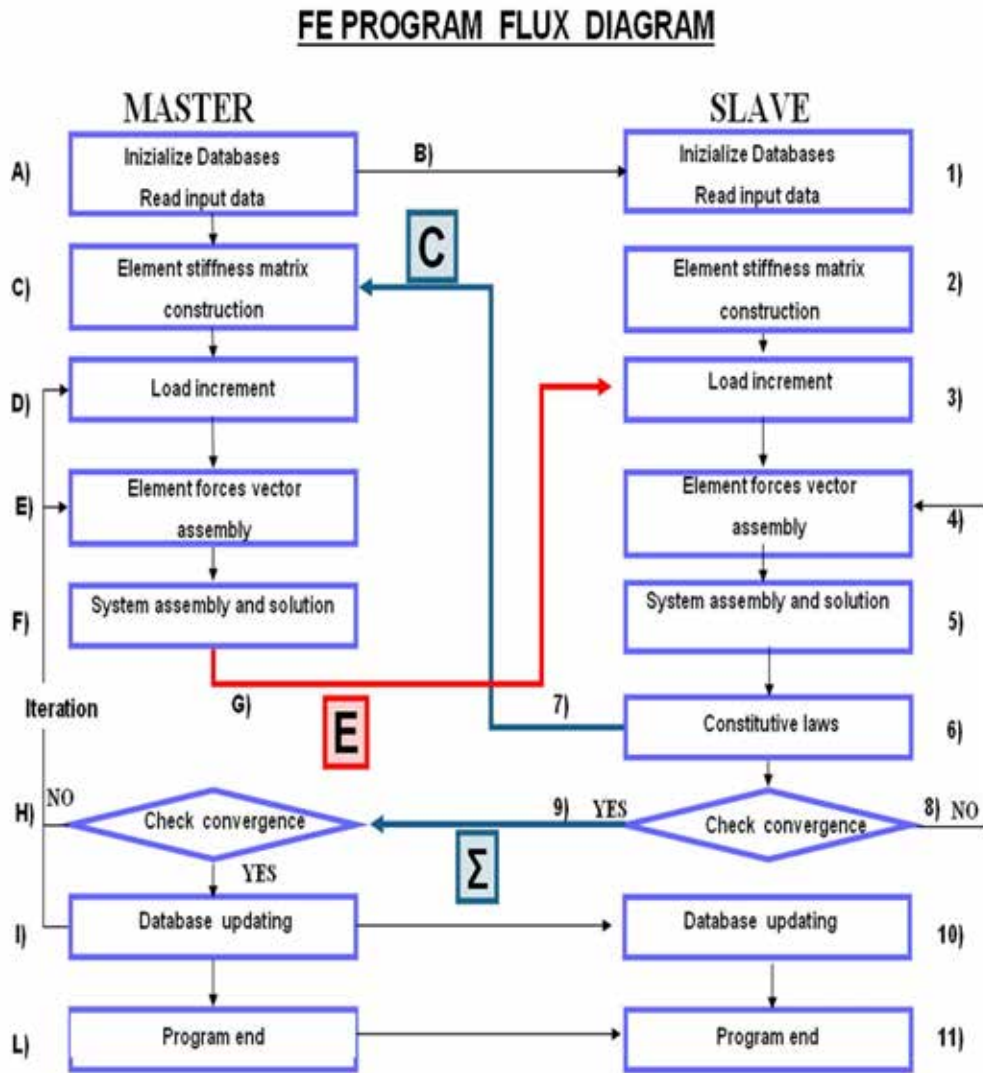
Figure 4.13: Fully iterative algorithm.

the SLAVE.

1) Only one SLAVE calculate the aforementioned tensor.

The SLAVE gets three " ad hoc " macroscopic strain tensors from the input file.

These are the perturbation data input in terms of homogenized strains.

The cell solves the static problem undergoing periodic conditions and calculates nodal displacements and the local strain and stress fields.

The cell calculates the corresponding homogenized stress tensors and obtains the homogenized elastic constitutive second order tensor.

The SLAVE sends the tensor,in vector form, to the MASTER.

D) The MASTER constructs the stiffness matrix and solves the system for the first load step: it calculates the displacements and obtains the stain tensor for every Gauss point. These tensors are sent to the respective SLAVES that utilize them as input data.

2) Every SLAVE accepts the received homogenized strain tensor as input data and solves the system. In the case of nonlinearity onset the resulting displacements are obtained at the end of the Newton-Raphson iteration process.

The SLAVES calculate the homogenized stresses as a volume average of the local stress field.

The SLAVES calculate the tangent constitutive tensor if the MASTER sends the corresponding request.

Every SLAVE sends the homogenized stress tensor to the respective Gauss point of the MASTER.

E) The MASTER constructs the internal forces vector and verifies the equilibrium. In the case of violation of equilibrium (the residual is greater than the tolerance)the MASTER comes back to the D) and solves the system considering the residual as the new incremental load. The procedure is repeated iteratively till the convergence is satisfied.
The local and global databases are actualized when, for a given load step, the MASTER achieves the convergence and, in this case, a new load step is considered and the process restarts from D).
A quasi-Newton iterative method is adopted in order that, for every global new step, a tangent stiffness matrix is calculated (perturbing the cells corresponding to every gauss point).

Consistent iterative algorithm

A consistent procedure for the formulation of equilibrium-based non-linear multi-scale problems is here proposed.
On the basis of different examples available in literature as by Hughes and Pister (1978) and by Petrangeli and Ciampi (1997) (specialized for non-linear beam problems) the idea is to avoid the fully iterative scheme in the nested problems.
As it has been underlined, the micro-level equilibrium problem is a non-linear boundary value problem. When at the macro-level trial strain values are calculated, corresponding to an iteration of a certain load step, the values are sent as input values to each related RVE and, at the micro-level, the solution is achieved iteratively checking the residual values in terms of difference between external and internal global forces. When the residual is less than a fixed tolerance the problem is solved and the last obtained

stress values are homogenized and are sent to the corresponding macro-level integration point.

Since the nested problems are substantially driven by the macro-level problem, it is possible to define the following alternative strategy: in the linearized solution procedure at the micro-level, the first obtained results, when the new input, in terms of macro-level strain, is considered, are the trial stress values and the residual. If the residual is expressed in terms of stresses, it is possible to send to the macro-level a twofold information and the residual at the macro-level can account for the macro-level and, at the same time, the micro-level residual.

In this way, when the convergence is reached at the macro-level, surely it is achieved also at the micro-level.

The evident advantage is that usually the solution of the micro-level problem is the most costly part of the procedure since the adopted meshed are quite refined and the *RVE* are numerous. It is surely convenient to need more macro-level iterations, each corresponding to one *RVE* step, than to adopt the standard procedure.

In Figure 4.14 the algorithm corresponding to the Consistent iterative procedure is shown.
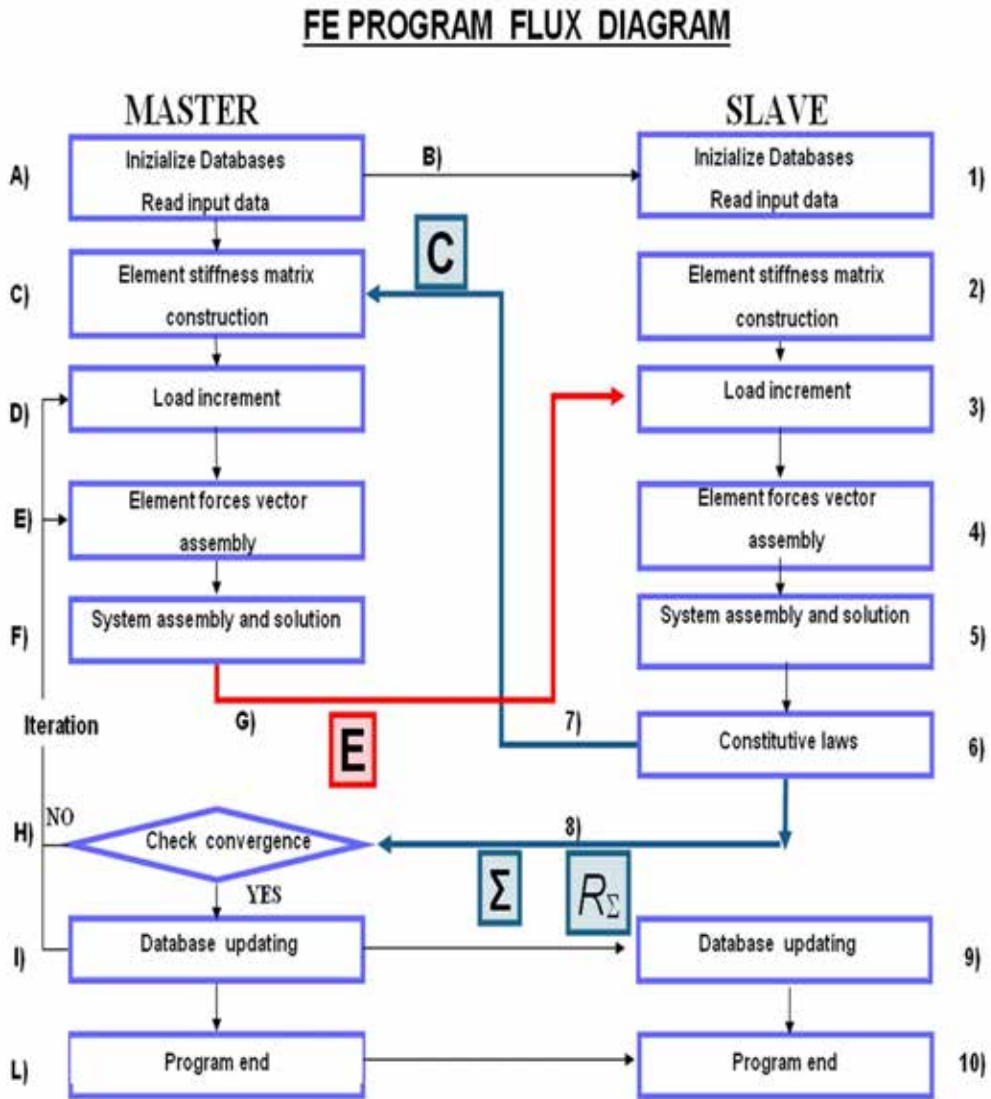
Figure 4.14: Consistent iterative algorithm.

4.6.4   Message passing

The message passing between scales is executed exploiting the potentialities of the libraries MPI.

MPI, the Message Passing Interface, is a message passing library interface specification. MPI addresses primarily the message passing parallel programming model, in which data is moved from the address space of one process to that of another process through cooperative operations on each process. MPI is a specification for a *library interface*. All MPI operations are expressed as functions, subroutines or methods according to to the appropriate language bindings, which for C, C++, Fortran 77 and Fortran 95 are part of MPI Standard. The standard defines the syntax and semantics of a core of library routines useful to a wide range of users writing portable message-passing programs. Several well-tested and efficient implementations of MPI already exist, including some that are free and in the public domain.
As for the actual work, the MPICH2 implementation of MPI has been adopted.

In Figure 4.15 it is clearly represented the correspondence between each macro-level integration point and the related *RVE*. In the figure, by way of example, as for both discretization levels, bilinear 4 node elements with 4 integration points have been considered, but no restrictions are imposed in the applications.
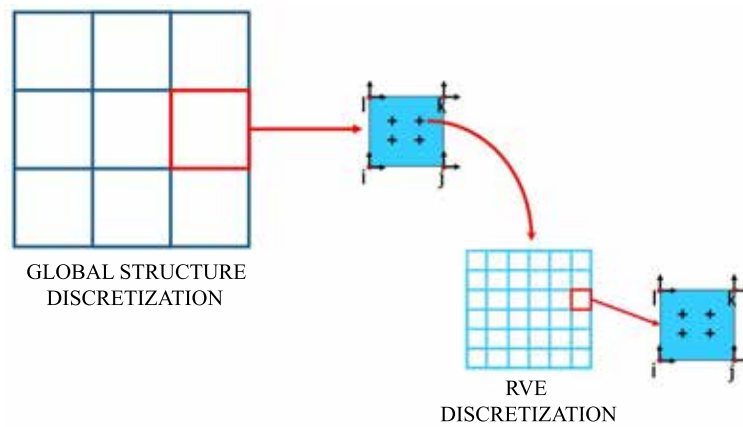
Figure 4.15: Shear test on masonry panel.

4.7 Numerical Applications

In this section some numerical examples are shown in order to display the capabilities of the proposed multi-scale technique in the reproduction of the composite material response.

The attention is first focused on the *RVE* behavior (section 4.7.1): the homogenized constitutive tensors are obtained in linear range as for different types of *RVEs* and, in the case of masonry like structures, a comparison is made in terms of orthotropic Young and Poisson's modula as for different bond patterns. In the second part, structural analyses are performed (section 4.7.2); lineal elastic and damage constitutive laws are considered. Two dimensional problems are implemented for plane stress and plane strain conditions.

4.7.1 Micro-mechanical linear elastic examples

This section is devoted to the analysis of the micro-level behavior: the *RVE* response undergoing different input is investigated. A careful study of the lower scale behavior into the nested macro-micro solution scheme is crucial in order to understand the multi-scale procedure.

As aforementioned, the *RVE* plays the role of a numerical constitutive equation since it can be considered as a black box that receives, as input, macro-level strain measures and sends back, as output, homogenized stress measures. Particularly interesting is the identification of homogenized modula extracted by perturbing the *RVE* and then used for the construction of the stiffness matrix at the macro-level.

In the sequel, different *RVEs* are considered and the results (homogenized modula, displacement, stress and strain fields) are compared with respective values available in literature.

As first example, a very simple square *RVE* is considered: it is made up of two constituents, arranged in echelon formation, used by Bendsoe and Kikuchi (1998) to extract the Cauchy homogenized constitutive tensors.

The second one presents a more elaborate square *RVE* reproducing a portion of masonry panel characterized by running bond masonry patterns employed by Casolo (2006) to extract the constitutive parameters of the masonry like structure.

As for the third example, an *RVE* of running bond masonry is considered, it was studied by Luciano and Sacco (1997b).

The section ends with a brief discussion about the influence of different masonry bonds on the overall elastic constitutive parameters: it is clear that the respective arrangement of constituents (bricks and mortar joints) in a masonry panel affects the stiffness of the resulting macroscopic structure.
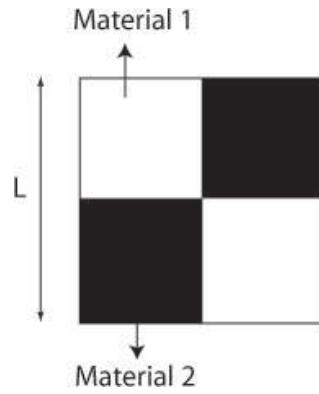
Simple Square RVE

The geometry of the simple square *RVE* is reproduced in Figure 4.16.

The edge is L=2.4 mm and each material portion occupies a square of $L/2$ x $L/2$ (see Figure 4.16). Linear elastic behavior is considered for the two materials and the mechanical parameters, i.e. Young modulus (E) and Poisson ratio (ν), are shown in Table 4.8 for Material 1 and 2 respectively.

Material 1	Material 2
$E = 10N/m^2$	$E = 100N/m^2$
$\nu = 0.3$	$\nu = 0.3$

Table 4.2: Mechanical parameters table

The Figure 4.17 shows the mesh adopted in the discretization (256 elements), while in Figure 4.18 the simple deformation modes, corresponding to single perturbation components are presented: the first two modes are extensional in horizontal and vertical directions respectively, while the third one is due to

Figure 4.16: Simple Square *RVE* geometry.

symmetric tangential deformation.
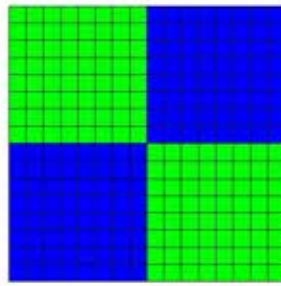
Figure 4.17: Simple Square *RVE* geometry.
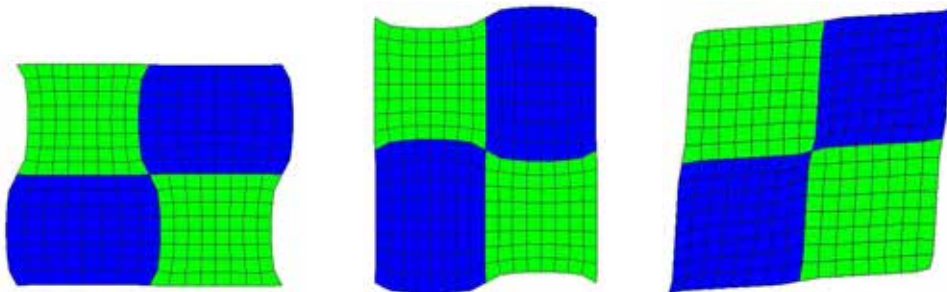
Figure 4.18: Deformation due to 1)Exx component; 2)Eyy component; 3)Exy component. .

In Bendsoe and Kikuchi (1998) the asymptotical method is used to obtain the elastic parameters for the composite. The hypothesis of orthotropic behavior is fulfilled for the periodic composite and the structure of the homogenized elastic tensor is the same as in 4.45.
A direct comparison is possible between results obtained via the methodology used in the present work and those obtained by the aforementioned author because the same discretization mesh has been adopted. In Table 4.3 the comparison for homogenized modula are presented.
A very good agreement with the results obtained by Bendsoe has been found.

Author	C_{XXXX}	C_{XXYY}	C_{YYYY}	C_{XYXY}
De Bellis	149.7998	71.6086	149.7998	87.1283
Bendsoe	149.8	71.61	149.8	87.12

Table 4.3: Elastic parameters obtained for the same *RVE* by different authors

Masonry like structure RVE (Casolo)

The same geometry and the material parameters proposed by Casolo (2006) have been adopted in this example for the *RVE*. A portion of masonry reproducing running bond pattern has been chosen; in Figure 4.19 the bond scheme together with the adopted discretization mesh (434 4-node isoparametric FE are used with four Gauss integration points) are shown:
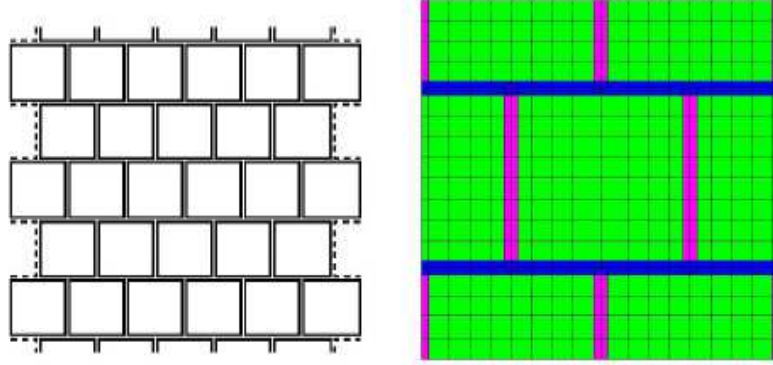
Figure 4.19: *RVE* geometry and simple square finite element mesh.

Square blocks of $120x120mm$ are used and the thickness of all the mortar joints is $10mm$. Different values of elastic modulus are assigned to horizontal and vertical mortar joints (it is supposed that that the vertical joints are weaker than the horizontal ones). In the Table 4.4 the material parameters are summarized both for bricks and mortar joints.

Bricks	Horizontal joints	Vertical joints
$E = 10000N/m^2$	$E = 1000N/m^2$	$E = 100N/m^2$
$\nu = 0.1$	$\nu = 0.1$	$\nu = 0.1$

Table 4.4: Elastic parameters of bricks, horizontal and vertical mortar joints [MPa]

Plane stress hypotheses are assumed. As well as for the former identification test, the simple deformation modes are presented (see Figure 4.20).

In the following Figure 4.21 the most significant strain fields in the *RVE* due to single perturbation
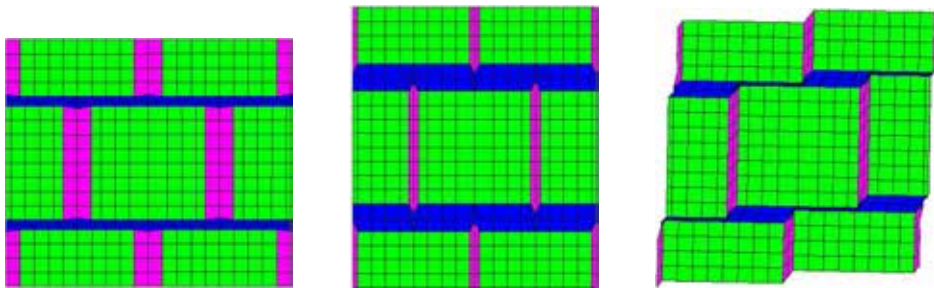
Figure 4.20: Deformation due to 1)Exx component; 2)Eyy component; 3)Exy component.

components are shown: in the first picture the ϵ_x strain field (corresponding to the first perturbation component), in the second ϵ_y strain field (corresponding to the second perturbation component), while in the third ϵ_{xy} strain field (corresponding to the third perturbation component) are presented.

In Figure 4.22 the respective stress fields are shown: σ_x; σ_y and σ_{xy} respectively.
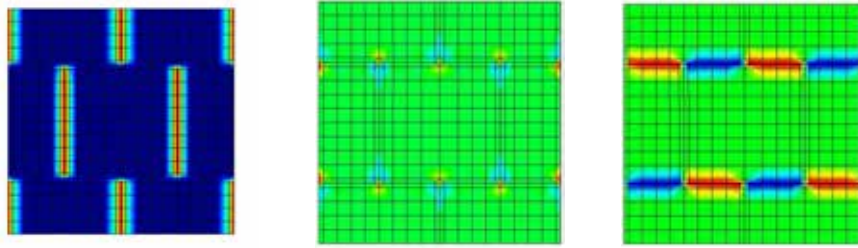Both for strains and stresses, periodic fields are obtained in agreement with the periodicity boundary conditions.

Figure 4.21: Strain fields 1)ϵ_x component due to Exx; 2)ϵ_y component due to Eyy; 3)ϵ_{xy} component due to Exy.
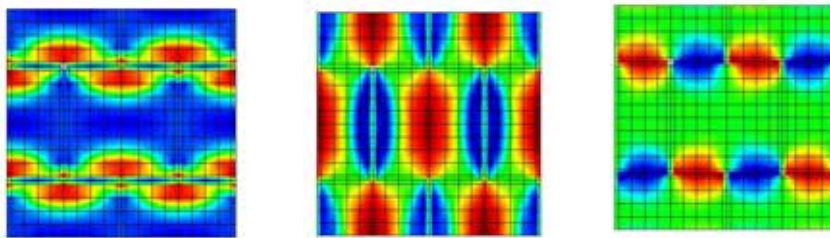
Figure 4.22: Strain fields 1) σ_x component due to Exx; 2) σ_y component due to Eyy; 3) σ_{xy} component due to Exy.

In Table 4.5 the obtained values of homogenized constitutive parameters are presented both for Casolo and for the actual procedure. He adopted a homogenization procedure "una tantum" with the aim of obtaining the homogenized modula and not to use a nested scheme with fully two scales coupling. He evaluates the axial modula by straightforward applying anti-symmetric tractions under symmetric essential boundary conditions (Anthoine (1995)). A very good agreement is obtained with the Casolo's results and the highest percentage difference 1.8 as for $\mathbf{C}_{XXYY}$.

Author	C_{XXXX}	C_{XXYY}	C_{YYYY}
Casolo	3.11	0.194	12.63
DeBellis	3.058	0.223	12.56

Table 4.5: Elastic parameters obtained for the same *RVE* by different authors [MPa]

Only the axial coefficients are here considered since the example of Casolo has been obtained in the Cosserat framework where both non-symmetric shear components have been considered. In the Section 5.6.3 the comparison with the results obtained by the author will be completed.

Masonry like structure RVE(Sacco-Luciano)

At this point the comparison with the results obtained by Luciano and Sacco (1997b) for the homogenized constitutive tensor of a running bond masonry portion is carried out. The related *RVE* discretization (2600 isoparametric 4 node elements) is showed in Figure 4.23.
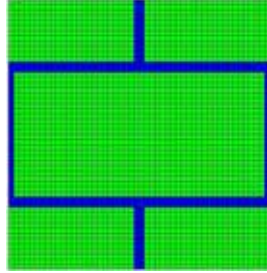The brick is 240 x 120 mm while the mortar joint thickness is 10 mm.
The elastic parameters adopted by the authors are:

Bricks	Mortar joints
$E = 18000 MPa$	$E = 1000 MPa$
$\nu = 0.15$	$\nu = 0.15$

Table 4.6: Mechanical parameters table

Plane strain hypotheses are assumed.

Figure 4.23: Finite element mesh for the *RVE* proposed by Sacco

The results obtained are summarized in the Table 4.7.

Author	C_{XXXX}	C_{XXYY}	C_{YYYY}	C_{XYXY}
Sacco	10860.33	872.13	7932.17	2885.01
DeBellis	10941	881	7745	2880

Table 4.7: Elastic parameters obtained for the same *RVE* by different authors [MPa]

In Luciano and Sacco (1997b) only the micro-mechanical periodic problem is solved by adopting the so-called *periodic elements* instead of solving for the superposition of kinematic map and periodic fluctuations:

$$(4.51) \qquad \mathbf{u}(\mathbf{x}) = \underline{\mathbf{E}}\,\mathbf{x} + \mathbf{u}^p(\mathbf{x});$$

The highest difference in success rate is 2.36% as for C_{YYYY} and it justified by the different discretization used by Luciano and Sacco (1997b) (6932 isoparametric 4 node elements). A good agreement has been found and the highest difference in success rate is 2.36% as for C_{YYYY}.

Different bonds constitutive identification

The previous examples have shown the capability of the adopted procedure in the proper extrapolation the homogenized constitutive tensors.
At this point a brief study is carried out in order to evaluate the effects of the bricks and mortar relative arrangements on the definition of the elastic properties in masonry.
Different bonds have been chosen: stack bond, running bond, English, 1/3 running and Flemish bond(See Figures 4.24 and 4.25).
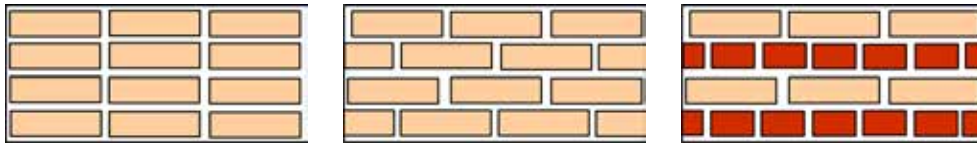
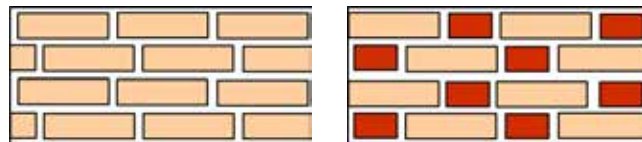Figure 4.24: Stack bond (left), running bond (center) and English bond (right).

Figure 4.25: 1/3 running bond (left) and Flemish bond (right).

The *RVE*s are chosen according to the suggestions proposed by Anthoine (1995). The brick is 204 x 98 x 50mm and the mortar joint thickness is 10mm.
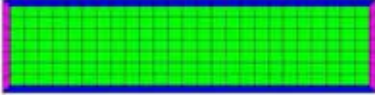The elastic parameters obtained experimentally by Magenes (1992) and adopted in the numerical simulations are:

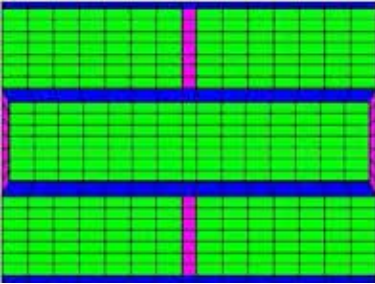| Bricks	Mortar joints
$E = 6000 MPa$	$E = 2000 MPa$
$\nu = 0.2$	$\nu = 0.25$

Table 4.8: Mechanical parameters table

The results are:

Stack Bond

Figure 4.26: *RVE* Stack Bond

$$(4.52)$$
$$C^x_{Cauchy} = \begin{bmatrix} 5134.516 & 938.084 & 0 \\ 938.084 & 4614.440 & 0 \\ 0 & 0 & 1743.679 \end{bmatrix}$$

Running Bond

Figure 4.27: *RVE* Running Bond

$$(4.53)$$
$$C^x_{Cauchy} = \begin{bmatrix} 5145.655 & 946.239 & 0 \\ 946.239 & 4610.071 & 0 \\ 0 & 0 & 1754.155 \end{bmatrix}$$

English Bond
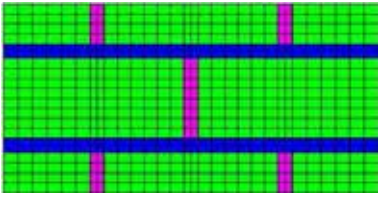
Figure 4.28: *RVE* English Bond

(4.54)

$$C_{Cauchy}^x = \begin{bmatrix} 4974.276 & 931.482 & 0 \\ 931.482 & 4552.296 & 0 \\ 0 & 0 & 1717.286 \end{bmatrix}$$

1/3 Running Bond
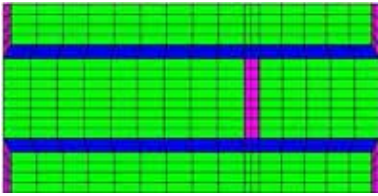
Figure 4.29: *RVE* 1/3 Running Bond

(4.55)

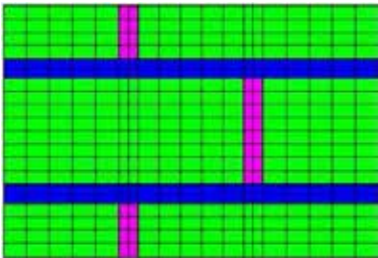$$C_{Cauchy}^x = \begin{bmatrix} 5167.471 & 959.711 & 0 \\ 959.711 & 4632.899 & 0 \\ 0 & 0 & 1776.268 \end{bmatrix}$$

Flemish Bond

Figure 4.30: *RVE* Stack Bond

(4.56)

$$C_{Cauchy}^x = \begin{bmatrix} 5027.550 & 936.739 & 0 \\ 936.739 & 4570.867 & 0 \\ 0 & 0 & 1730.005 \end{bmatrix}$$

In order to summarize the results obtained for the different arrangements in masonry, in the Table 4.9 the identified horizontal E_h and vertical E_v homogenized Young modulus (in the hypothesis of orthotropic material behavior) and the homogenized Poisson coefficient ν are shown.

The identified values are very close together: the maximum percentage difference for E_h is 3.6% and for E_v is 1.6% between 1/3 Running and English bonds. As for the equivalent ν the highest value is obtained for 1/3 Running while the lowest for Stack bond, anyway the difference is 1.88%.

	Stack	*Running*	*1/3 Running*	*English*	*Flemish*
E_h	4943	4951	4783	4968	4836
E_v	4443	4436	4378	4455	4396
ν	0.203	0.205	0.205	0.207	0.205

Table 4.9: Elastic parameters obtained for the same *RVE* by different authors [MPa]

4.7.2 Multi-scale examples

In this section two scale analyses are carrier out. The whole procedure coupling the micro and macro-level is here tested. An *RVE* is chosen corresponding to every integration point of the macro-level finite element discrete structure.

The study is firstly focused on the linear elastic constitutive behavior of a simple striped structure and then a non-linear case is investigated: a test commonly used in the calibration of numerical models of masonry is reproduced and the adopted constitutive laws of masonry constituents are characterized dy damaging processes.

Two materials linear elastic tests

A very simple case is considered for the first test of the adopted two scales procedure.

A composite material structure subjected to plane stress conditions is studied in linear range.

The specimen is a two-dimensional square structure measuring 18 x 18 meters, it is made of sixteen horizontal stripes of two different materials neatly alternating arranged.

Linear elastic behavior is considered for the two materials and the mechanical parameters, i.e. Young modulus (E) and Poisson ratio (ν), are shown in Table 4.10 for Material 1 and 2 respectively:

Material 1	Material 2
$E = 3.5e5 N/m^2$	$E = 2.1e6 N/m^2$
$\nu = 0.2$	$\nu = 0.3$

Table 4.10: Mechanical parameters table

Three analysis cases are considered:

1. uniform lateral traction imposed on the whole right end of the structure;

2. one point traction imposed on the right top edge;

3. two displacements equal and opposed applied on the top and bottom points of the right edge.

The geometry, the loading cases and the material arrangement are shown in Fig.4.31.
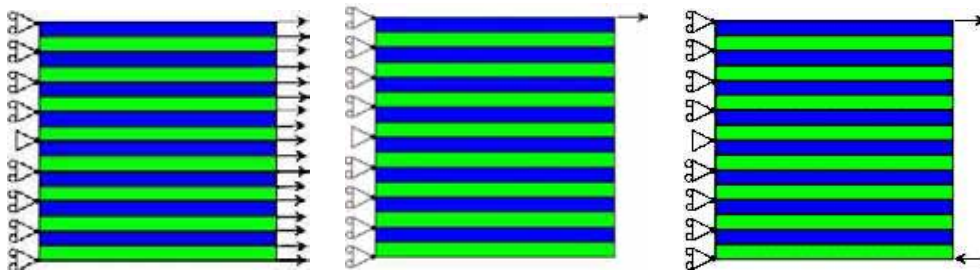

Figure 4.31: case 1; case (b); case (c)

In order to compare the multi-scale procedure response with the respective one of a micro-model, the current problem is solved using two different finite element codes: the two-scales code based on the

computational homogenization and a standard finite element code.

Different discretizations are chosen for the multi-scale procedure: a course macrostructural mesh is chosen made of 16 square elements while different discretizations are considered for the *RVE*: 4, 16 and 64 square elements (see Figure 4.32).

As for the micro-structural discretization a mesh is considered constituted by 16 x 16 elements.
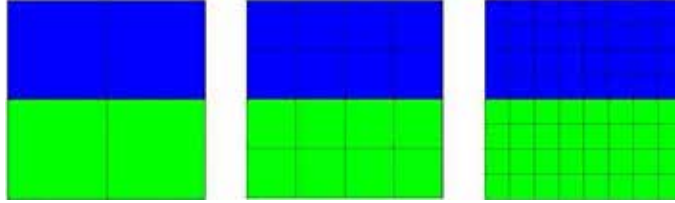

Figure 4.32: RVE_1: 2x2; RVE_2: 4x4; RVE_3: 8x8

As for the first loading case (uniform displacement on the right edge) no differences in results are detected at the macroscopic level using different discretizations for the *RVE*.

In Figure 4.33 the horizontal displacement fields obtained with the multi-scale procedure (left) and with the micro-model(right) are compared: the values fit well together and no differences are evident.

As for the obtained horizontal stress fields, they are consistent with the expected values: in the micro-model the stripes of alternating materials are reproduced in detail and the stress distribution provides different values corresponding to different materials; in the multi-scale model, instead, the global homogenized stresses are obtained by averaging the lower level fields. It is thus clear that the the homogenized stress field is uniform and the respective value is exactly the mean value between the corresponding values of the micro-model (see Figure 4.34).
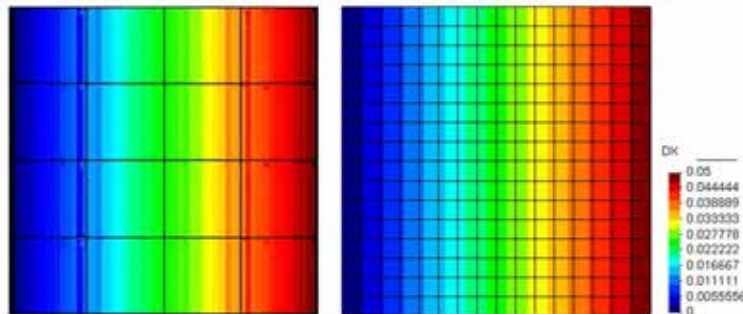

Figure 4.33: Horizontal displacement for homogenization model and micro-model: I loading condition

As for the other two loading cases, the obtained values for the multi-scale and micro models are shown in the sequel.

Those loading conditions have been chosen with the aim of investigating the multi-scale model response in cases where localization effects are predominant.

In the second loading condition, the comparison between multi-scale model and micro model as for the displacement fields (Figures 4.35 and 4.36) shows a good agreement: clearly in the micro-model the response is more localized and refined.

As for the stress fields, the averaging procedures, inner in the multi-scale approach, clearly tend to smooth the response both in terms of values and distributions. Qualitatively the same behavior is preserved. See Figures (4.37, 4.38 and 4.39).

Similar comments are valid in the third loading condition.

In this case, as expected, the stress distributions of the multi-scale model are symmetric (being the volume
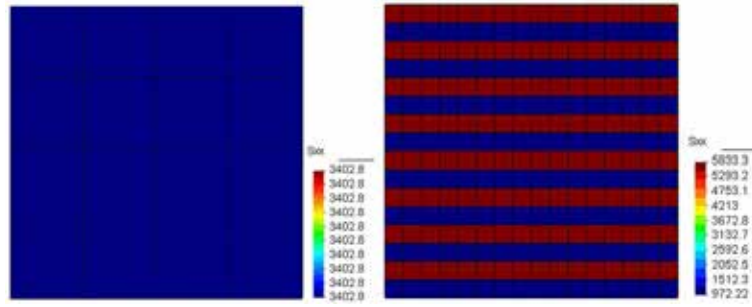
Figure 4.34: Horizontal stress Σ_x for homogenization model and micro-model: I loading condition
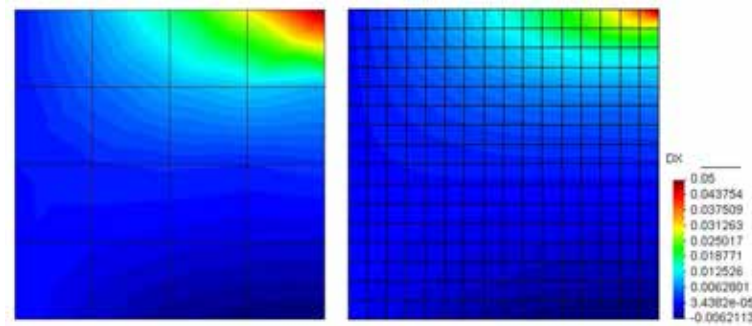

Figure 4.35: Horizontal displacement for homogenization model and micro-model: II loading condition
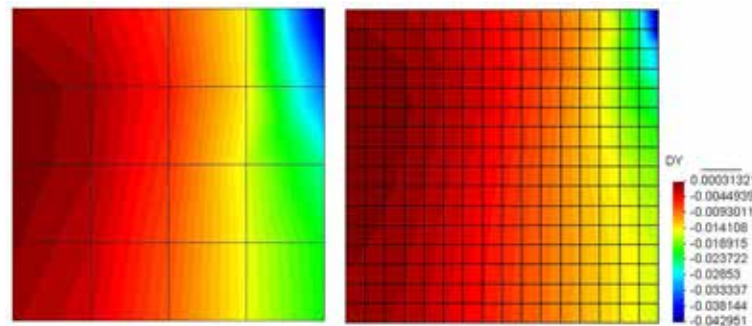

Figure 4.36: Vertical displacement for homogenization model and micro-model: II loading condition
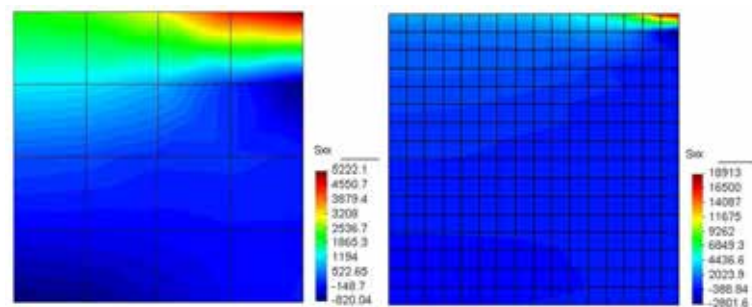

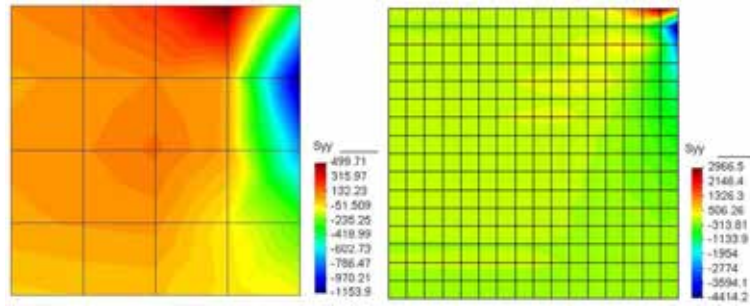Figure 4.37: Horizontal stress Σ_x for homogenization model and micro-model: II loading condition

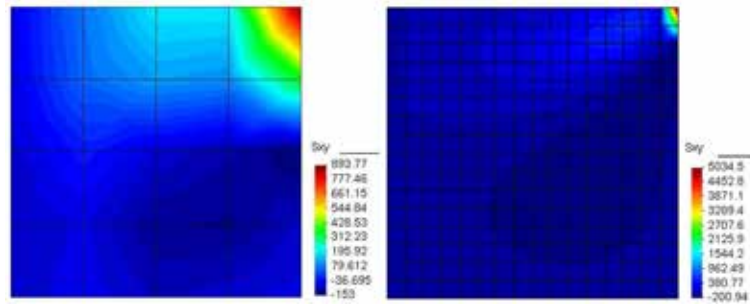Figure 4.38: Vertical stress Σ_y for homogenization model and micro-model: II loading condition

Figure 4.39: Shear stress Σ_{xy} for homogenization model and micro-model: II loading condition

fraction of each component 0.5) while the micro-model response is not symmetric because the top and bottom stripes are of different materials, thus it is clear that a stress concentration is shown in the top right corner of the structure (where the hard material is present). See Figures (4.40 , 4.41, 4.42, 4.43 and 4.44).
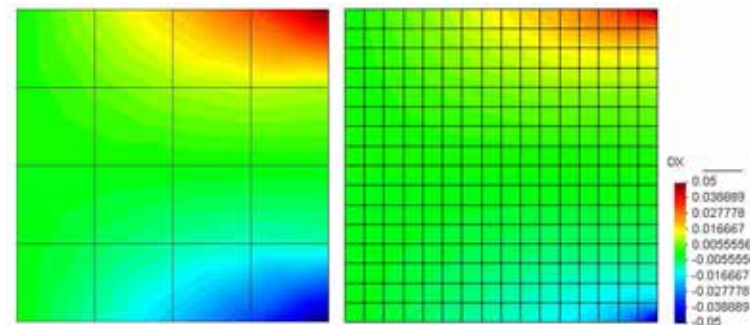

Figure 4.40: Horizontal displacement for homogenization model and micro-model: III loading condition

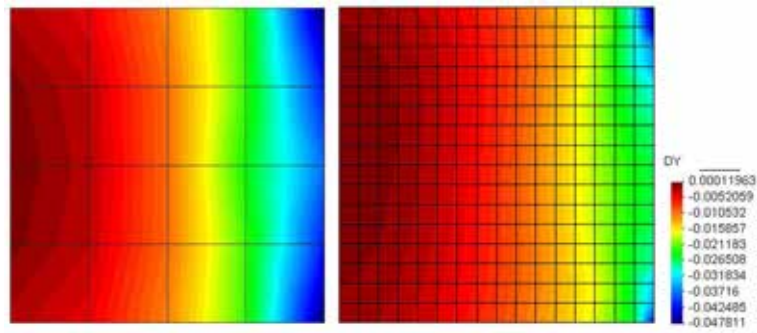Figure 4.41: Vertical displacement for homogenization model and micro-model: III loading condition

Figure 4.42: Horizontal stress Σ_x for homogenization model and micro-model: III loading condition

Figure 4.43: Vertical stress Σ_y for homogenization model and micro-model: III loading condition
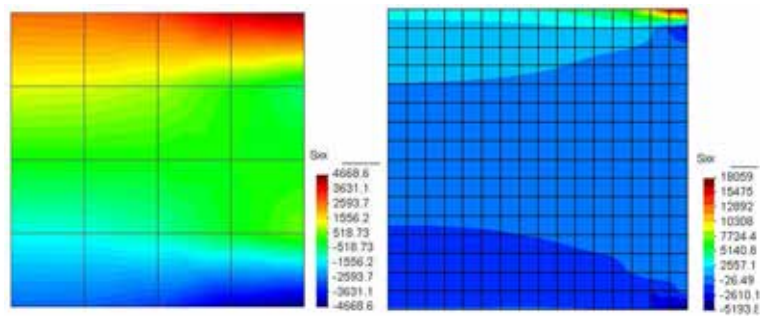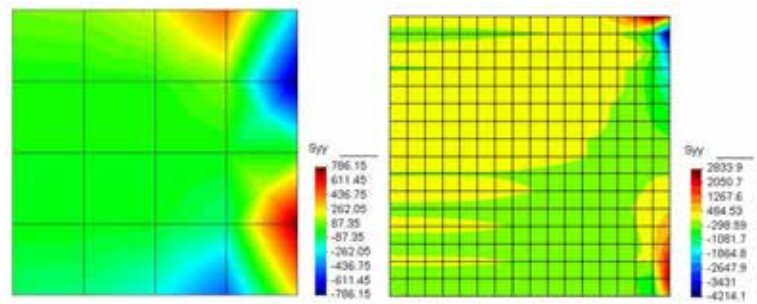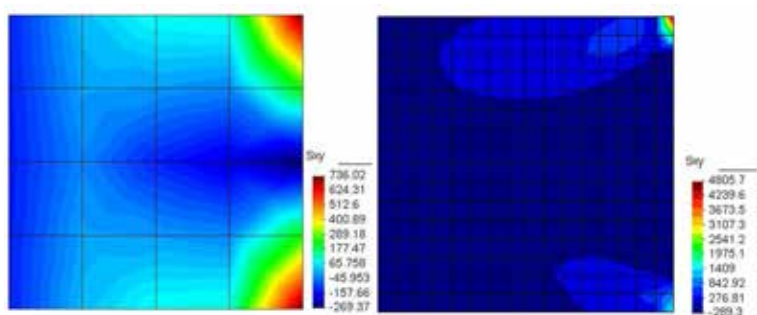

Figure 4.44: Shear stress Σ_{xy} for homogenization model and micro-model: III loading condition

Page test

The *Page Test* (Page (1978)) is one of the most commonly used academic tests in the calibration of numerical models for masonry. Loureno (1996) and also Lopez et al. (1999) used this test for calibrating their models.

The dimensions of the panel were 757 x 457 x $54mm^3$, using bricks of 122 x 37 x 54 mm^3 with joints 5 mm thick.

The adpted mechanical properties are summarized in Table 4.11. The experimental test provides values of stresses and vertical strains along a line of gauges positioned at 186.5 mm from the baseline. The load (P that is $20 - 40 - 60$ kN successively imposed) is applied with a piston and transmitted through a steel beam over a length of 381 mm (see Figure 4.45).

  Since no measurements of fracture energies and plastic deformations in compression were made in the
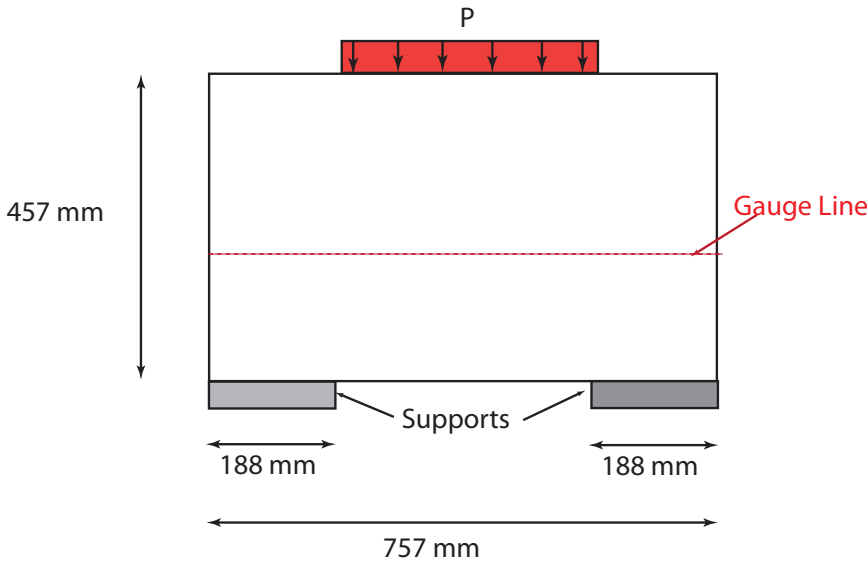

Figure 4.45: Page test: geometry and boundary conditions.

experimental test, the values proposed by Lopez et al. (1999) have been assumed.

  The generated mesh has 16 four-node elements (only one half of the structure has been discretized due

Material 1	Material 2
$E = 7400 MPa$	$E = 788 MPa$
$\nu = 0.167$	$\nu = 0.167$
$fc = 35.5 MPa$	$fc = 3.13 MPa$
$ft = 2 MPa$	$ft = 1.5 MPa$
$G = 207.36 N/mm$	$G = 8.32 N/mm$

Table 4.11: Mechanical parameters table

to geometric and loading condition symmetries), each with 4 Gauss points (see Figure 4.46).

The gauges coincide with the positions of the top Gauss points of the elements in the intermediate band. The chosen *RVE* is shown in Figure 4.47: a brick surrounded by half a mortar joint has been chosen in order to represent the stack bond masonry patterns of the experimental specimen. Every *RVE* has 44 elements, each with 4 Gauss points.

In the discretization at the macro and micro levels quadrilateral 4-nodes finite elements are used (with 4

integration points).
As for both constituents (bricks and mortar joints) the constitutive behavior is described by a damage law of course characterized by different parameters (as for the details of the constitutive model see Appendix A).
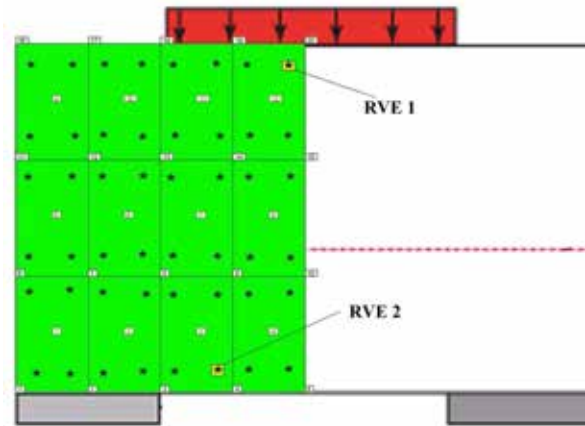

Figure 4.46: Macro-level mesh and placement of the *RVEs* examined in detail.
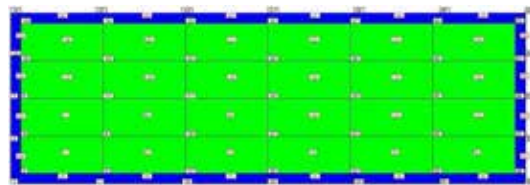

Figure 4.47: *RVE* discretization.

Since the referential experimental data are related, as said before, to a loading control test, no information are available about the post peak behavior.
Thus, the numerical two-scale application has been executed twice:

1. by reproducing the same experimental conditions, i.e. the vertical load (20 kN) is imposed and the vertical stresses are evaluated along the panel abscissa so that a direct comparison is possible with the referential results;

2. by imposing a displacement control loading condition, in order to follow the post peak behavior.

With respect to the first application, in Figure 4.48 a comparison is executed between experimental data (the red solid curve), the result of the adopted first order computational homogenization (black dashed line) and the result obtained by Lopez et al. (1999) (blue dashed line). The procedure followed by Lopez et al. (1999) is based on the definition of a constitutive model based on the homogenized anisotropic elastoplasticity previously developed by the authors. The effect of anisotropy is introduced by means of fictitious isotropic stress and strain spaces. The material properties in the fictitious isotropic spaces are mapped into the actual anisotropic space by means of a consistent fourth-order tensor.
The results obtained using the first order computational homogenization are in good agreement with the experimental data with the exception of the extremes. Possible causes are the fact that the Gauss point does not coincide exactly with the position of gauge since this is not specified or that experimental local effects in the band of measurements. Also, the lack of adequate discretization could cause this poor approximation. In the second application, the fracture energy regularization technique is adopted.
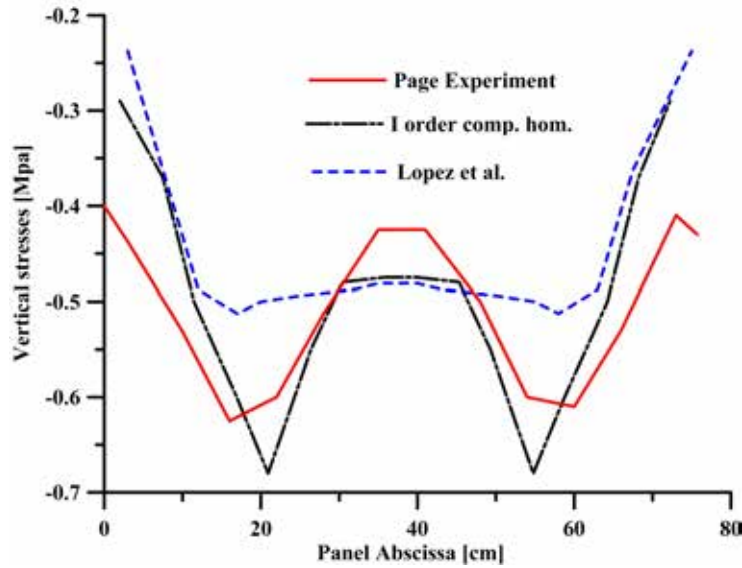
Figure 4.48: Page test: stress distribution along the horizontal gauge line.

The technique is well known in the standard finite element framework: the main idea is the preservation of the fracture energy. Depending on a characteristic length l_c that is related to the dimensions of the finite elements, the post-peak behavior of the stress-strain constitutive law is modified (by changing the area under the curve), without modifying the pre-peak behavior.

This lead to free the response from the adopted finite element mesh.

In the multi-scale framework, a double localization problem arise, each for every discretizazion level.

In the following Figure 4.49 the global response of the considered structure is presented in terms of vertical displacements in the top central point under the load and vertical reaction at the bottom left point.

Tho curves are shown: the blue one is obtained by adopting a characteristic length l_{cm} that is related to the dimensions of the finite elements at the micro-level, while the red one is obtained by adopting a characteristic length l_{cm} that is related to the dimensions of the finite elements at the macro-level.

The results obtain for the RVE 1 and 2 are examined in detail. The first one is in the zone where maximum values of distortions while the zone where the second one (corresponding to a macro-level fixed point) is characterized by maximum stress and strain gradients.

The following results are referred to the last equilibrium point reached in the curve 4.49. In the Figures 4.50 and 4.51 the displacement fields at the macro level are shown.

At this point the stress fields at the macro-level are shown. Figure 4.52 reproduces Σ_X stress distribution. Compressive stresses are obtained in the top right zone (corresponding to RVE_2), while tensile stresses in the bottom right (corresponding to RVE_2). As for the vertical stress distribution Σ_Y, it is shown in Figure4.53. The growth of a diagonal compressive strut appears evident. As for the RVE_1, Figures 4.55 and 4.56 show the displacement fields, while Figures 4.57 and 4.58 stress distributions.

While as for the RVE_2, Figures 4.59 and 4.60 show the displacement fields, while Figures 4.61 and 4.62 stress distributions.
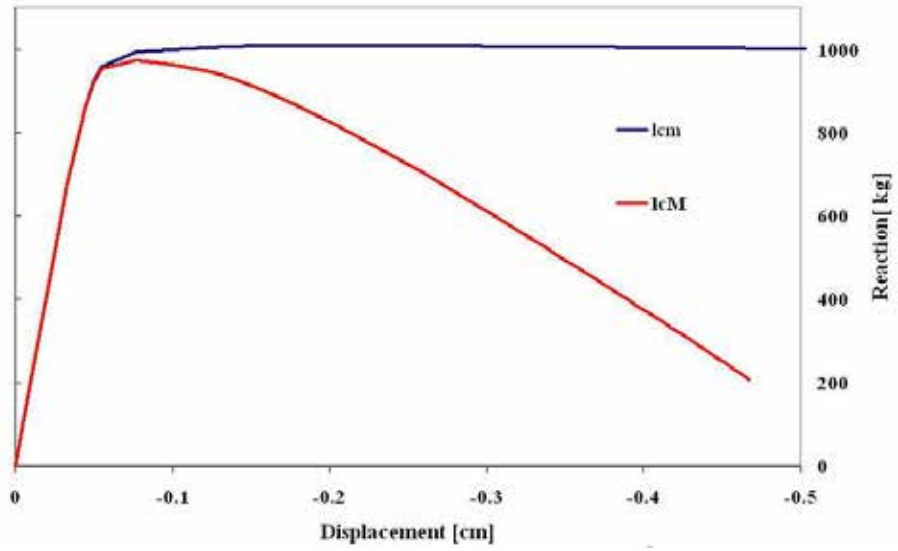
Figure 4.49: Global response comparisons
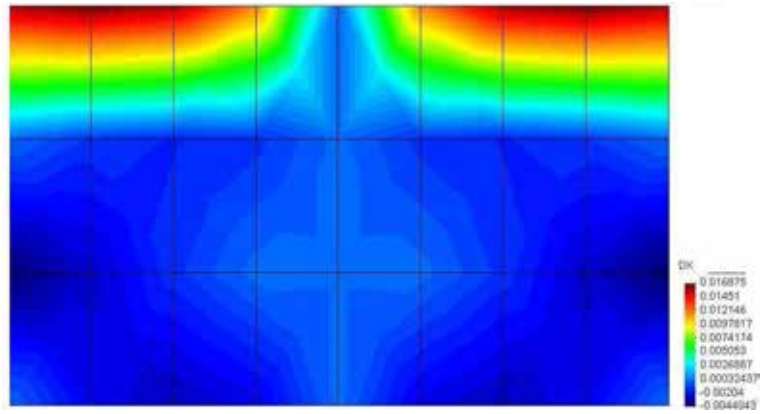
Figure 4.50: Horizontal displacement components.
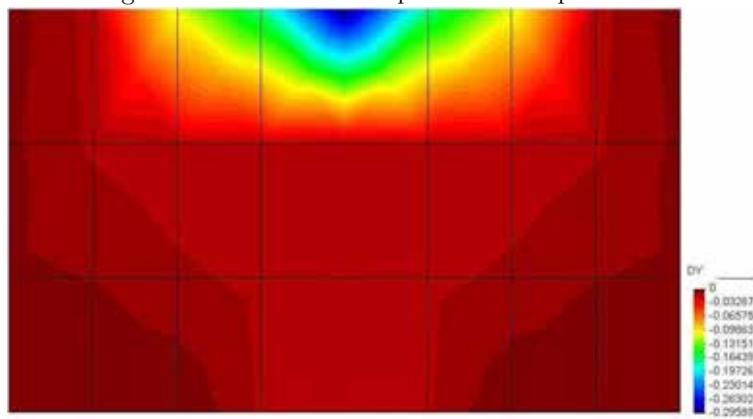
Figure 4.51: Vertical displacement components.
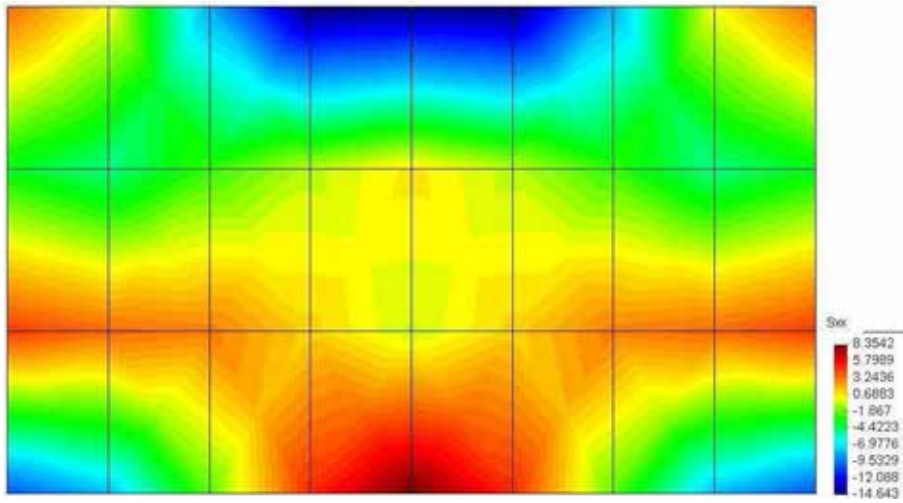
Figure 4.52: Stress components Σ_X.
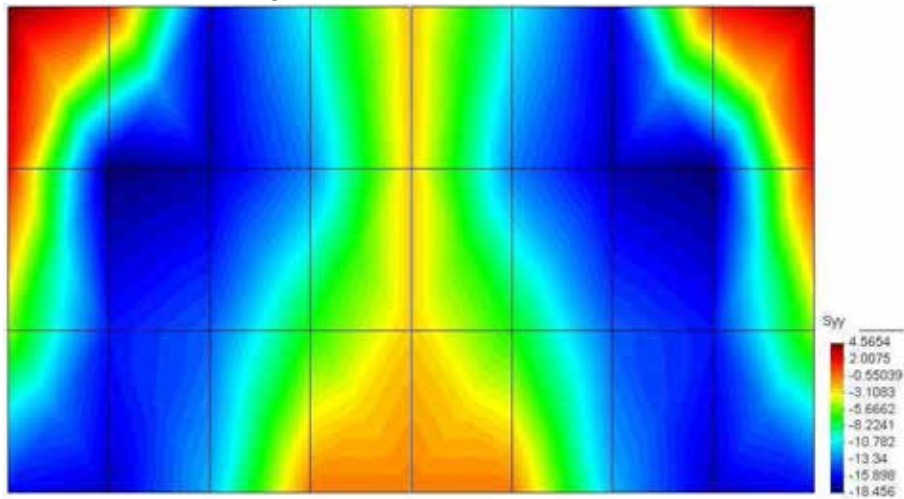
Figure 4.53: Stress components Σ_Y.
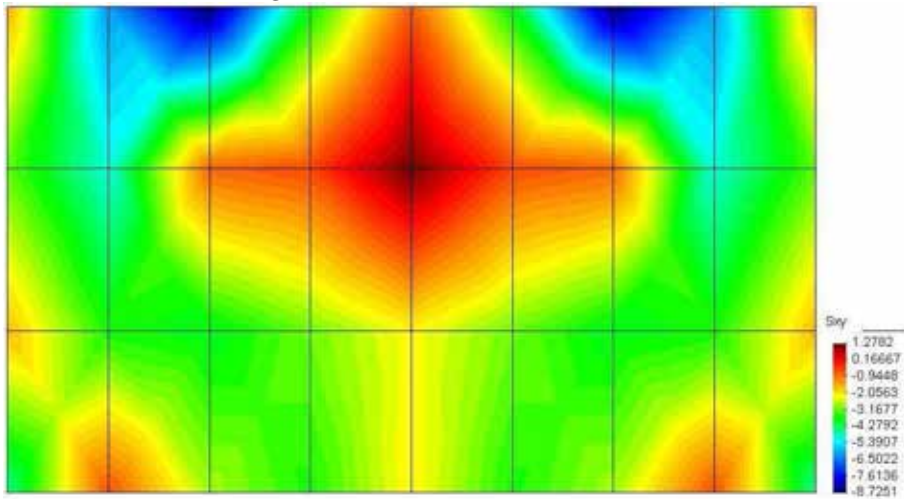
Figure 4.54: Stress components Σ_{XY}.
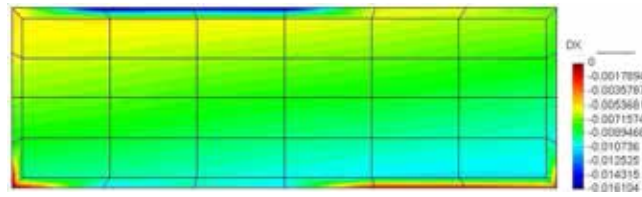
Figure 4.55: RVE finite element mesh.
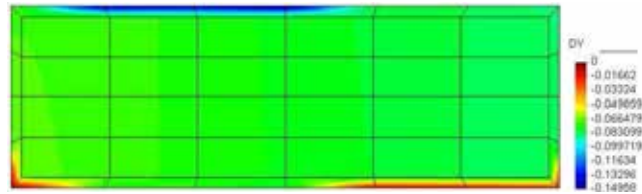
Figure 4.56: RVE finite element mesh.
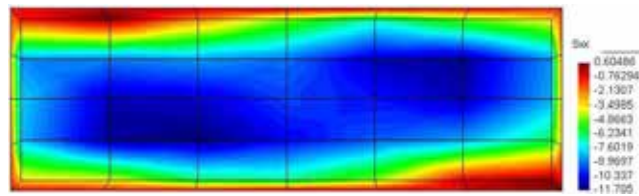
Figure 4.57: RVE finite element mesh.
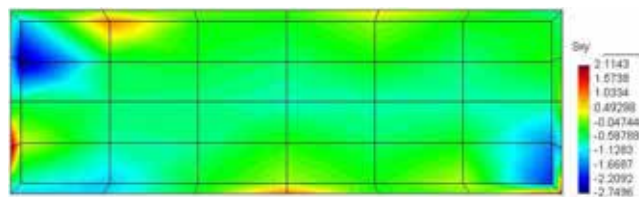
Figure 4.58: RVE finite element mesh.
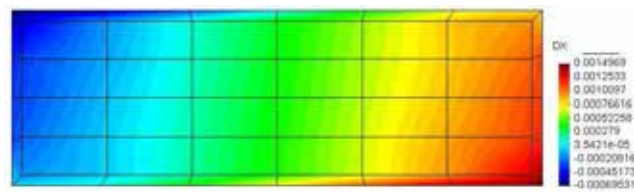
Figure 4.59: RVE finite element mesh.
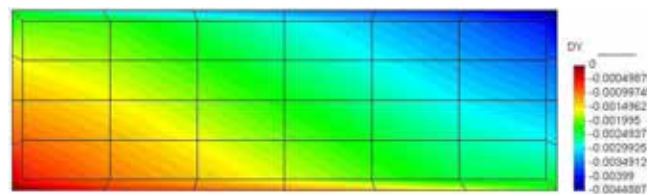
Figure 4.60: RVE finite element mesh.
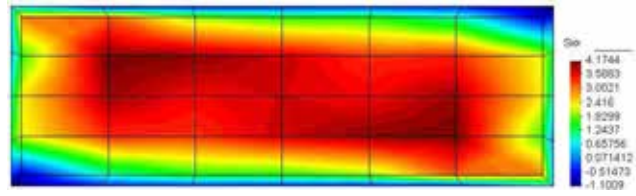
Figure 4.61: RVE finite element mesh.
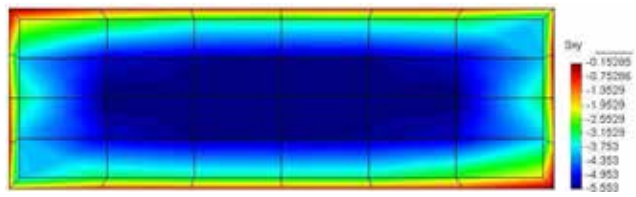
Figure 4.62: RVE finite element mesh.

Chapter 5

Enhanced Cosserat-Cauchy homogenization

5.1 Introduction

In the Chapter 4, the theoretical bases and the numerical implementation of the first order computational homogenization technique have been presented.
It has been shown that such a technique is a very effective tool to reproduce, in a natural way, the global behavior of composite material structures, by directly examining the micro-structure.

Despite that, many authors as Kouznetsova (2002), Forest and Sab (1998) and Feyel (2001) have extensively pointed out the inner limits of such a computational strategy.
In fact, since standard Cauchy continuum media are employed at both the analysis levels (macro and micro), the following considerations arise:

1. the Principle of local action fully holds, i.e. the formulation is valid only if the microstructure is very small with respect to the characteristic size at the macro-level and with respect to the length of the spatial variation of macroscopic loading, thus only very small macroscopic loading gradients can be applied to the microstructure;

2. the absolute size of the constituents does not affect the effective properties of the homogenized medium;

3. this formulation is unable to objectively reproduce localization phenomena in presence of strain-softening material behavior and typical spurious mesh dependencies appear;

Even if the aforementioned features, in case of other applications, can be acceptable, for the considered case of masonry structures, seem to be roundly invalidating.
In fact the first consideration is controverted by the experimental evidence that, in masonry, the microstructural typical size are comparable with the macrostructural one and, additionally, the constitutive material behavior with damage can trigger high deformation gradients. Then a formulation in which only first-order deformation modes (tension, compression, shear or combinations thereof) of the microstructure can be retrieved is, therefore, highly advised against since this is not capable to describe high deformation gradients.
With respect to the second requirement, it is proved that not only shape and arrangement of the constituents, but also the size, strongly affect the mechanical global response of masonry structures.

Finally, as for the third observation, due to the typical softening behavior experimentally exhibited by masonry panels undergoing seismic like loading conditions, localization phenomena frequently occur and it is necessary to employ a suitable regularization technique, in the numerical approach, in order to avoid spurious mesh dependencies.

On the basis of the aforementioned observations, it stands to reason that an enhanced formulation is required in order to overcome the limits of the standard first order one and to obtain a more realistic description of the actual response for the structural cases to be considered.
A decisive choice in this direction is the adoption of generalized continua in order to account for a material length scale in a natural manner and enriched deformation modes.
Several strategies have been proposed in the two-scale computational homogenization framework.
In Kouznetsova (2002), for instance, a second gradient continuum formulation for the macro-level has been adopted; another option is the employment of a Cosserat continuum at macro-level together with a classical continuum at the micro-level as in Forest and Sab (1998) in the framework of a continuum approach and Feyel (2001) in the computational homogenization multi-scale technique or, again, the adoption of Cosserat continuum at both levels (Forest et al. (1999)).

In this work the selected strategy is to couple two different continua as for the description of the macro-level and micro-level. At the macro-level a Cosserat continuum is adopted while the Cauchy medium is preserved at the micro-level.
This choice has been turned out to be very suitable for approaching the study of masonry structures.
Substantially the first reason is that it allows the introduction of a material length scale so that the overall response of the composite material is spontaneously bound to the the absolute size of the constituents.
The effect of considering a Cosserat continuum at the macro-level, in fact, is to enrich the displacement, strain and stress descriptions and, thus, to pass additional information to the micro-level: apart from the standard Cauchy three deformation modes (two axial and one shear symmetric deformation) that are however preserved, three additional deformation modes are considered (a skew-symmetric shear and two bending deformations). This means that, at least for shear and bending behaviors, with this formulation is possible to account for size effects (directly related to the *RVE* dimensions).
In the second gradient continuum formulation further additional deformation modes arise (10 instead of 6), raising the computational effort. Being, in masonry structures subjected to seismic like loading conditions, the predominant observed mechanisms related to shear and bending effects, the Cosserat continuum is already appropriate to handle the problem and it has been thought needless to look to the higher order continuum.

The adoption of a Cosserat continuum also at the micro-level has been avoided essentially because only the elastic constitutive model is well established in this case, while several non-linear models are available for classical continuum; thus it has been regarded as convenient to use a Cauchy continuum at the lower level where the constitutive behavior description is a crucial part of the formulation.

The nodal point of the strategy is the coupling between scales, because a one to one correspondence between strain and stress variables defined at two levels not longer arises and, therefore, an *ad hoc* kinematic map has to be formulated in order to manage the communications from the higher to the lower level.
Moreover a properly stated rule to obtain averaged stresses has to be obtained as an extension of the Hill-Mandel principle. (See Figure 5.1).

From the Figure 5.1, it is clear that the conceptual scheme remains the same as for the first order computational homogenization; the fundamental difference is the increased number of deformation modes that are to imposed to the *RVE* as boundary conditions and the higher number of homogenized stress components that have to be evaluated as output variables, by averaging the micro-level stress fields.

MACRO-COSSERAT

$$E \cdot \Sigma$$

KINEMATIC MAP

AVERAGED STRESSES

$$\sigma = f(\varepsilon)$$

MICRO-CAUCHY
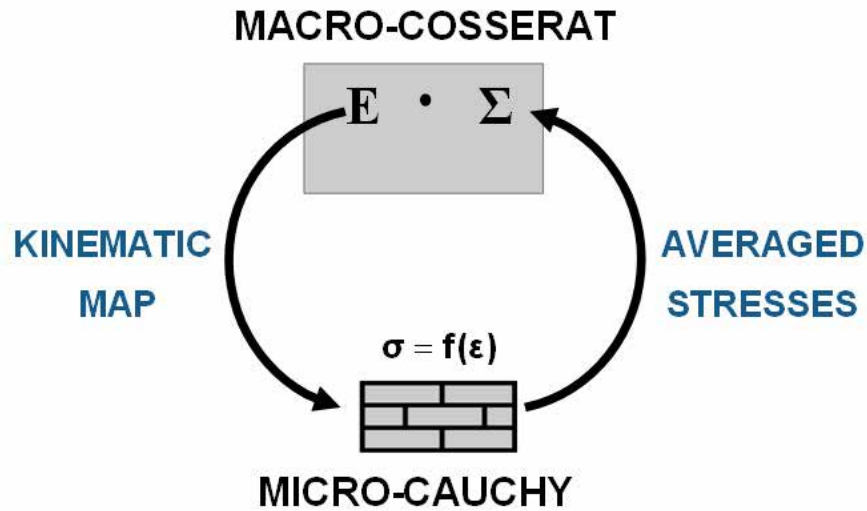
Figure 5.1: Enhanced Cosserat-Cauchy homogenization working scheme.

As aforementioned, one of the main goal to fulfill in the study of masonry structures is the effectiveness of the regularization strategy in order to tackle the localization phenomena. With this respect, as for the macro-level it is reasonable to suppose that the Cosserat medium can provide, thanks to its inner properties, regularization effects, at least for dominant shear and bending failure mechanisms; at the micro-level, instead, the standard fracture energy technique is adopted.

To the knowledge of the author, this work is the first example of enhanced first order computational homogenization applied to localization problems related to the study of masonry structures.

5.2   Statement of the *two scale* problem

The conceptual scheme of the scale transition procedure remains the same as for the standard first order homogenization (Cauchy-Cauchy). The correspondence one-to-one between macroscopic material point and underlaying *RVE* is preserved.

Again Ω is the domain at the macro-level, while ω is the domain of the *RVE*.

The fundamental differences can be established as follows: at the macro-scale additional degrees of freedom appear enriching as the strain as the stress descriptions; at the micro-scale, where the Cauchy medium is maintained, new input and output bridge conditions have to be established, i.e. a new kinematic map in order to impose the *BVP* and a new definition of the averaged stresses.

In the following, as for the Chapter 4, the macro and micro level problems are presented and the bridging conditions are discussed.

5.3   Statement of the Macroscopic problem

At the macro-level, a case of 2-D Cosserat continuum is considered in the hypothesis of infinitesimal deformations and infinitesimal displacements.

5.3.1   Compatibility equations

As it is well known, the Cosserat medium can be considered as a continuum enriched with respect to the Cauchy one. In the classical continuum mechanics, indeed, as for a 2-D case, a material point has two degrees of freedom (the displacements in two independent directions), while in the Cosserat theory each material point is provided with three degrees of freedom, i.e. an additional rotational degree of freedom is introduced with respect to the Cauchy medium and the displacement vector results as $\mathbf{U} = [U, V, \Phi]^T$. From a physical standpoint, it is possible to imagine that each material point is equipped with a rigid frame and that Φ describes the rotation angle of such a local structure, with respect to the initial configuration.

As for the strain measures the kinematic equations, defining the strains, are:

$$(5.1) \qquad\qquad \dot{\mathbf{E}} = \underline{\mathbf{D}}\dot{\mathbf{U}} \quad \text{in} \quad \Omega$$

where the expanded form holds as:

$$(5.2) \qquad
\left\{
\begin{array}{c}
\dot{E}_X \\
\dot{E}_Y \\
\dot{E}_{XY} \\
\dot{E}_{YX} \\
\dot{K}_X \\
\dot{K}_Y
\end{array}
\right\}
=
\left[
\begin{array}{ccc}
\frac{\partial}{\partial X} & 0 & 0 \\
0 & \frac{\partial}{\partial Y} & 0 \\
0 & \frac{\partial}{\partial X} & 1 \\
\frac{\partial}{\partial Y} & 0 & -1 \\
0 & 0 & \frac{\partial}{\partial X} \\
0 & 0 & \frac{\partial}{\partial Y}
\end{array}
\right]
\left\{
\begin{array}{c}
\dot{U} \\
\dot{V} \\
\dot{\Phi}
\end{array}
\right\}$$

where $\dot{\mathbf{E}}$ is the increment, in the infinitesimal time increment dt, of the strain vector (called *Homogenized strain vector*), $\underline{\mathbf{D}}$ is the compatibility operator and $\dot{\mathbf{U}}$ is the increment of the displacement vector.

Therefore in such a model the incremental form of the six strains components is defined, in particular $\dot{E}_X$ nd $\dot{E}_Y$ are axial components as in the Cauchy continuum, $\dot{E}_{XY}$ and $\dot{E}_{YX}$ are non-symmetric shear components and $\dot{K}_X$ and $\dot{K}_Y$ are curvatures.

It is possible to manipulate the expressions of the shear components of strains $\dot{E}_X$ nd $\dot{E}_Y$ in order to separate the symmetric and non symmetric parts. Two different measures, namely $\dot{E}_{XY}^{sym}$ and $\dot{\Theta}$, are thus

defined. The former corresponds to symmetric shear strain component (the third component of strains as for Cauchy continuum model) as:

$$\dot{E}_{XY}^{sym} = \frac{1}{2}\left(\frac{\partial \dot{U}}{\partial Y} + \frac{\partial \dot{V}}{\partial X}\right) \tag{5.3}$$

while the latter is defined as:

$$\dot{\Theta} = \dot{\Phi} - \frac{1}{2}\left(\frac{\partial \dot{V}}{\partial X} - \frac{\partial \dot{U}}{\partial Y}\right) \tag{5.4}$$

If $\partial\Omega = \partial\Omega_U \cup \partial\Omega_T$ is the boundary contour of the domain Ω, divided into the contour on which only the displacements are prescribed $\partial\Omega_U$ and the other on which only tractions are prescribed $\partial\Omega_T$, the Dirichlet boundary condition are defined as follows:

$$\dot{\mathbf{U}} = \dot{\bar{\mathbf{U}}} \quad \text{on} \quad \partial\Omega_U \tag{5.5}$$

5.3.2 Forces and stresses

The static local equilibrium using the incremental form of the Cosserat stress tensor $\dot{\boldsymbol{\Sigma}}$ is:

$$\underline{\mathbf{D}}^T\dot{\boldsymbol{\Sigma}} + \dot{\mathbf{B}} = \mathbf{0} \quad \text{in} \quad \Omega; \tag{5.6}$$

The vector of the increment of the stress components is :

$$\dot{\boldsymbol{\Sigma}} = \left\{\begin{array}{c} \dot{\Sigma_X} \\ \dot{\Sigma_Y} \\ \dot{\Sigma_{XY}} \\ \dot{\Sigma_{YX}} \\ \dot{M_X} \\ \dot{M_Y} \end{array}\right\} \tag{5.7}$$

and the increment of the body forces $\dot{\mathbf{B}}$ in the Ω domain is formed by two components of body forces namely B_X and B_Y and one component of body moment C_Z.

The incremental form of the traction boundary condition, resulting from the Cauchy's theorem, are defined as follows:

$$\underline{\mathbf{N}}\dot{\boldsymbol{\Sigma}} = \dot{\mathbf{T}} \quad \text{on} \quad \partial\Omega_T \tag{5.8}$$

where $\underline{\mathbf{N}}$ is the matrix containing the unit vectors normal to the traction boundary contour $\partial\Omega_T$ and $\dot{\mathbf{T}}$ is the vector of the increment of surface forces defined on the same contour.

5.3.3 Constitutive relations

As for the constitutive laws at the macro level, the lack of closed form global relations, between strains and stresses, requires the construction of a numerically based strategy with the aim of properly extracting from the micro-level the required information at the macro-level.
In a strain-driven framework, the values of the dependent variables (i.e. $\dot{\boldsymbol{\Sigma}}$) are obtained by averaging the related measures at the micro-scale (See 4.5) and also the homogenized tangent constitutive tensor $\underline{\mathbf{C}}$ is obtained from the *RVE*.
The differential constitutive relation linking homogenized stresses and strains by means of the homogenized constitutive tensor holds as:

(5.9)
$$\dot{\mathbf{\Sigma}} = \underline{\mathbf{C}} \quad \dot{\mathbf{E}}$$

The assumed form of the homogenized tangent constitutive matrix, obtained in the hypothesis of orthotropic behavior, is as follows:

(5.10)
$$\underline{\mathbf{C}} = \begin{bmatrix} C_{11} & C_{12} & 0 & 0 & 0 & 0 \\ C_{12} & C_{22} & 0 & 0 & 0 & 0 \\ 0 & 0 & C_{33} & C_{34} & 0 & 0 \\ 0 & 0 & C_{34} & C_{44} & 0 & 0 \\ 0 & 0 & 0 & 0 & C_{55} & 0 \\ 0 & 0 & 0 & 0 & 0 & C_{66} \end{bmatrix}$$

5.4   Statement of the Microscopic problem

At the micro-level the Cauchy continuum is maintained, hence for the description of Compatibility equations; Forces and stresses and for the constitutive relationships it is directly referred to 4.4.

5.4.1   Boundary value problem

The statement of the BVP at the micro level is the key part of the multi-scale homogenization procedure. Properly conceived bridging conditions between the two scales have to be imposed, by extending the method used for the Cauchy-Cauchy homogenization.

The displacement field $\mathbf{u}$, on the RVE, has to de defined as the superposition of an assigned field $\mathbf{u}^*$, depending on the macro deformations $\mathbf{E}$, and an unknown periodic fluctuation field $\mathbf{u}^p$, namely:

(5.11)
$$\mathbf{u} = \mathbf{u}^*(\mathbf{E}) + \mathbf{u}^p$$

In this section the derivation of field $\mathbf{u}^*$ is first pointed out and later the imposition of periodicity conditions is explained in detail.

For the sake of generality the RVE is rectangular shaped with b and h being respectively the base and the height. To the knowledge of the author, this is the first attempt to consider a rectangular RVE in this formulation as only square $RVEs$ have been used up to now.
Let's consider a material point at the macro level, whose displacement vector is $\mathbf{U} = \{U, V, \Phi\}^T$; the related RVE is characterized by the displacement field $\mathbf{u} = \{u, v\}^T$ varying within the domain ω. In Figure 5.2 the RVE is shown together with its reference frame.

As proposed in Forest (1998), it is postulate that the displacement components of the macroscopic point $\mathbf{U} = [U, V, \Phi]^T$ represent the generalized displacements characterizing the rigid body motion of the underlying RVE.

This means that the rigid body displacement field can be defined in $\omega = [-\frac{b}{2}, \frac{b}{2}] \times [-\frac{h}{2}, \frac{h}{2}]$ as:

(5.12)
$$u(x,y) = U - \Phi(y - y_C) \qquad v(x,y) = V + \Phi(x - x_C)$$

where $\mathbf{x}_C = [x_C, y_C]^T$ is the position vector of the center C of the RVE in the RVE reference frame. This condition is imposed via the least square method, together with the hypothesis that the rotation center coincides with the geometric center of the RVE.
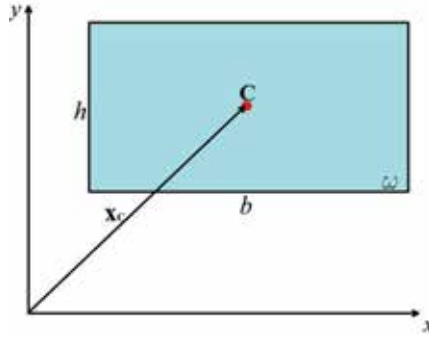
Figure 5.2: RVE and reference frame.

If $\mathbf{U}^* = [U, V]^T$ and $\boldsymbol{\Phi} = \Phi\mathbf{a}$ (where $\mathbf{a}$ is the versor normal to the plane) the following expression has to be minimized:

$$(5.13) \qquad F = \int_{x_C-b/2}^{x_C+b/2} \int_{y_C-h/2}^{y_C+h/2} \|\mathbf{u}(\mathbf{x}) - \mathbf{U}^*(\mathbf{x}_C) - \boldsymbol{\Phi} \wedge (\mathbf{x} - \mathbf{x_C})\|^2 d\Omega$$

where $\wedge$ denotes the vector product, $\|\cdot\|$ is the norm operator, and $\mathbf{x}$ the coordinates of a generic point in the RVE.

Namely the minimization of F corresponds to require that:

$$(5.14) \qquad \frac{\partial F}{\partial U} = 0; \quad \frac{\partial F}{\partial V} = 0; \quad \frac{\partial F}{\partial \Phi} = 0.$$

Simple algebraic manipulations lead to three expressions relating the macroscopic point displacement components to the corresponding RVE fields:

$$(5.15) \qquad U(x_C, y_C) = \langle u(x, y) \rangle_\omega$$

$$(5.16) \qquad V(x_C, y_C) = \langle v(x, y) \rangle_\omega$$

$$(5.17) \qquad \Phi = \frac{12}{(b^2 + h^2)} \langle v(x - x_C) - u(y - y_C) \rangle_\omega$$

The previous expressions (5.15), (5.16) and (5.17) correspond to a homogenization rule in terms of displacements that relates the entire displacement field of the RVE to the displacement vector characterizing the correspondent macro-level material point. Once assumed a properly conceived general expression as for the micro-level displacement fields (a third order polynomial with two variables has been chosen and it will be shown in the sequel), such a homogenization rule is used in order to express the coefficients of the aforementioned displacement fields in terms of macro-level strains.

Aiming to establish the main steps of the adopted procedure, the first step is the definition of the strains at the two scales. In 4.4.1 and 5.3.1 the compatibility equations as for micro and macro-level have been pointed out in the incremental forms, and, for the sake of completeness are repeated in the following.
As for the micro-level, the strain vector results as:

$$(5.18) \qquad \mathbf{e} = \underline{\mathbf{d}}\mathbf{u} \quad \text{in} \quad \omega$$

and the expanded form is:

$$(5.19) \qquad \left\{ \begin{array}{c} \epsilon_x \\ \epsilon_y \\ \epsilon_{xy} \end{array} \right\} = \left[\begin{array}{cc} \frac{\partial}{\partial x} & 0 \\ 0 & \frac{\partial}{\partial y} \\ \frac{1}{2}\frac{\partial}{\partial y} & \frac{1}{2}\frac{\partial}{\partial x} \end{array} \right] \left\{ \begin{array}{c} u \\ v \end{array} \right\}$$

while at the macro-level, by taking into account the aforementioned partition of the shear components into the symmetric and the antisymmetric part, the strain vector can be split into three sub-vectors in order to deal separately with the different components. The first three components describe axial and shear symmetric strains:

$$(5.20) \qquad\qquad \mathbf{E}^* = \underline{\mathbf{D}}^* \mathbf{U}^* \quad \text{in} \quad \Omega$$

$$(5.21) \qquad \left\{ \begin{array}{c} E_X \\ E_Y \\ E_{XY}^{sym} \end{array} \right\} = \left[\begin{array}{cc} \frac{\partial}{\partial X} & 0 \\ 0 & \frac{\partial}{\partial Y} \\ \frac{1}{2}\frac{\partial}{\partial Y} & \frac{1}{2}\frac{\partial}{\partial X} \end{array} \right] \left\{ \begin{array}{c} U \\ V \end{array} \right\}$$

where the vector $\left\{ \begin{array}{c} E_X \\ E_Y \\ E_{XY}^{sym} \end{array} \right\}$ is called $\mathbf{E}^*$ moreover the antisymmetric shear is:

$$(5.22) \qquad\qquad \Theta = \Phi - \frac{1}{2}\left(\frac{\partial V}{\partial X} - \frac{\partial U}{\partial Y} \right)$$

and at last the vector collecting curvatures components is defined as:

$$(5.23) \qquad\qquad \mathbf{K} = \left\{ \begin{array}{c} K_X \\ K_Y \end{array} \right\}$$

A set of hypotheses is formulated as for the strain fields:

- scale invariance in the homogenization process and quadratic variation for the symmetric strain tensor, i.e. it is supposed that the strain vector at the micro-scale, to be calculated in the center of the *RVE*, is equal to the sub-vector $\mathbf{E}^*$ corresponding to the same point:

  $$(5.24) \qquad\qquad \mathbf{E}^* = \mathbf{e}(\mathbf{x}_C)$$

  both defined by quadratic functions of the point coordinates;

- linear variation for Φ;

- constant curvatures $\mathbf{K}$.

In order to fulfill the aforementioned hypotheses it is now possible to define the analytical form of the assumed displacement field on the *RVE* and third order complete polynomials are chosen so that the following expressions hold:

$$(5.25) \qquad u^* = A_1 + A_2 x + A_3 y + A_4 x^2 + A_5 y^2 + 2A_6 xy + A_7 x^3 + A_8 y^3 + 3A_9 x^2 y + 3A_{10} xy^2$$

$$(5.26) \qquad v^* = B_1 + B_2 x + B_3 y + B_4 x^2 + B_5 y^2 + 2B_6 xy + B_7 x^3 + B_8 y^3 + 3B_9 x^2 y + 3B_{10} xy^2$$

where the expressions of the 20 coefficients A_i and B_i can be obtained as a function of the macroscopic strain vector, received as input from the macro-level.

Considerable simplifications in the polynomial expressions arise when the above requirement are imposed on the strains:

$$(5.27) \qquad E_X = \epsilon_x(\mathbf{x}_C) \quad \longrightarrow \quad A_7 = -A_{10}\frac{h^2}{b^2}$$

$$(5.28) \qquad E_Y = \epsilon_y(\mathbf{x}_C) \quad \longrightarrow \quad B_9 = -B_8\frac{h^2}{b^2}$$

$$(5.29) \qquad E_{XY} = \epsilon_{xy}(\mathbf{x}_C) \quad \longrightarrow \quad (A_9 + B_7) = -(A_8 + B_{10})\frac{h^2}{b^2}$$

$$(5.30) \qquad \Phi \quad linear \quad \longrightarrow \quad \begin{aligned} B_7 &= A_9\frac{h^2}{b^2} \\ B_{10} &= A_8\frac{h^2}{b^2} \\ B_9 &= A_{10}\frac{h^2}{b^2} \end{aligned}$$

while the requirement on the curvature is directly fulfilled. At this point it is possible to express all the coefficients appearing in (5.27), (5.28),(5.29) and (5.30) in terms of 2 independent coefficient as, for example, A_9 and A_{10}.

Additional hypotheses are imposed, namely:

- no constant terms are considered in the polynomials because displacement fields have to be expressed in terms of macro-level strains and thus no rigid body motions are admitted:

$$(5.31) \qquad A_1 = B_1 = 0;$$

- ϵ_x does not depend on the variable x:

$$(5.32) \qquad A_4 = A_{10} = 0;$$

- ϵ_y does not depend on the variable y:

$$(5.33) \qquad B_5 = 0;$$

- ϵ_{xy} does not depend neither on x nor on y:

$$(5.34) \qquad B_4 = -A_6; \qquad A_5 = -B_6;$$

The identification of polynomial coefficients is carried on, according to Forest and Sab (1998), by imposing that the center of the *RVE* overlaps the origin of the reference frame $\mathbf{x}_C = 0$, and that the macro-strains components, evaluated on the basis of the micro-level displacement fields in the center of the *RVE*, are equal to the macro-level imposed values $\overline{\mathbf{E}}^*$, $\overline{\Theta}$ and $\overline{\mathbf{K}}$:

$$(5.35) \qquad\qquad\qquad\qquad \mathbf{E}^*(\mathbf{0}) = \overline{\mathbf{E}}^*;$$

$$(5.36) \qquad\qquad\qquad\qquad (\Phi - \Omega)(\mathbf{0}) = \overline{\Theta};$$

$$(5.37) \qquad\qquad\qquad\qquad \mathbf{K}(\mathbf{0}) = \overline{\mathbf{K}};$$

The coefficients of the polynomials are, thus, identified as:

$$(5.38) \qquad\qquad\qquad A_2 = \overline{E}_X; \qquad B_3 = \overline{E}_Y; \qquad B_2 = \overline{E}_{XY}^{sym};$$

$$(5.39) \qquad\qquad\qquad A_6 = -\frac{1}{2}\overline{K}_X; \qquad B_6 = \frac{1}{2}\overline{K}_Y;$$

$$(5.40) \qquad\qquad\qquad A_9 = \frac{5}{b^2 h^2}\left[(b^2 - h^2)\overline{E}_{XY}^{sym} - (h^2 + b^2)\overline{\Theta}\right];$$

so that the following resulting expressions arise:

$$(5.41) \qquad
\begin{aligned}
u^* &= \overline{E}_X x + \overline{E}_{XY} y - \tfrac{1}{2}\overline{K}_Y y^2 - \overline{K}_X xy - 5\frac{b^2+h^2}{b^4}\left[\overline{E}_{XY}\left(\frac{h^2-b^2}{b^2+h^2}\right) + \overline{\Theta}\right]\left(y^3 - 3\frac{h^2}{b^2}x^2 y\right) \\
v^* &= \overline{E}_{XY} x + \overline{E}_Y y + \tfrac{1}{2}\overline{K}_X x^2 + \overline{K}_Y xy - 5\frac{b^2+h^2}{b^4}\left[\overline{E}_{XY}\left(\frac{h^2-b^2}{b^2+h^2}\right) + \overline{\Theta}\right]\frac{h^2}{b^2}\left(\frac{h^2}{b^2}x^3 - 3y^2 x\right)
\end{aligned}$$

Figure 5.4 depicts the associated elementary deformation mechanisms, where the first three are the typical Cauchy modes and the last are the Cosserat additional ones.
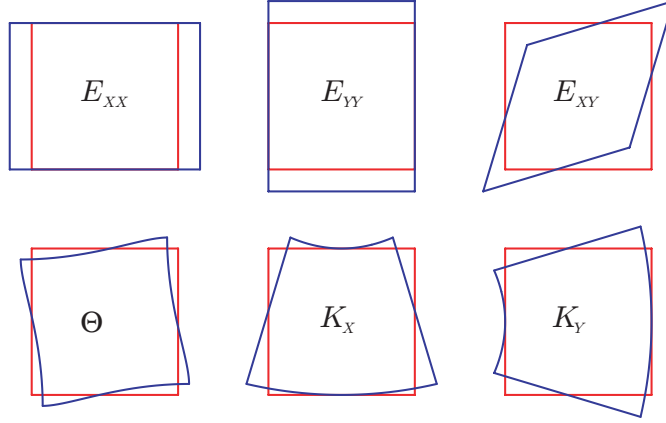
Figure 5.3: Elementary deformation modes.

Using a compact notation the kinematic map may be expressed by $\mathbf{u}^* = \mathbf{A}\mathbf{E}$ where $\mathbf{A}$ is the localization matrix that is defined as:

(5.42)

$$\mathbf{A} = \begin{bmatrix} x & 0 & \left[y - 5\frac{b^2+h^2}{b^4} \left(\frac{h^2-b^2}{b^2+h^2} \right) \left(y^3 - 3\frac{h^2}{b^2}x^2 y \right) \right] & -5\frac{b^2+h^2}{l^4} \left(y^3 - 3\frac{h^2}{b^2}x^2 y \right) & -xy & -\frac{1}{2}y^2 \\ 0 & y & \left[x - 5\frac{b^2+h^2}{l^4} \left(\frac{h^2-b^2}{b^2+h^2} \right) \frac{h^2}{b^2} \left(\frac{h^2}{b^2}x^3 - 3y^2 x \right) \right] & -5\frac{b^2+h^2}{l^4} \frac{h^2}{b^2} \left(\frac{h^2}{b^2}x^3 - 3y^2 x \right) & \frac{1}{2}x^2 & xy \end{bmatrix}$$

At this point the kinematic map $\mathbf{u}^*$ to be imposed on the *RVE* has been completely defined, and the periodicity conditions have to be imposed on the edge of the *RVE* as follows (In Figure 5.4 the position of vertices and periodic points of RVE are shown):

1. conditions imposed at the corner points were the periodic fluctuation displacement fields are equal to zero:

   (5.43)
   $$\mathbf{u}_{\mathrm{ai}} = \mathbf{u}^*{}_{\mathrm{ai}} \qquad i = 1, 4$$

2. conditions imposed between pears of periodic points:

   (5.44)
   $$\mathbf{u}_{\mathrm{a+}} - \mathbf{u}_{\mathrm{a-}} = \mathbf{u}^*{}_{\mathrm{a+}} - \mathbf{u}^*{}_{\mathrm{a-}}$$

3. Additional conditions, with respect to the first order homogenization framework, are required to ensure that the fluctuation field produces zero averaged strains. Those statements are straight derived from the Equations 5.36 and 5.37. In fact if all the displacement fields, solution of the *RVE*, are taken into account, the expression 5.36 is:

   (5.45)
   $$\frac{1}{h^2 + b^2} [B_2(b^2 - h^2) - A_9 \frac{b^2 h^2}{5}] + \frac{12}{(b^2 + h^2)} \langle xv^p - yu^p \rangle_\omega = \Theta;$$

   while the expression 5.37 results in components:

   (5.46)
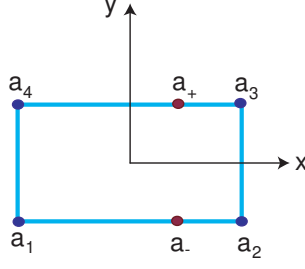 $$-2A_6 + \frac{12}{(b^2 + h^2)} \langle x \frac{\partial v^p}{\partial x} \rangle_\omega = K_X;$$

Figure 5.4: Point periodicity conditions.

$$2B_6 + \frac{12}{(b^2 + h^2)} \langle y \frac{\partial u^p}{\partial y} \rangle_\omega = K_X;$$

thus the additional integral conditions to be imposed on the whole domain of the *RVE* arise as:

$$\int_\omega (xv^p - yu^p)d\omega = 0;$$

$$\int_\omega x \frac{\partial v^p}{\partial x} d\omega = 0; \, ;$$

$$\int_\omega y \frac{\partial u^p}{\partial y} d\omega = 0;$$

by simply manipulating the (5.48), (5.49) and (5.50) it is possible to obtain strong simplifications. It is assumed the following notation: A is the bottom edge of the *RVE* and B, C and D are respectively the right, the top and the left edges.

By starting with the first condition, expressed in Equation 5.48, if the vector $\mathbf{r}$ is defined as $\mathbf{r} = [x, y]^T$, then $*\mathbf{r} = [-y, x]^T$ is the rotate vector , it becomes:

$$\int_\omega (*\mathbf{r}) \, \mathbf{u}^p \, d\omega = \int_\omega \mathbf{r} \, (*\mathbf{u}^p) \, d\omega = \int_\omega \frac{1}{2} [\nabla \|\mathbf{r}\|^2] \, (*\mathbf{u}^p) \, d\omega = 0$$

by substituting:

$$\frac{1}{2} [\nabla \|\mathbf{r}\|^2] \cdot (*\mathbf{u}^p) = \nabla \cdot [\frac{1}{2} \|\mathbf{r}\|^2 (*\mathbf{u}^p)] - \frac{1}{2} \|\mathbf{r}\|^2 \nabla \cdot (*\mathbf{u}^p)$$

moreover

$$\nabla \cdot (*\mathbf{u}^\mathbf{P}) = -\mathbf{curl}(\mathbf{u}^\mathbf{P})$$

it leads to:

$$\int_\omega \nabla \cdot [\frac{1}{2} \|\mathbf{r}\|^2 \, (*\mathbf{u}^p)] \, d\omega + \int_\omega \frac{1}{2} \|\mathbf{r}\|^2 \cdot curl(\mathbf{u}^p) \, d\omega = 0$$

by applying the divergence theorem to the first term and the curl theorem to the second term:

$$(5.55) \qquad \int_{\partial\omega} \frac{1}{2}\|\mathbf{r}\|^2 (*\mathbf{u}^p) \cdot \mathbf{n}\, d\,\partial\omega + \int_{\partial\omega} \frac{1}{2}\|\mathbf{r}\|^2 \mathbf{n} \wedge \ \mathbf{u}^p\, d\,\partial\omega = 0$$

it results as:

$$(5.56) \qquad \int_{\partial\omega} \frac{1}{2}\|\mathbf{r}\|^2 (un_y - vn_x)\, d\partial\omega + \int_{\partial\omega} \frac{1}{2}\|\mathbf{r}\|^2 (vn_x - un_y)\, d\partial\omega = 0$$

It stands to reason that the (5.56) is identically zero as the terms at the left hand side cancel each other out.

The second condition to be imposed, according to Equation 5.49, it turns out to be:

$$(5.57) \qquad \int_\omega x \frac{\partial v^p}{\partial x}\, d\omega = \int_\omega \frac{\partial(xv^p)}{\partial x}\, d\omega - \int_\omega v^p\, d\omega$$

The second term in the right hand side is equal to zero by definition of periodic fluctuation field on the *RVE* domain, thus applying the divergence theorem to the first term it leads to:

$$(5.58) \qquad \int_{\partial\omega} x\, v^p\, n_x\, \mathbf{e}_x\, d\,\partial\omega = \int_{\partial\omega_B} x_B\, v^p\, n_B\, \mathbf{e}_x\, d\,\partial\omega_B + \int_{\partial\omega_D} x_D\, v^p\, n_D\, \mathbf{e}_x\, d\,\partial\omega_D = 0$$

where $\mathbf{n} = \{n_x\mathbf{e}_x + n_y\mathbf{e}_y\}^T$;the periodicity conditions assure that:

$$(5.59) \qquad v_B^p(s) = v_D^p(s)$$

where s is the abscissa along the edges and moreover it is clear that:

$$(5.60) \qquad n_B\mathbf{e}_x = -n_D\mathbf{e}_x$$

for the considered case of small displacements and small deformation hypotheses, the following very simple expression holds, relating the coordinates of opposite edges of the *RVE*:

$$(5.61) \qquad \mathbf{x}_B = \mathbf{x}_D + b \quad \mathbf{n}_B$$

where b the distance between the right and left edges and $\mathbf{n}_B$ is the normal associated to the right edge. therefore the expression in 5.58 becomes:

$$(5.62) \qquad \int_{\partial\omega_D} x_D\, v^p\, n_D\, \mathbf{e}_x d\,\partial\omega_D - \int_{\partial\omega_B} (x_D + b\, n_B\, \mathbf{e}_x)\, v^p\, n_D\, \mathbf{e}_x\, d\,\partial\omega_D = 0$$

and it leads to:

$$(5.63) \qquad B\|n_D\|^2 \int_{\partial\omega_B} v^p\, d\,\partial\omega = 0$$

the final expression is:

$$(5.64) \qquad \int_{\partial\omega_B} v^p\, d\,\partial\omega = 0$$

The last additional integral condition is:

(5.65)
$$\int_\omega y \, \frac{\partial u^p}{\partial y} \, d\omega = 0$$

by following a similar path with respect to the previous one, it leads to the final expression:

(5.66)
$$\int_{\partial \omega_A} u^p \, d \, \partial\omega = 0$$

in order to summarize, the integral conditions to be imposed simply result as:

(5.67)
$$\int_{\partial \omega_B} v^p d \, \partial\omega = 0, \qquad \int_{\partial \omega_A} u^p d \, \partial\omega = 0$$

These conditions need to be imposed only on the bottom (A) and left (D) edge of the *RVE*. See Figure 5.5.
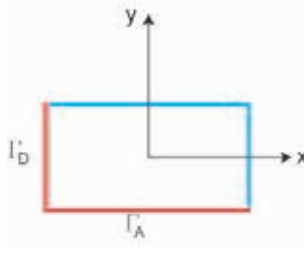

Figure 5.5: Point periodicity conditions.

5.5   Homogenization procedure

In this case, as for the homogenization procedure, an extension of the *Hill-Mandel principle* assures that the the averaging procedure is valid in an energetic sense, thus:

(5.68)
$$\boldsymbol{\Sigma}^T \boldsymbol{E} = \langle \boldsymbol{\sigma} \rangle_\omega^T \langle \mathbf{e} \, \rangle_\omega$$

where the stress and strains vectors have been introduced before. The final expressions of the averaging procedure, relating macro and micro stresses are obtained via basic calculations and result as:

(5.69)
$$\Sigma_X = \langle \sigma_x \rangle_\omega$$

(5.70)
$$\Sigma_Y = \langle \sigma_y \rangle_\omega$$

(5.71)
$$\Sigma_{XY} = \left\langle 15xy \frac{b^2 - h^2}{b^2 h^2} (\sigma_x - \sigma_y) + \left\{ 1 + \frac{15}{2} \left[\left(\frac{1}{b^2} - \frac{b^2}{h^4} \right) y^2 + \left(\frac{1}{h^2} - \frac{h^2}{b^4} \right) x^2 \right] \right\} \sigma_{xy} \right\rangle_\omega$$

(5.72)
$$Z = \left\langle 30xy \frac{b^2 + h^2}{b^2 h^2} (\sigma_y - \sigma_x) + \left[\left(\frac{30}{h^2} + \frac{15}{b^2} + \frac{15b^2}{h^4} \right) y^2 - \left(\frac{30}{b^2} + \frac{15}{h^2} + \frac{15h^2}{b^4} \right) x^2 \right] \sigma_{xy} \right\rangle_\omega$$

$$(5.73) \qquad\qquad M_X = \langle -y\sigma_x \rangle_\omega$$

$$(5.74) \qquad\qquad M_Y = \langle x\sigma_y \rangle_\omega$$

Set of governing equations at the two level: summarizing table

To sum up the analytical problems are stated by defining two sets of governing equations, both at the micro and macro levels, as shown in the following summarizing table:

Macro-level		Micro-level	
$\underline{\mathbf{D}}^T\dot{\boldsymbol{\Sigma}} + \dot{\mathbf{B}} = \mathbf{0}$	in Ω;	$\underline{\mathbf{d}}^T\dot{\boldsymbol{\sigma}} = \mathbf{0}$	in ω;
$\dot{\boldsymbol{\Sigma}} = \underline{\mathbf{C}}\ \ \dot{\mathbf{E}}$	in Ω;	$\dot{\boldsymbol{\sigma}} = \underline{\mathbf{c}}\ \ \dot{\boldsymbol{\epsilon}}$	in ω;
$\dot{\mathbf{U}} = \dot{\bar{\mathbf{U}}}$	on $\partial\Omega_U$	$\mathbf{u}(\mathbf{x}) = \mathbf{u}^*(\underline{\mathbf{E}}) + \mathbf{u}^p(\mathbf{x})$	on $\partial\omega_U$;
$\underline{\mathbf{N}}\dot{\boldsymbol{\Sigma}} = \dot{\mathbf{T}}$	on $\partial\Omega_T$		

Table 5.1: Summarizing table

5.6 FE solution alghorithms

As for the first order computational homogenization, the FEM has been used to discretize both levels problems.

5.6.1 Discrete problem at the micro-level

At this level the imposition of the *BVP* is carried out via the use of Lagrange multipliers as in the first order standard scheme. In this case, however, also the additional integral conditions have to be imposed using the same technique. As above-mentioned, indeed, additional integral conditions have to be imposed when the enriched formulation is considered. The integral expressions initially defined on the whole domain of the *RVE* (refer to5.4.1) can be simplified by straightforward manipulations. Thus the conditions are fulfilled by simply imposing two line integrals:

$$(5.75) \qquad\qquad \int_{\partial\omega_L} v^p d\partial\omega = 0, \qquad \int_{\partial\omega_B} u^p d\partial\omega = 0$$

The first expression means that the integral of the periodic vertical displacement components evaluated on one vertical edge of the *RVE* (*L*) is imposed to be identically equal to zero, in other words this is equivalent to impose that the vertical displacement components v, solution of the RVE, along one vertical edge have to be equal to the integral of the vertical displacements component derived by the kinematic map v^* on the same edge; similarly a dual integral condition is imposed on the horizontal displacement components on one horizontal edge (*B*).

(5.76)
$$\int_{\partial\omega_L} v\,d\partial\omega = \int_{\partial\omega_L} v^*\,d\partial\omega, \qquad \int_{\partial\omega_B} u^p\,d\partial\omega = \int_{\partial\omega_B} u^*\,d\partial\omega$$

The numerical form of expressions (5.76), by considering a composite trapezoid rule in the general case of not equispaced nodes, is:

$$\frac{1}{2}\triangle y_1\, v(1) + \sum_{i=2}^{N-1}\left(\frac{1}{2}\triangle y_{i-1} + \frac{1}{2}\triangle y_i\right)v(i) + \frac{1}{2}\triangle y_{N-1}\, v(N) =$$

(5.77)
$$\frac{1}{2}\triangle y_1\, v^*(1) + \sum_{i=2}^{N-1}\left(\frac{1}{2}\triangle y_{i-1} + \frac{1}{2}\triangle y_i\right)v^*(i) + \frac{1}{2}\triangle y_{N-1}\, v^*(N)$$

where N is the number of nodes on the vertical edge; $\triangle y_i$ is the distance, between node i and i+1.

$$\frac{1}{2}\triangle x_1\, u(1) + \sum_{i=2}^{M-1}\left(\frac{1}{2}\triangle x_{i-1} + \frac{1}{2}\triangle x_i\right)u(i) + \frac{1}{2}\triangle x_{M-1}\, u(M) =$$

(5.78)
$$\frac{1}{2}\triangle x_1\, u^*(1) + \sum_{i=2}^{M-1}\left(\frac{1}{2}\triangle x_{i-1} + \frac{1}{2}\triangle x_i\right)u^*(i) + \frac{1}{2}\triangle x_{M-1}\, u^*(M)$$

where M is the number of nodes on the horizontal edge; $\triangle x_i$ is the distance, between node i and i+1.

5.6.2   Discrete problem at the macro-level

As for the macro-level, the Cosserat 2D finite element has been implemented, by generalizing the Cauchy finite element. The additional degree of freedom for independent rotations has been considered and the debate modifications in order to expand the strain and stress descriptions have been afforded.
Both 4-node and 8-node isoparametric FE are used with one or four integration points.

In Figure 5.6 it is clearly represented the correspondence between each macro-level integration point and the related *RVE*. In the figure, by way of example, as for both discretization levels, bilinear 4 node elements with 4 integration points have been considered, but no restrictions are imposed in the applications.
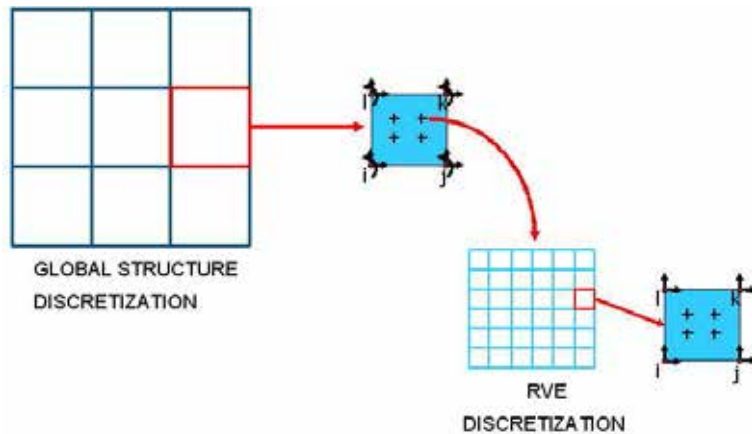

Figure 5.6: Shear test on masonry panel.

5.6.3 Numerical Applications

Influence of additional boundary conditions

In the framework of the Cosserat-Cauchy computational homogenization, the imposition of the bridge conditions between scales (i.e. kinematic map and averaged stresses) requires, as aforementioned, that the *RVE* is submitted to additional integral boundary conditions, in order to assure that the periodic fluctuation displacement fields do not produce any mean strain nor curvature. This means that, in the nested solution scheme, the deformed shape of the *RVE*, as a response of the input (deformation measure) received from the higher level, respects not only the periodicity conditions but also the integral conditions.

(a) *Horizontal extension* (b) Σ_X *field* (c) *Vertical extension*

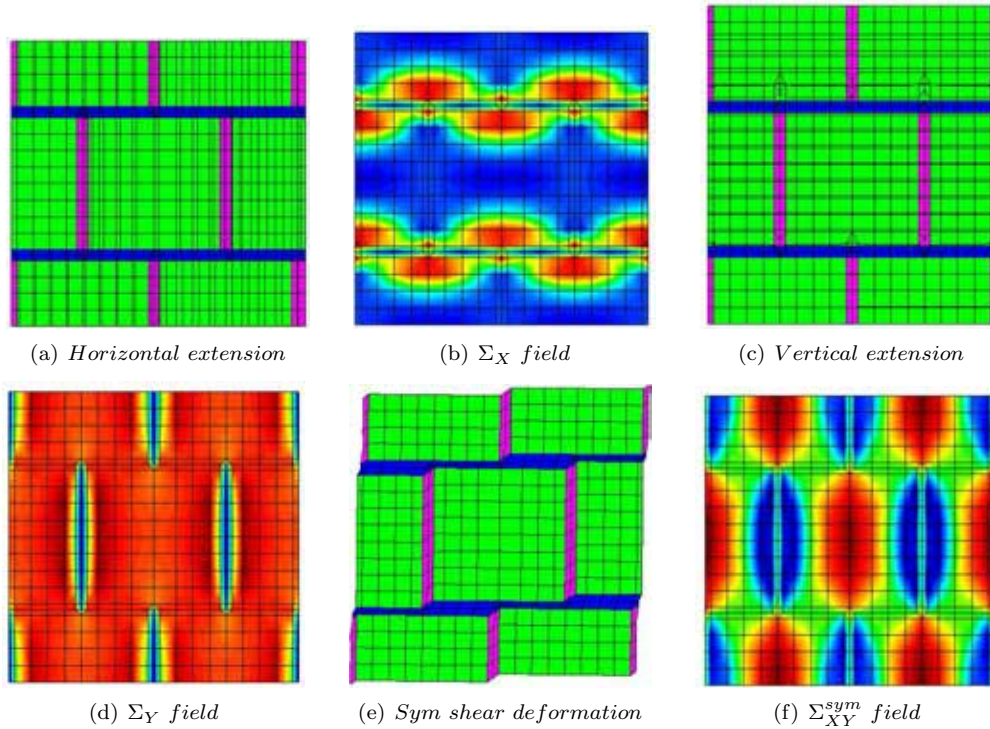(d) Σ_Y *field* (e) *Sym shear deformation* (f) Σ_{XY}^{sym} *field*

Figure 5.7: Cauchy simple deformation modes.

In the case of the enhanced computational homogenization, when a Cosserat continuum at the macro level is coupled with a Cauchy continuum at the micro one, it is not possible to strictly speak of "periodic" boundary conditions: as for the extensional and the symmetric shear modes nothing changes with respect to the Cauchy homogenization, but, when the additional Cosserat modes are taken into account, it is clear that the deformed shape is not periodic anymore.
In Fig.5.7 the deformed shapes (left column) and the associated prevalent periodic stress states (right column) are shown for the Cauchy deformation modes (two axial extensions and symmetric shear) considering the *RVE* of square blocks used in Casolo (2006) and presented in Section 4.7.1 for the Cauchy modes and in 5.6.3 for the additional Cosserat modes.
In Fig.5.8, instead, the deformed shapes (left column) and the associated prevalent non periodic stress states (right column) are shown for the Cosserat additional deformation modes (skew-symmetric shear and two flexures) considering the same *RVE* as before.

It is interesting to understand the effects of the additional condition on the deformed shape of the *RVE* and, as a consequence, on the estimation of the associated overall properties.

(a) *Skewsym shear*   (b) Σ_X *field*   (c) *Flexure K_x*

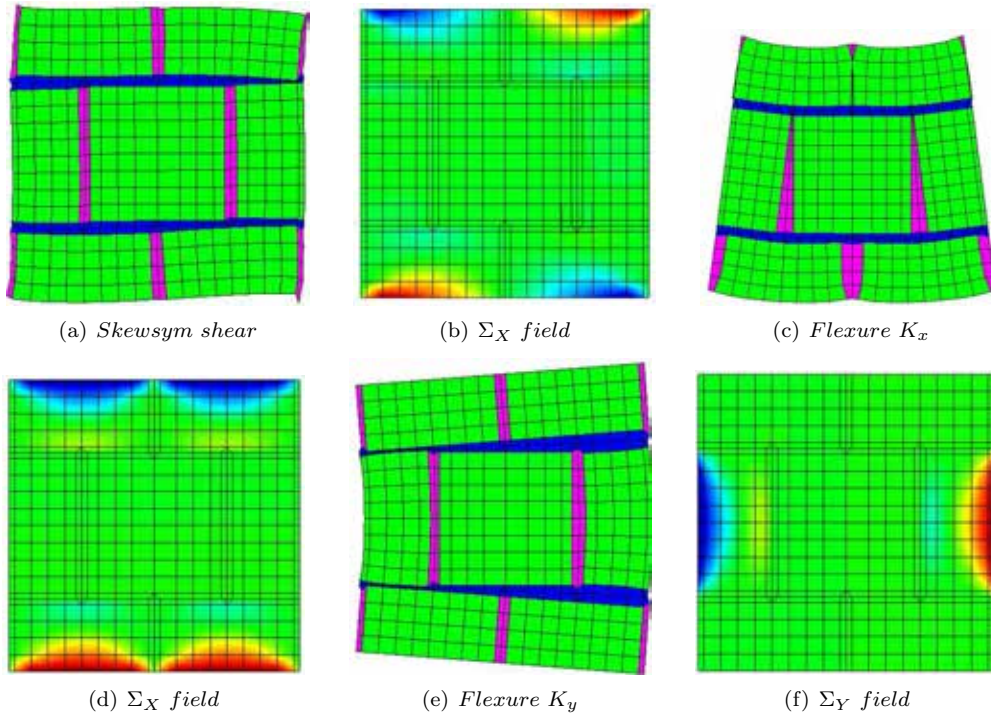(d) Σ_X *field*   (e) *Flexure K_y*   (f) Σ_Y *field*

Figure 5.8: Cosserat additional deformation modes.

In order to describe the influence of the integral conditions, four different *RVEs* have been considered both square and rectangular. They are shown in Figure 5.9.

For each *RVE*, the homogenized elastic constitutive matrix has been obtained both considering and

(a) *cross*   (b) *square*   (c) *blocks*   (d) 1 *block*
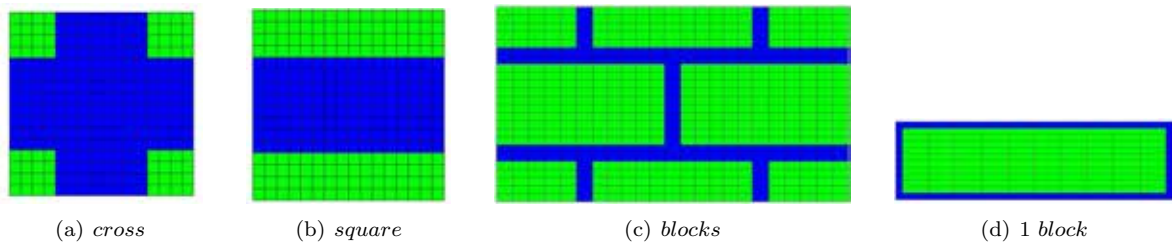
Figure 5.9: Cosserat additional deformation modes

discarding the additional boundary conditions.

The deformed shapes and related stress states associated to simple deformation modes have been analyzed. In Table 5.2 the results in terms of coefficient of the homogenized constitutive matrix are summarized for the four *RVEs*. For each case in the first row the results without additional boundary conditions are reported, while in the second row the respective with additional boundary conditions.

The additional integral conditions provide results in between the standard periodic boundary conditions and the fully prescribed displacement.

It is clear that the Cauchy simple deformation modes are not affected by the additional conditions, as the edges remain linear and the coefficients of the homogenized constitutive matrix are the same with or without additional boundary conditions.

		C_{1111}	C_{1212}	C_{2222}	C_{3333}	C_{3434}	C_{4444}	C_{55}	C_{66}
		Mpa	*Mpa*	*Mpa*	*Mpa*	*Mpa*	*Mpa*	*kN*	*kN*
cross	no a.b.c.	489.472	194.67	489.472	3143.1887	-2862.997	3143.1887	411728.212	411728.212
	a.b.c.	489.472	194.67	489.472	3143.1887	-2862.997	3143.1887	407834.44	407834.44
square	no a.b.c.	69557	5563	14359.088	57993.743	-51074.814	60293.666	25814.31	58635.44
	a.b.c.	69557	5563	14359.088	57993.743	-51074.814	60293.666	26387.327	59318.495
1 block	no a.b.c.	1203.47	251.29	1046.73	7998.1	-1134.96	13119	670619.66	5381595
	a.b.c.	1203.47	251.29	1046.73	7998.1	-1134.96	13119	674412.76	5524650.1
blocks	no a.b.c.	1143.16	243.52	997.38	8581.384	-3705	8758.53	2882069.46	5614297.435
	a.b.c.	1143.16	243.52	997.38	8581.384	-3705	8758.53	2896872.86	5660745.45

Table 5.2: Summarizing table

As for the skew-symmetric shear components, again, no differences are recognized.
Finally the stronger effects of the application of such conditions are evident in the case of the bending modes. Anyway the effect is quite low, in fact the differences with respect to the standard periodic boundary conditions are restricted to 2-3%.

In the Figures 5.10 and 5.11 the six deformation modes for the first presented *RVE*, the *cross* are shown by comparing the results without additional boundary conditions (left columns) and with them (right columns). It is noteworthy that the effect of such additional conditions is to create, for the bending modes, a local oscillating shape. The associated homogenized constitutive components are higher, thus the effect is to obtain a stiffer response.

(a) *Axial horizontal deformation E_X*

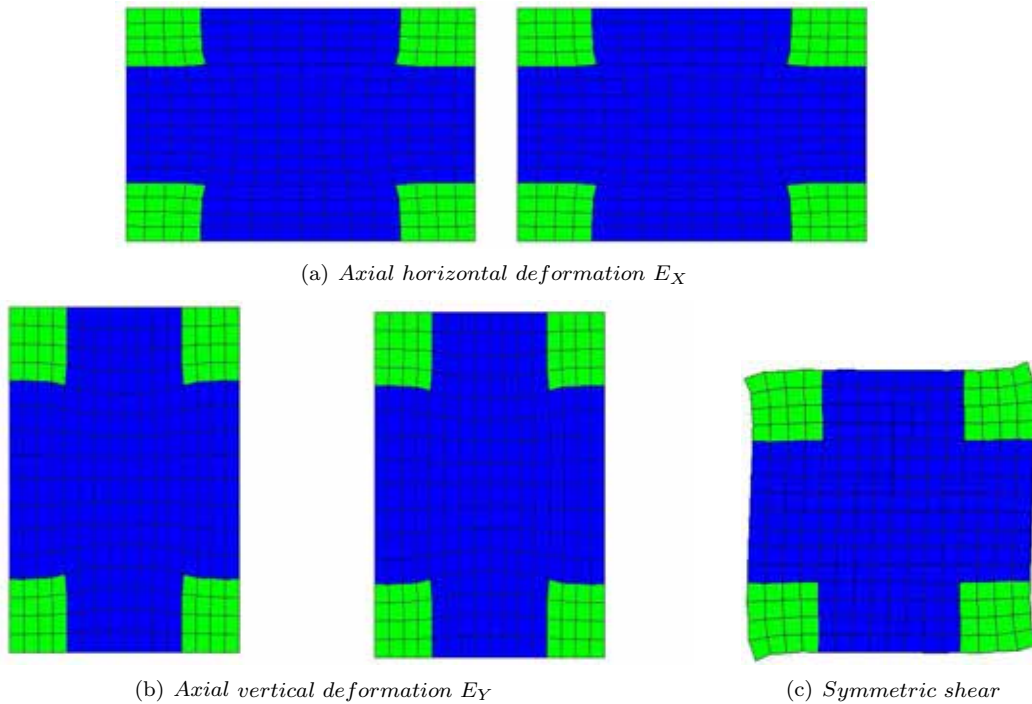(b) *Axial vertical deformation E_Y*   (c) *Symmetric shear*

Figure 5.10: Cauchy standard deformation modes. Results without additional boundary conditions (left column) and with additional boundary conditions (right column).

(a) *Skew-sym shear*
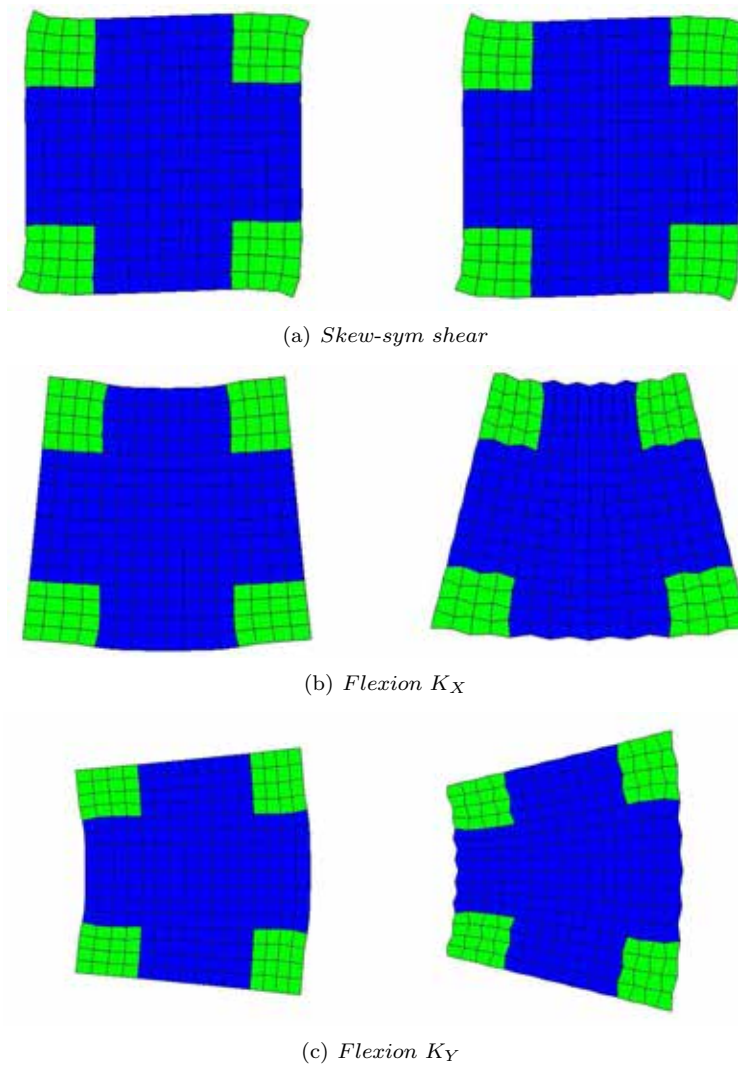

(b) *Flexion K_X*

(c) *Flexion K_Y*

Figure 5.11: Cosserat additional deformation modes. Results without additional boundary conditions (left column) and with additional boundary conditions (right column).

Masonry like structure RVE (Casolo)

The example proposed by Casolo (2006) and analyzed in Section 4.7.1 is, here, considered in order to show the additional Cosserat deformation modes and additional components of the homogenized elastic constitutive matrix. For geometric and material parameters refer to Section 4.7.1.

The simple additional Cosserat deformation modes are presented (see Figure 5.12).

In the following Figure 5.13 the most significant stress fields in the RVE due to single perturbation
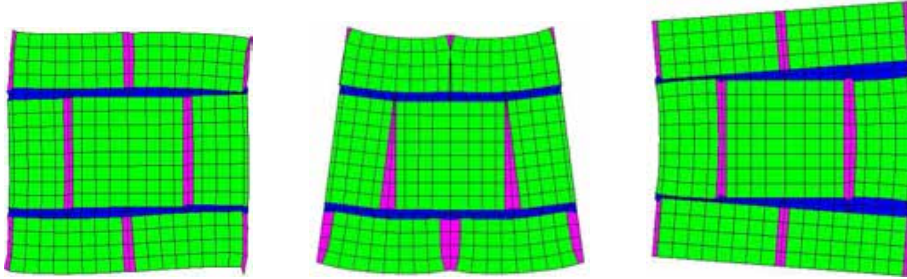

Figure 5.12: Deformation due to 1)Θ component; 2)K_X component; 3)K_Y component.

components are shown: in the first picture the σ_x strain field (corresponding to the fourth perturbation component, i.e. the application of macro-level Θ), in the second σ_x strain field (corresponding to the fifth perturbation component, i.e. the application of macro-level K_X), while in the third σ_y strain field (corresponding to the sixth perturbation component, i.e. the application of macro-level K_Y) are presented.

It is clear that the stress fields related to the additional Cosserat deformation modes are not periodic.
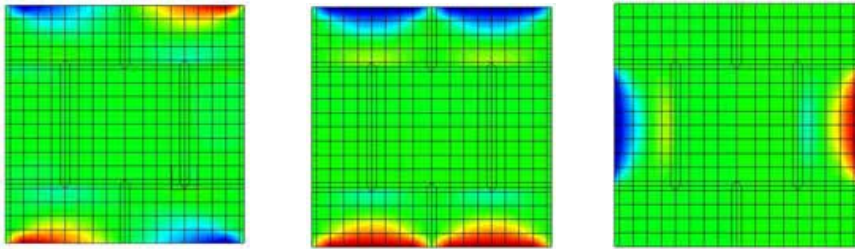

Figure 5.13: Strain fields 1) σ_x component due to Θ; 2) σ_x component due to K_X; 3) σ_y component due to K_Y.

In Table 5.3 the obtained values of homogenized constitutive parameters are presented both for Casolo and for the actual procedure: the residual components of the constitutive matrix with respect to the values presented in Section 4.7.1 are here shown. Casolo evaluates the shear modula by means of the two tests. The first one aims to reproduce symmetric shear and it is made considering a refined finite element mesh of the representative volume element with periodic displacement boundary conditions and loaded by anti-periodic shear stresses that have equal absolute value on all the four sides. The macroscopic values of E_{XY}^{sym} and Θ are measured on the deformed finite element mesh. The second test aims to reproduce, instead, a skew-symmetric shear state and it is performed by considering a representative volume element with displacement boundary conditions that produce null symmetric shear strain, while the periodic local couples are applied to the blocks. In this case the macroscopic quantity measured on the finite element meshes is the local rotation.

By merging the constitutive relations for these two tests, the unknown shear modula are obtained as a solution of a linear system. The differences are justified by the different way to apply the boundary conditions imposed to the RVE.

Author	C_{34}	C_{34}	C_{44}	C_{55}	C_{66}
Casolo	2.76	1.565	3.11	0.016	0.071
DeBellis	2.81	0.9	2.9	0.0146	0.0667

Table 5.3: Elastic parameters obtained for the same *RVE* by different authors; [MPa] for C_{33}, C_{34} and C_{44}; [N] for C_{55} and C_{66}

Cosserat patch test

With the aim of testing the correct formulation and implementation of the proposed multi-scale procedure a patch test properly conceived for Cosserat continua is performed. This test was introduced by Providas and Kattis (2002) in the framework of linear isotropic Cosserat elasticity.

As well known, considering a standard patch test for Cauchy continuum, boundary conditions on the boundaries of the considered domain are imposed in order to reproduce states of constant strains, the rigid body motions being eliminated.

As for the Cosserat elasticity, due to additional independent rotational degrees of freedom, particular conditions for displacement fields, body forces and couples, are required to guarantee the equilibrium with constant strains.

Providas and Kattis proposed a patch test on a rectangular region covered completely by a number of distorted, non overlapping triangular elements undergoing prescribed displacement and force fields. A plane strain assumption was used for the Finite element analysis.

In this work the test has been fit to the multi-scale procedure so it is necessary to define the meshes adopted at both levels.

In the Fig.5.14 the macro-level Finite Element mesh, constituted by five distorted quadrilateral elements, with 8 nodes and four integration points, is shown; in Fig. 5.15 the coordinates of the internal nodes are reported with respect to a 2D reference system [Oxy] with the origin in node 5.
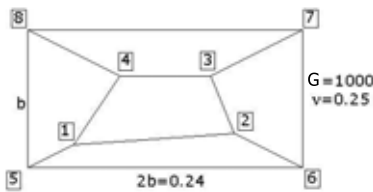
Node	x	y
1	0.04	0.02
2	0.18	0.03
3	0.16	0.08
4	0.08	0.08

Figure 5.14: Finite element mesh   Figure 5.15: Node Coordinates

As for the micro-level, a square *RVE* with unit edge is chosen and it is discretized with a mesh of 256 elements with biquadratic interpolation of the displacement field.

The test is passed if three different strain states, other than the classical strain states conceived for Cauchy medium, are properly reproduced:

1. constant strain with symmetric shear and zero curvatures;

2. constant strain with non-symmetric shear and zero curvatures;

3. constant curvatures;

In the sequel prescribed displacements and rotations on the boundary nodes and loading conditions on the whole domain are defined for the three aforementioned tests together with the expected solutions

in terms of stresses.

For *Test 1* the displacements fields are the following:

$$(5.79) \qquad u = 10^{-3}(x + \frac{1}{2}y); \quad v = 10^{-3}(x + y); \quad \phi = 10^{-3}(\frac{1}{4});$$

that is linear fields for the translational degrees of freedom and constant rotations. The nodal values are imposed to the the fixed nodes 5,6,7,8 and no body forces neither body couples are required to fulfill the equilibrium conditions. The test is passed if the following exact solution in terms of stress fields is recovered in the whole domain:

$$(5.80) \qquad \Sigma_{xx} = \Sigma_{yy} = 4; \quad \Sigma_{xy} = \Sigma_{yx} = 1.5; \quad M_x = M_y = 0;$$

In Fig. 5.16 the Finite Element solutions are shown where a perfect correspondence with the exact solution can be noted:
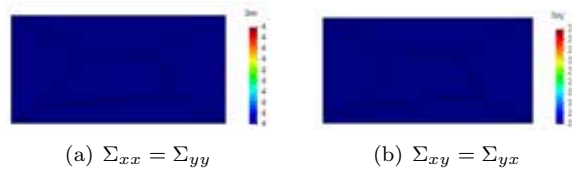

(a) $\Sigma_{xx} = \Sigma_{yy}$ (b) $\Sigma_{xy} = \Sigma_{yx}$

Figure 5.16: Stress state for patch *Test 1*

For *Test 2* the following displacement fields are chosen:

$$(5.81) \qquad u = 10^{-3}(x + \frac{1}{2}y); \quad v = 10^{-3}(x + y); \quad \phi = 10^{-3}(\frac{1}{4} + \frac{1}{4\alpha});$$

that is linear fields for the translational degrees of freedom and constant rotations (but this time depending on a Cosserat parameter i.e. $\alpha = \frac{G_c}{G}$). The nodal values are imposed to the fixed nodes 5,6,7,8 and no body forces and constant body couples ($q = 1$)are required to fulfill the equilibrium conditions. The solution expected in terms of stresses is:

$$(5.82) \qquad \Sigma_{xx} = \Sigma_{yy} = 4; \quad \Sigma_{xy} = 1; \quad \Sigma_{yx} = 2; \quad M_x = M_y = 0;$$

As before, the Finite Element solutions are in perfect agreement with the exact solution (see Fig. 5.17).
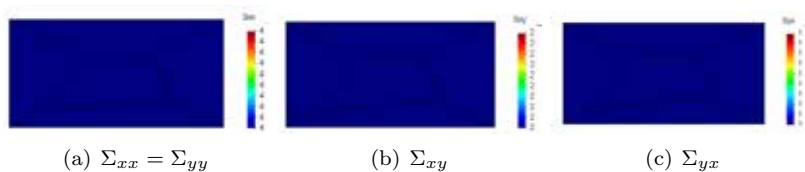

(a) $\Sigma_{xx} = \Sigma_{yy}$ (b) Σ_{xy} (c) Σ_{yx}

Figure 5.17: Stress state for patch *Test 2*

Until this point the ability of the element in simulating constat curvatures state has not been tested, therefore, for the last case, *Test 3*, linear fields both for translational and rotational degrees of freedom are considered.

$$(5.83) \qquad u = 10^{-3}(x + \frac{1}{2}y); \quad v = 10^{-3}(x + y); \quad \phi = 10^{-3}(\frac{1}{4} + \frac{1}{2\alpha}(x - y));$$

as usual, nodal values are imposed to the fixed nodes 5,6,7,8 and constant body forces $(p_x = p_y = 1)$ and linear body couples $(q = 2(x - y))$ are required to fulfill the equilibrium conditions. The solution is showed in term of the exact stresses in the expression 5.84and the numerical FE solution in Fig 5.18:

(5.84) $\qquad \Sigma_{xx} = \Sigma_{yy} = 4; \quad \Sigma_{xy} = 1.5 - (x - y); \quad \Sigma_{yx} = 1.5 + (x - y); \quad M_x = -M_y = \dfrac{2l^2}{\alpha};$
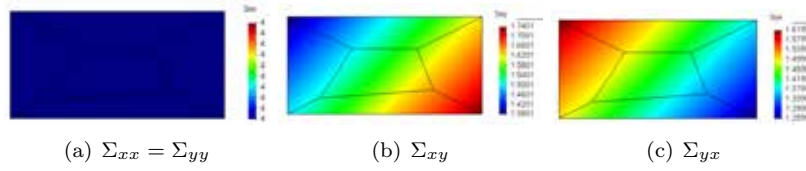

(a) $\Sigma_{xx} = \Sigma_{yy}$ (b) Σ_{xy} (c) Σ_{yx}

Figure 5.18: Stress state for patch *Test 3*

Linear elastic multilayered membrane

A simple test is here reproduced, similar to the one proposed by Forest and Sab (1998) in the framework of multi-scale Cosserat elasticity. A multilayered planar structure is considered at the macro-level (see Figure 5.20).

As for the boundary conditions, the left hand side is fixed, while on the right hand side of the structure a vertical uniform displacement is imposed.

The structure consists of two layers of different materials, for the sake of simplicity named "Hard" and "Soft"; in the following Table 5.19 the elastic properties of both materials are summarized:

Material	E [Mpa]	ν
Hard	210000	0.3
Soft	1000	0.3

Figure 5.19: Material parameters.

The global dimensions are 6x8 mm and at the micro-level a square *RVE* is considered (edge lenght 1 mm) constituted by two soft half layers surrounding a central hard layer (see Figure 5.20 right side) and the volume fraction of each component is 0.5. Plane strain assumption have been adopted.
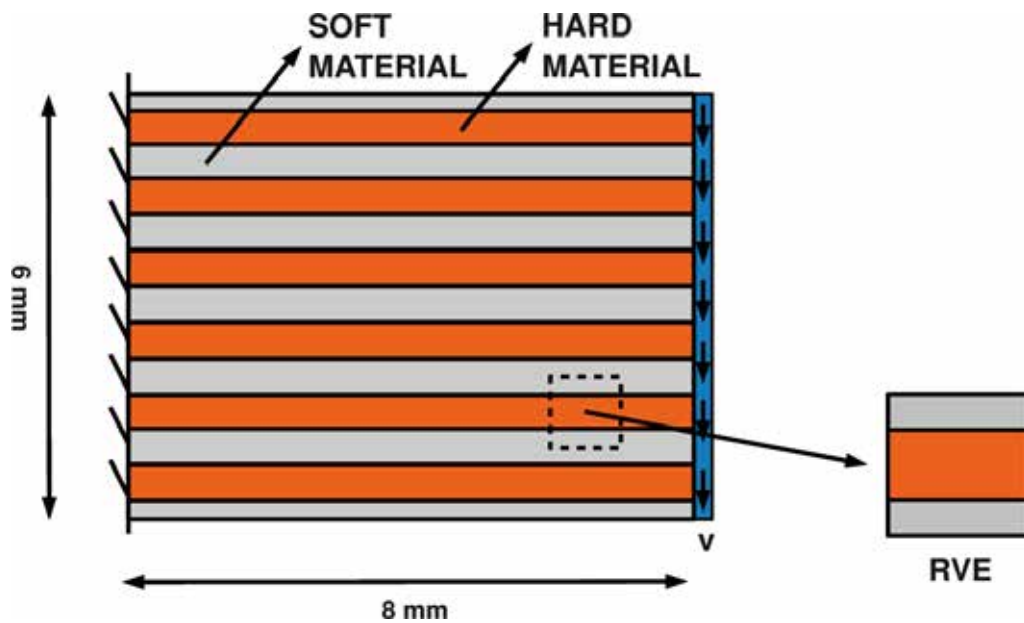

Figure 5.20: Geometry, boundary and loading conditions for elastic layered structure; definition of the *RVE*.

The aim of this example is two-fold:

1. to test the correct working of the implemented two-scale Cosserat-Cauchy computational homogenization finite element program;

2. to perform a direct quantitative comparison, in terms of displacements, between the results of a finite element micro-model and the respective obtained with the multi-scale procedure.

In order to fulfill the proposed objectives the following steps have been taken.
A micro-model has been realized, using 3072 4-node isoparametric elements with four integration points. A standard finite element program in linear elasticity has been adopted. In Figure 5.21 the deformed shape of the structure, with this micro-model, is shown.
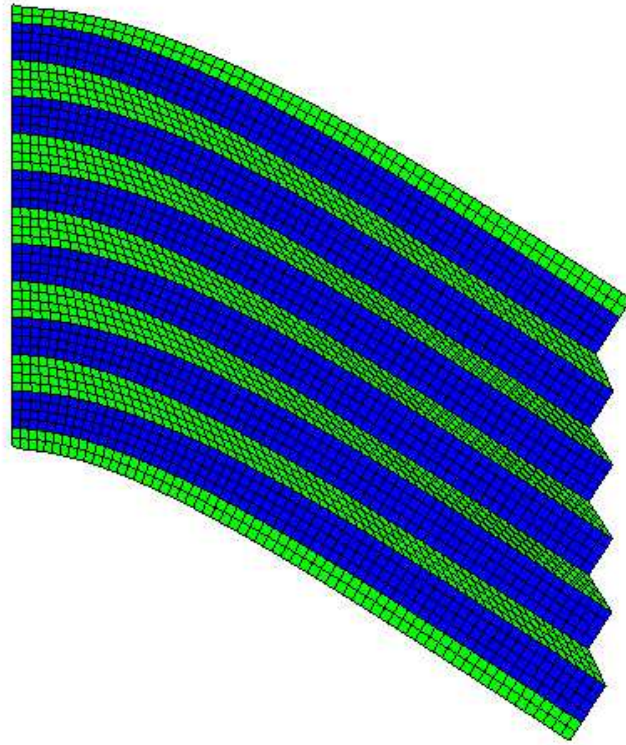

Figure 5.21: Simple Cosserat deformation modes for the *RVE* .

As second step, the values of the effective elasticity constants, i.e. the components of the homogenized constitutive tensor, have been obtained considering an *RVE* discretized by using 256 elements with 8 nodes and 4 Gauss points (in order to avoid shear locking) and 4 integration point per element.
In table 5.5 the results are shown:

	C_{1111}	C_{1212}	C_{2222}	C_{3333}	C_{3434}	C_{4444}	C_{55}	C_{66}
	Mpa	Mpa	Mpa	Mpa	Mpa	Mpa	kN	kN
De Bellis	131617	22420	32274	57320	-55983	57320	2510	3003

Table 5.4: Summarizing table: effective elastic constants

In the Figure 5.22 the six simple deformation modes, obtained as superposition of kinematic map and

periodic fluctuation field of the *RVE*, are shown. The shear components have been obtained by separating the symmetric and the antisymmetric parts of the deformation tensor.
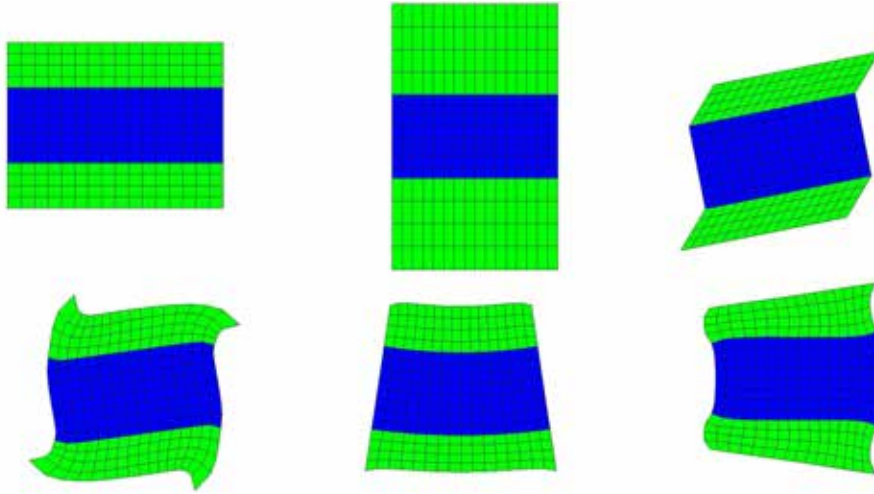

Figure 5.22: Simple Cosserat deformation modes for the *RVE* .

As a linear elastic analysis is performed, in this case the fully coupled multi-scale procedure is redundant because additional computational costs are required with respect to a macro-model Cosserat membrane analysis afforded with the obtained homogenized constitutive modula.

The third step, hence, has been the adoption of the homogenized constitutive modula as input data for a macro-model Cosserat membrane and, finally, in order to test the multi-scale program, the fully coupled multi-scale analysis has been anyway performed.

The vertical displacements of the points of the macro-level model along an horizontal abscissa corresponding to the hard material at the mid height of the structure is finally measured. A direct comparison between the aforementioned displacements obtained with a homogenized Cauchy model, the homogenized Cosserat model and the micro-mechanical model is proposed.

In Figure 5.23 the blue solid curve represents the response of the micro-model, considered as exact solution. The red curve is the solution of the homogenized Cauchy model with 48 quadrilateral elements with 8 nodes (a finer mesh has also been considered leading to the same result). The three remaining curves are obtained with the homogenized Cosserat model considering different discretizations with quadrilateral 4-nodes elements. It is clear that the exact solution is reached from above by refining the mesh from 24 elements (the green solid curve), passing to 48 elements (the violet solid curve), up to 96 elements (the light-blue dashed curve).

No differences in terms of displacements are found by comparing the results obtained, by fixing the same macro-level discretization, between the fully-coupled multi-scale technique and the homogenized Cosserat model.

Hereafter some results obtained with the multi-scale procedure are presented.

The deformed shape of the structure is shown in Figure 5.24 together with the deformed shape of the *RVEs* corresponding to five representative macroscopic points. It is clear that the *RVEs* nearest to the clamped end undergo a mixed shearing and bending deformation mode, while, moving towards the free end, only shearing mechanisms are left.

As for the stress fields, in Figures 5.25 and 5.26 the Σ_X and Σ_Y distributions are shown and also the respective micro-level fields are reported corresponding to three macroscopic points.
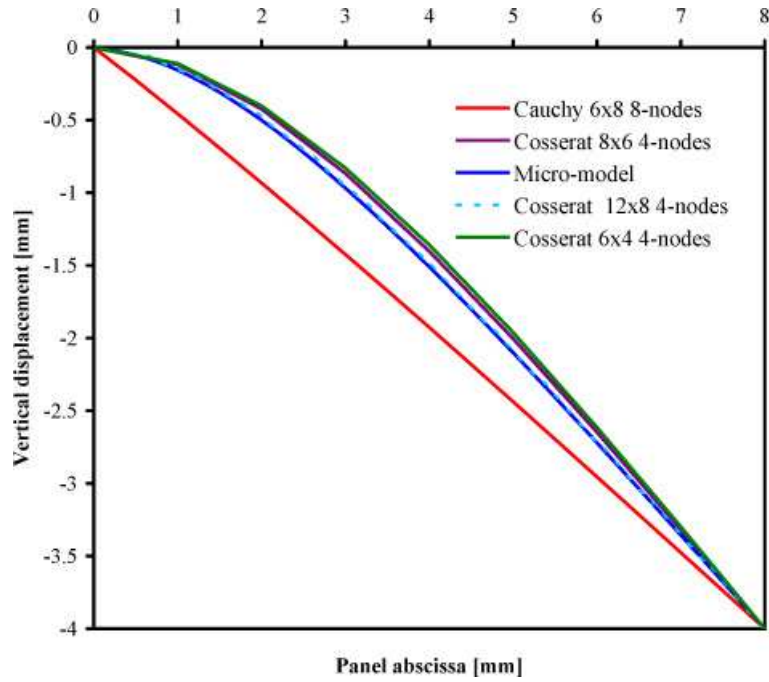
Figure 5.23: Comparison between the response of the Cauchy continuum, the reference micro-mechanical structure and the Cosserat multi-scale procedure.
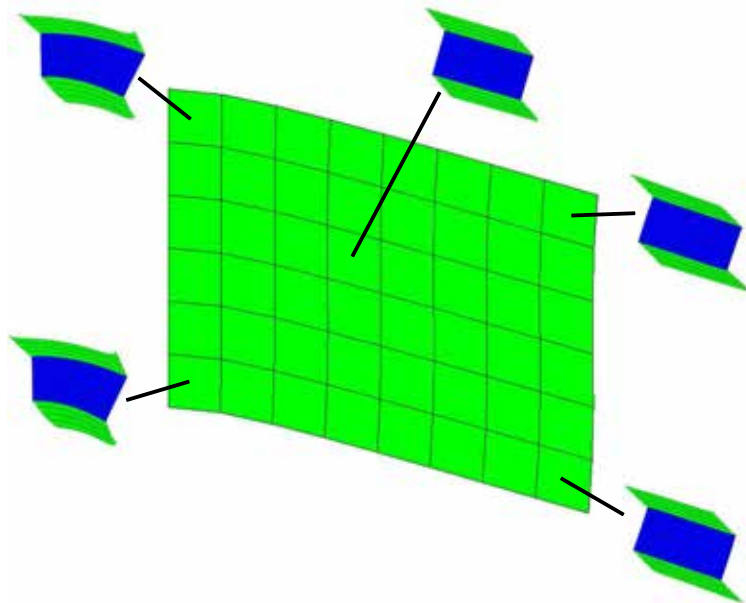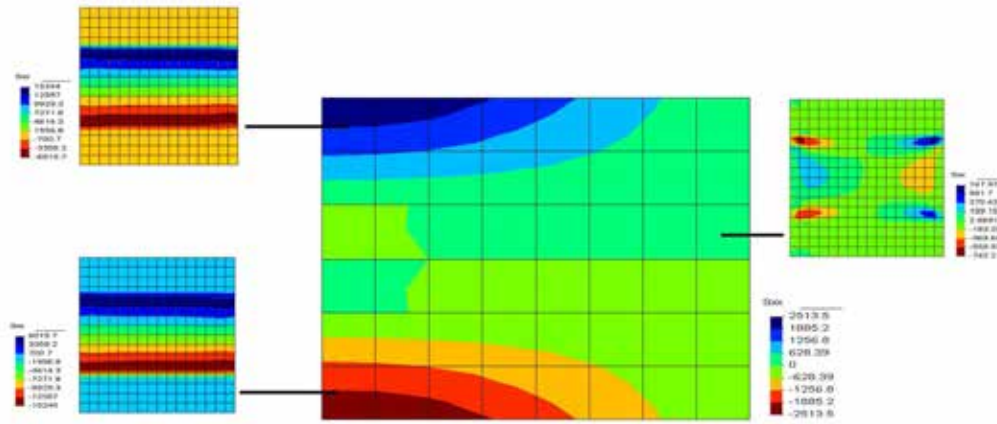

Figure 5.24: Macro and micro deformed shapes.
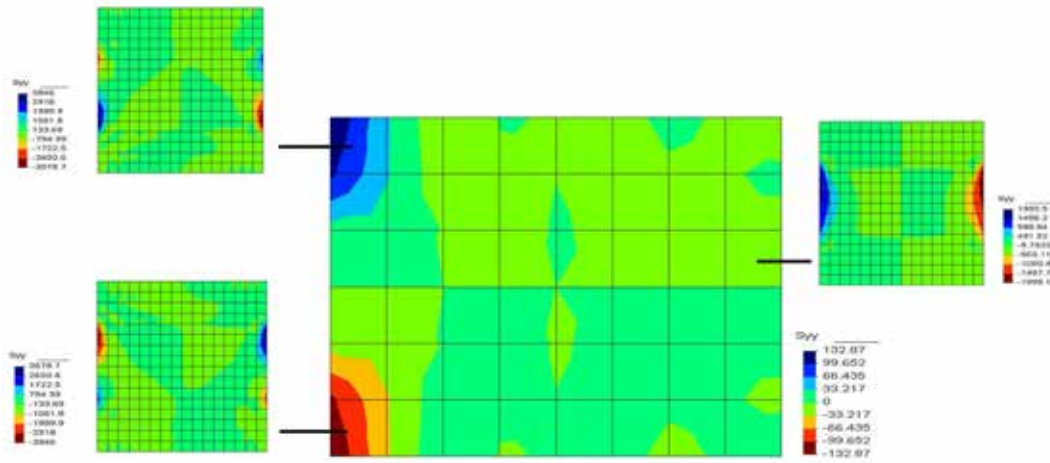
Figure 5.25: Macro and micro Σ_{xx} field.

Figure 5.26: Macro and micro Σ_{yy} field.

Full masonry wall: non-linear damage shearing test

A test on a shearing wall proposed by Massart (2003) is performed. The test is conceived on the basis of experimental results obtained by Raijmakers and Vermeltfoort (1992) on a panel of running bond masonry of dimensions 1000 x 1000 x 100 mm^3 made of bricks of dimensions 210 x 52 x 100 mm^3. For this experiment the ratio between macro and micro scale is very small (in practice no separation of scales exists) and the multi-scale procedure cannot be used. This is the reason why Massart designed a new test, by enlarging the dimensions of the panel 3000 x 3000 x 100 mm^3 and by reducing the dimensions of the single brick 140 x 65 x 100 mm^3, with the same boundary conditions, in order to qualitatively compare the results in terms of cracking evolution.

Massart developed a multi-scale framework, based on the first order computational homogenization, with a dedicated scale transitions obtained by introducing strain discontinuities that define a localization band on the *RVE* when macroscopic localization is detected.

In Fig. 5.27 the geometry of the panel together with the boundary and loading conditions are shown.

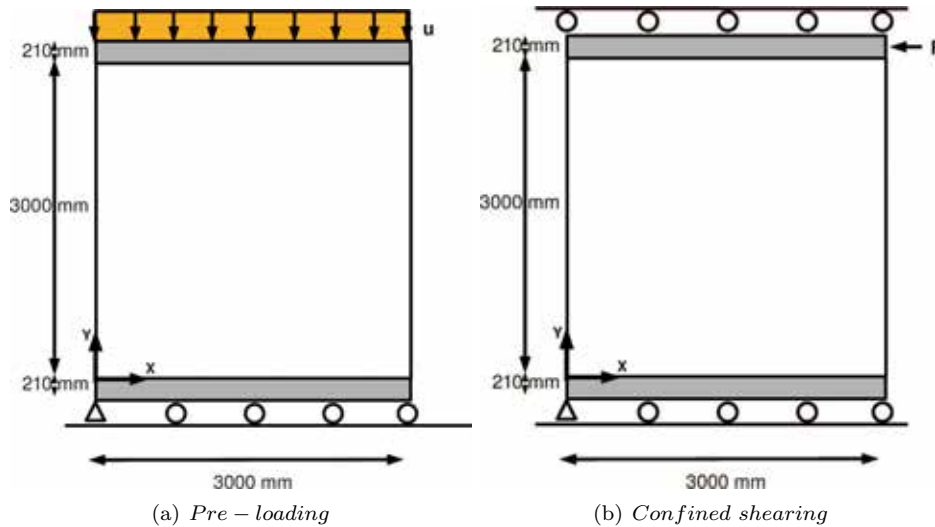(a) *Pre − loading*   (b) *Confined shearing*

Figure 5.27: Geometry and two-phases loading conditions for the shear masonry wall.

Two loading phases are imposed: an initial compressive load of 150 kN (see Fig.5.27(a)) followed by a confined shearing phase (Fig.5.27(b)). In order to better reproduce the actual experimental boundary conditions on the top and bottom edges of the wall, two stripes of elastic elements have been used, with a concrete-like stiffness.

In the numerical simulation, the structure is discretized by using an unstructured mesh of 126 triangular elements with a single integration point per element (see Fig.5.29). About the same mesh has been used by Massart (114 triangular elements).

A Plane stress assumption is used.

Damage isotropic laws are adopted, with different threshold in compression f_c and in traction f_t, both for bricks and mortar joints. Refer to the Appendix A where the constitutive model is presented.

At the micro-level the regularization technique is based on the fracture energy G_f.

The mechanical parameters adopted by Massart for bricks and for mortar joints respectively are summarized in Table 5.28:

The choice of the *RVE* requires a brief discussion.

Massart employs an *RVE* formed by 1 brick surrounded by half mortar joint (i.e. 5 mm) discretized by using 396 elements with a biquadratic interpolation of the displacement field. In order to reproduce

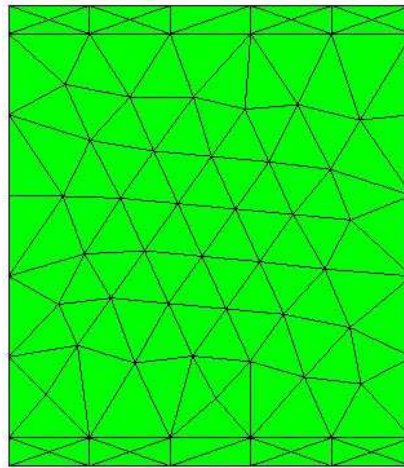| Material	E [Mpa]	ν	G_f [Nm/m^2]	f_t [Mpa]	f_c [Mpa]
Brick	16700	0.15	16.2	0.75	15
Mortar	3900	0.2	9	0.13	5.6
Concrete	24800	0.2	-	-	-

Figure 5.28: Material parameters.

Figure 5.29: $Mesh\ at\ the\ macro-scale$: 126 $triangular\ elements$.

the running bond arrangement, cross periodicity conditions on the top and bottom horizontal edges are imposed, i.e. the half right top edge is periodic with the half left bottom edge (a similar relation arises between top left and bottom right).

In the framework of the Cosserat model, adopted in the present macroscopic homogenization model, the actual dimensions and the shape of the RVE are essential in order to define the effective elastic constants of the composite material, being those constants dependent not only on the volume fraction and respective arrangement of the constituents but also on their absolute sizes.

Thus, with the aim of properly defining an RVE for such a case of analysis, a comparison is performed in terms of elastic constitutive tensors for different$RVEs$.

In Figure 5.30 the RVE used by Massart is shown (named RVE^1): it is the minimum periodic unit that can be considered in the framework of a first order homogenization based on the Cauchy continuum.

In Figure 5.31, instead, RVE^2 is a square RVE obtained considering the minimum portion of running bond masonry periodically repeated (if cross periodicity conditions are discarded). In the same Figure 5.31 RVE^3 and RVE^4 are obtained respectively by duplicating and quadruplicating the RVE^2.
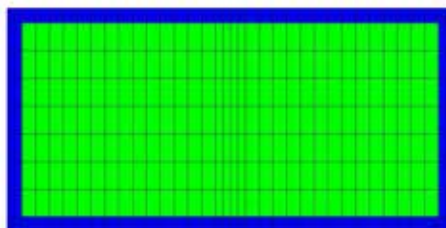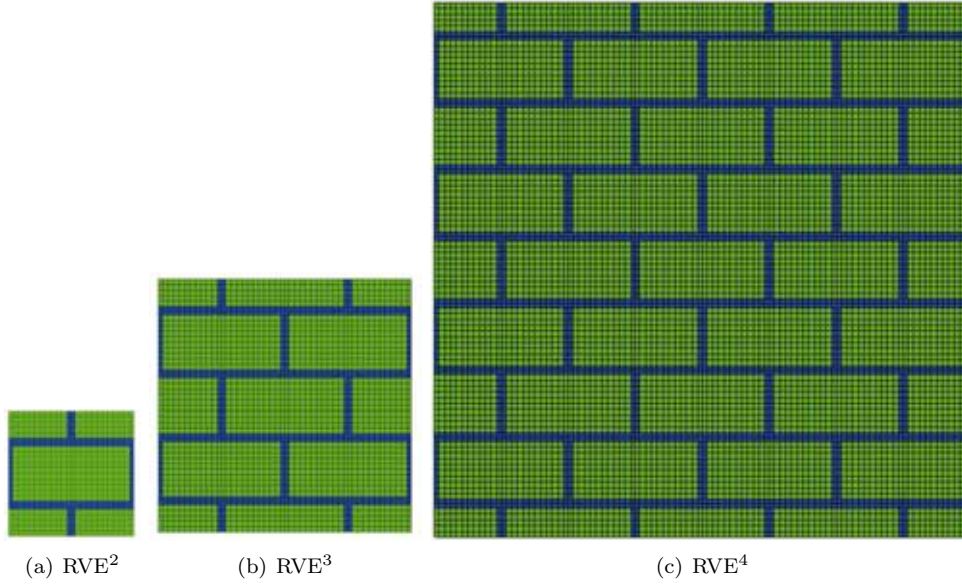

Figure 5.30: RVE^1: 396 $elements$.

(a) RVE^2 (b) RVE^3 (c) RVE^4

Figure 5.31: The three meshes contains 625, 2500 *and* 10000 *elements*, respectively.

	C_{1111}	C_{1212}	C_{2222}	C_{3333}	C_{3434}	C_{4444}	C_{55}	C_{66}
	Mpa	Mpa	Mpa	Mpa	Mpa	Mpa	kN	kN
RVE^1	12903.9	1721.7	11458.7	37594	-21886.3	98922.96	4908675.07	7857469
RVE^2	12910.7	1726	11464	64502	-55001	63891	25066286	21157905
RVE^3	12910.7	1726	11464	63462	-54379	63160	97738919	85192729
RVE^4	12910.7	1726	11464	63618	-54560	63541	387654887	341379545

Table 5.5: Summarizing table: effective elastic constants

In Table 5.5 the results in terms components of the homogenized constitutive tensor, obtained for the different *RVEs* discretized with 4-node elements with four integration points, are collected.
As expected, the axial components remains substantially the same for the four *RVEs* (the maximum observed difference is 0.2%) as those characteristics are not affected by size effects and being obtained on the basis of simple averages of stress fields on the volume of the *RVE*. It is, thus, recovered that RVE^1 and RVE^2 are perfectly equivalent if used in the first order computational homogenization and, clearly, RVE^1 has to be preferred being smaller than the other.
As for the shear components, a very considerable difference is detected between the values of RVE^1 and the remaining three others, while the values remain substantially unchanged (the maximum observed difference is 1.6%) in the cases of RVE^2, RVE^3, RVE^4. The reason is that the shear components are strongly affected by the shape of the *RVE* (RVE^1 is the only one rectangular, while the others are square), and, instead, if the same shape and the same microstructural respective arrangement of bricks and mortar joints are maintained the values are almost constant (as in the case of RVE^2, RVE^3, RVE^4).
Taking into account again RVE^2, RVE^3 and RVE^4, a transformation rule can be defined for the bending components, passing from one *RVE* to another:

(5.85) $$C_{ii}[\text{RVE}^2] = \left(\frac{l_2}{l_3}\right)^2 C_{ii}[\text{RVE}^3] = \left(\frac{l_2}{l_4}\right)^2 C_{ii}[\text{RVE}^4], \quad i = 5, 6$$

where l_2, l_3, l_4 are the edge dimensions for RVE^2, RVE^3 and RVE^4, respectively.
Since the bending components, keeping the respective arrangement of constituents, depend on the shape

and on the dimensions of the *RVE* very different properties are found in the case of RVE$_1$.

This analysis shows that, in the case of the actual homogenization technique based on the Cosserat continuum, the RVE^1 is not equivalent (not even up to a scale factor) to the other three *RVEs*. Instead RVE^2, RVE^3 and RVE^4 are equivalent between them up to a scale factor. This is the reason why in the following numerical example the RVE^2 has been adopted (the smallest reproducing conveniently the behavior of running bond masonry).

In Fig. 5.32 a comparison in terms of load-displacement curves in the shear loading phase between results obtained by Massart (the green dashed curve) and by the present approach (blue solid curve) is carried out. A good agreement is found out and it appears that the present approach provides a stiffer response. This is reasonable due to the presence of the flexural stiffness components. In the curve the points A, B and C are fixed: the following local and global results are referred to that points of the analysis.
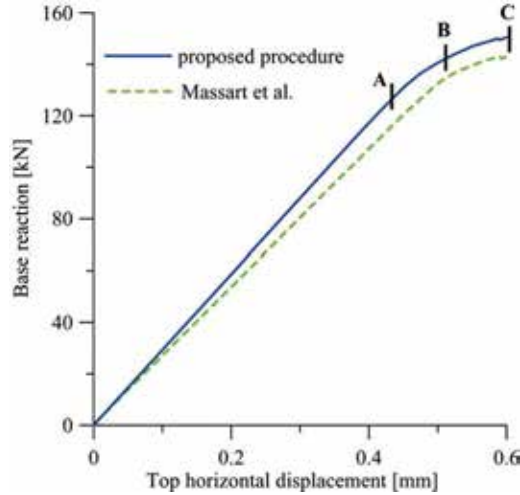

Figure 5.32: Comparison between the global response curves obtained with the proposed procedure and by Massart (2003).

In Fig.5.33 the macroscopic deformed shape of the structure together with the deformed shapes of five *RVEs* are shown (corresponding to point A in the global load-displacement curve). It is clear that in the bottom right and top left regions flexural modes are dominant (see point 1 and the respective); in the central region of the panel an about symmetric shear mode is obtained, while in the top right and bottom left regions the deformation modes are characterized both by shear and flexure.

In the sequel, for the same global point A, the macroscopic strain tensors, corresponding to three representative points of the structure (points 1, 2 and 3 in Figure 5.33), are presented: these tensors are the input information received by the *RVEs* in the form of kinematic map.

$$\mathbf{E}_1 = \begin{pmatrix} -4.63 \cdot 10^{-6} \\ +1.04 \cdot 10^{-6} \\ -6.26 \cdot 10^{-6} \\ +2.60 \cdot 10^{-7} \\ 0.0 \\ -9.00 \cdot 10^{-8} \end{pmatrix} \qquad \mathbf{E}_2 = \begin{pmatrix} +7.00 \cdot 10^{-6} \\ -4.98 \cdot 10^{-5} \\ -4.47 \cdot 10^{-5} \\ +4.10 \cdot 10^{-7} \\ -3.00 \cdot 10^{-8} \\ -6.00 \cdot 10^{-8} \end{pmatrix} \qquad \mathbf{E}_3 = \begin{pmatrix} +9.69 \cdot 10^{-6} \\ -9.51 \cdot 10^{-5} \\ -1.99 \cdot 10^{-5} \\ -1.25 \cdot 10^{-6} \\ 0.0 \\ 0.0 \end{pmatrix}$$

Point 1 is characterized by a state of low vertical traction combined with uniaxial bending; point 2 is characterized by a state of vertical compression, bending and also symmetric shear; finally, in point 3, a slightly higher vertical compression is coupled with a weak symmetric and skew-symmetric shear.
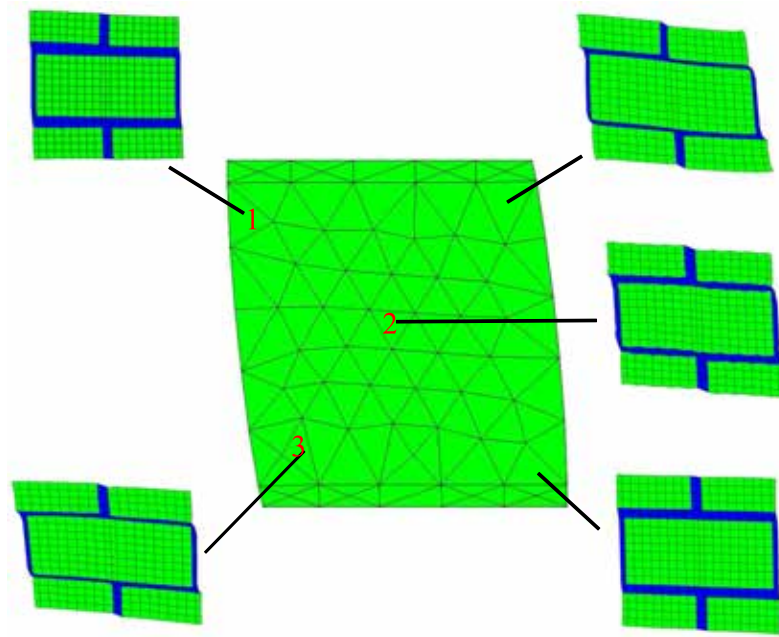
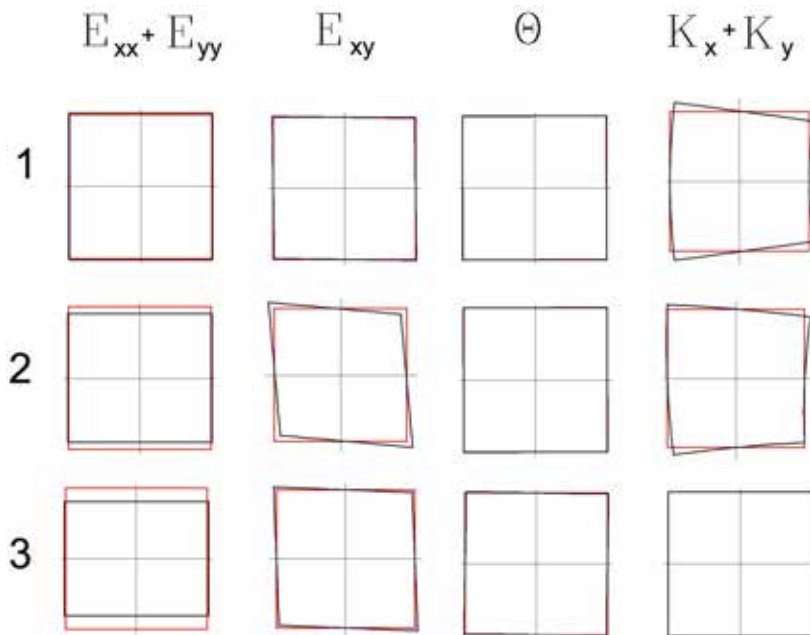Figure 5.33: Macro and micro deformed shapes.

Figure 5.34: Graphic visualization on a square *RVE* of the homogenized strain tensor passed as input data to points 1, 2 and 3 of the panel, for the point A of global curve. The scale factor is 10^4 for the deformed shapes shown in the first three columns, while 10^5 for the last one.

As for the stress and damage distributions, it is important to qualitatively understand the experimental response of the panel.

Fig.5.35 shows the damage mechanisms evolution and the orientation of cracks experimentally observed by Raijmakers and Vermeltfoort (1992). Depending on the value of the pre-compression load, as Massart underlined, a different global behavior can be observed.

In the actual case, a first phase of the shearing load is characterized by the appearance of horizontal tensile cracking, at the top and bottom zones of the panel, on opposite sides with respect to the application of the horizontal load. Successively, with the increasing of the shearing force, a diagonal crack appears in the central zone of the panel and, finally, failure is reached with a compressive crushing.
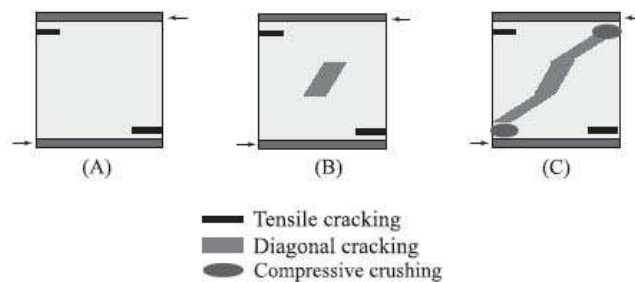

Figure 5.35: Crack distribution evolution.

With reference to points A, B and C in Fig. 5.32, the maps of representative stress and damage distributions are presented in Figures 5.36, 5.37, 5.38, 5.39, 5.40 and 5.41.

At point A, the vertical stress distribution Σ_Y is plotted both for the global structure and for three *RVEs* corresponding to points 1, 2 and 3 in Figure 5.33. A diagonal compressive strut visibly appears.
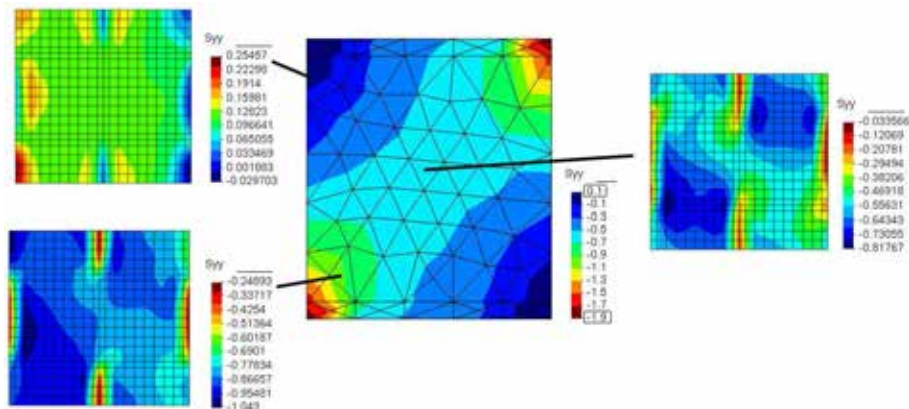
Figure 5.36: Macro and micro Σ_Y field (point A).

At point B, the symmetric shear stress Σ_{XY} is plotted, while at point C the horizontal axial stress is shown Σ_X (these choices are consistent with the Massart work). Qualitatively a good agreement has been found with the reference results.

In succession the damage distribution is shown for the global structure and for the most representative *RVEs*, corresponding to global points A, B and C.

In Figure 5.39 the macro and micro damage distribution are shown corresponding to point A of the global curve. The observed damage distribution is qualitatively compatible with the obtained experimental

Figure 5.37: Macro and micro Σ_{XY} field (point B).
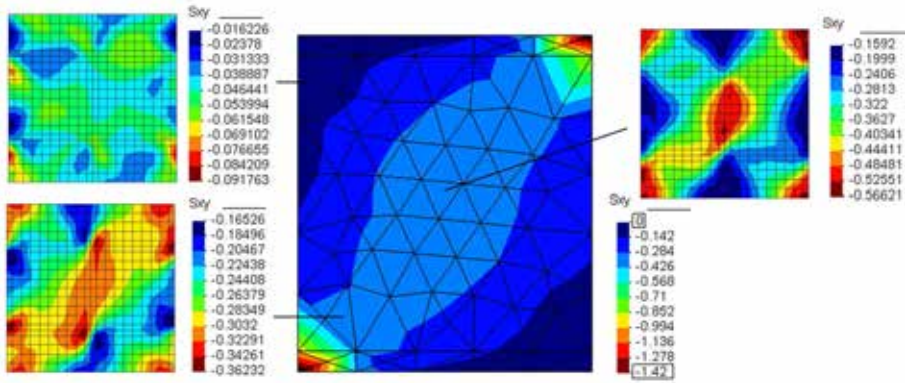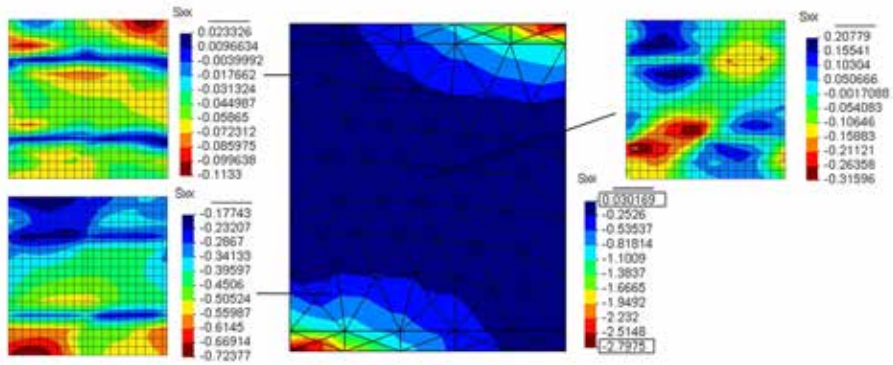

Figure 5.38: Macro and micro Σ_Y (point C).

results: in the first stage (point A) the bottom right and the top left corners of the panel show a damage concentration. This phase is characterized by typical bending damage distribution: the horizontal mortar joints are damaged in the zones where the tensile damage threshold is overcome.

In Figure 5.40, instead, the macro and micro damage distribution are shown corresponding to point B of the global curve.

It is clear, thus, that by proceeding with the shearing loading phase, the damage radiates out in a diagonal fashion towards the middle of the panel. A staircase damage distribution (confined into the vertical and horizontal mortar joints) is noticed for the *RVEs* corresponding to the middle zone of the panel where the central compressive strut is formed, as expected. In Figure 5.41, finally, the macro and micro damage distribution are shown corresponding to point C of the global curve.

In this last phase, the damaging process observed at point B is completely developed and the damaging mechanisms are totally formed.

With the multi-scale procedure, the damage is obtained at the micro-level: for each macro-level integration point, a corresponding damage distribution on the *RVE* is associated.

A homogenized measure of damage at the macro-level is still lacking.

An *ad hoc* definition of a scalar macro-level damage parameters is, therefore, here proposed. By observing the damage evolution at the micro-level, it is clear that two different evolution mechanisms are interesting the *RVEs*:

1. a so-called *mode 1* fracture for the *RVEs* corresponding to points at the right bottom and left top sides of the panel: in this case the damage is concentrated into the horizontal mortar joints;

2. a so-called *staircase* fracture mode for the *RVEs* corresponding to points towards the middle of the panel.

Once recognized the failure mode, for each *RVE*, the idea is to define a homogenized scalar damage value, varying between 0, when no damage appears, and 1, when all the elements, belonging to the respective damaging mechanisms at the micro-level, are completely damaged. In Figures 5.39, 5.40 and 5.41 the macro-level damage values are calculated on the basis of the aforementioned definition.
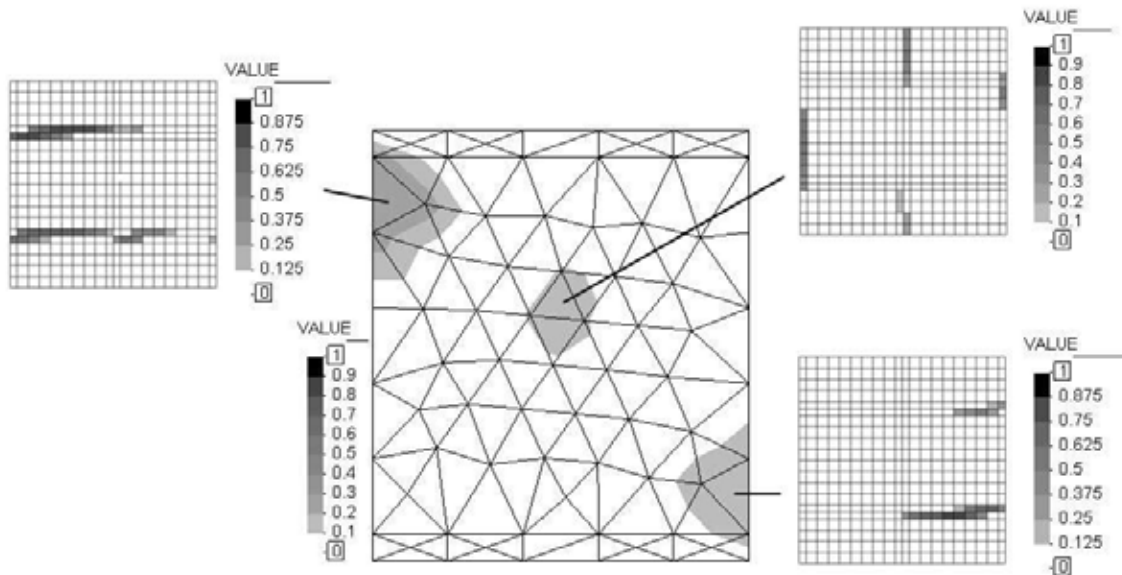

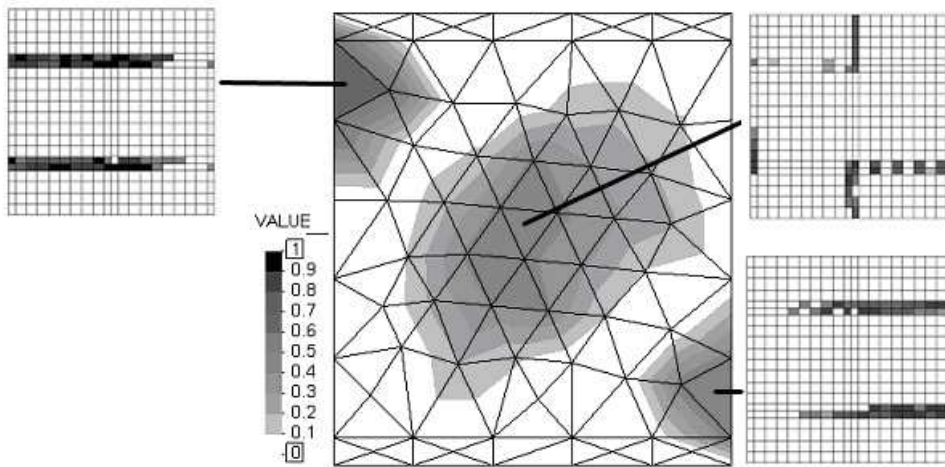Figure 5.39: Macro and micro damage distribution (point A).

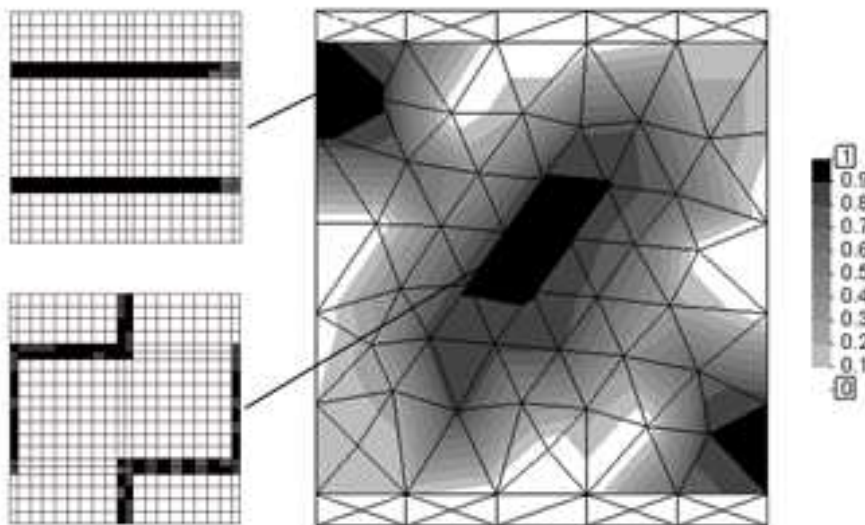Figure 5.40: Macro and micro damage distribution (point B).

Figure 5.41: Macro and micro damage distribution (point C).

Full masonry wall: Magenes experimental test

A a numerical simulation is performed on a rectangular panel under shear loading conditions. The response is compared with the experimental results obtained by Magenes (1992).

The dimensions of the panel are $1500 \times 2000 \times 380\,mm^3$, while the bricks ($250 \times 55 \times 120\,mm^3$) are arranged in Dutch bond with mortar joints of $10\,mm$. A vertical preloading of $1.2\,MPa$ is applied and a uniform horizontal displacement is imposed at the top edge. The geometry and boundary conditions are shown in Figure 5.42 (a). The bottom edge is completely restrained , while at the top edge, the horizontal displacement and the rotation are restrained during the preloading phase and in the second phase all three degrees of freedom are restrained. The selected RVE is a rectangular portion of masonry of $260 \times 130\,mm^2$ (Figure 5.42 (b)). The damage isotropic model described in Appendix A is adopted
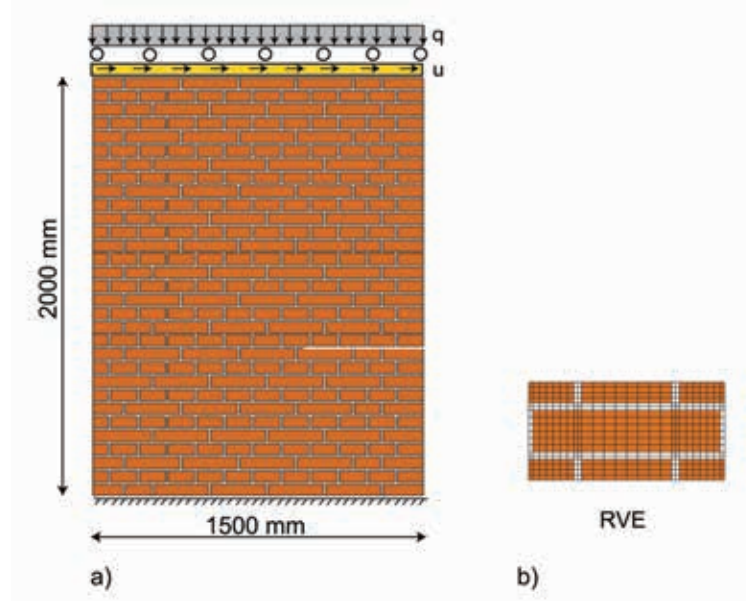
Figure 5.42: Shearing masonry panel: geometry and boundary conditions at structural level (a); RVE (b).

for both bricks and mortar joints.

The mechanical parameters assumed are the same as those reported by Magenes (1992)(except for the fracture energy which was not reported). See Table 5.6.

Material	E [MPa]	ν	G_f [Nm/m^2]	f_t [MPa]	f_c MPa]
Brick	6000	0.2	207.36	1.26	19.72
Mortar	2000	0.25	8.32	0.66	4.33

Table 5.6: Material parameters.

At the micro-level 468 quadrilateral FE for each RVE are used and the standard fracture energy regularization technique is employed. At the macro-level, instead, in order to highlight the inner regularization properties of the adopted Cosserat continuum, three different meshes are considered of 36, 81 and 144 elements, respectively. In Figure 5.43 the comparison between the global response curves obtained experimentally (continuous black curve) by Magenes (1992) and the ones evaluated with the proposed procedure (dashed curves) is shown. It should be noted that the three different meshes adopted at the

macro-level give an objective mesh-independent global response curve, confirming the effectiveness (for shear and bending predominant damaging mechanisms) of the Cosserat continuum in regularizing the numerical response in presence of strain-softening behavior. Furthermore, there is a satisfactory match
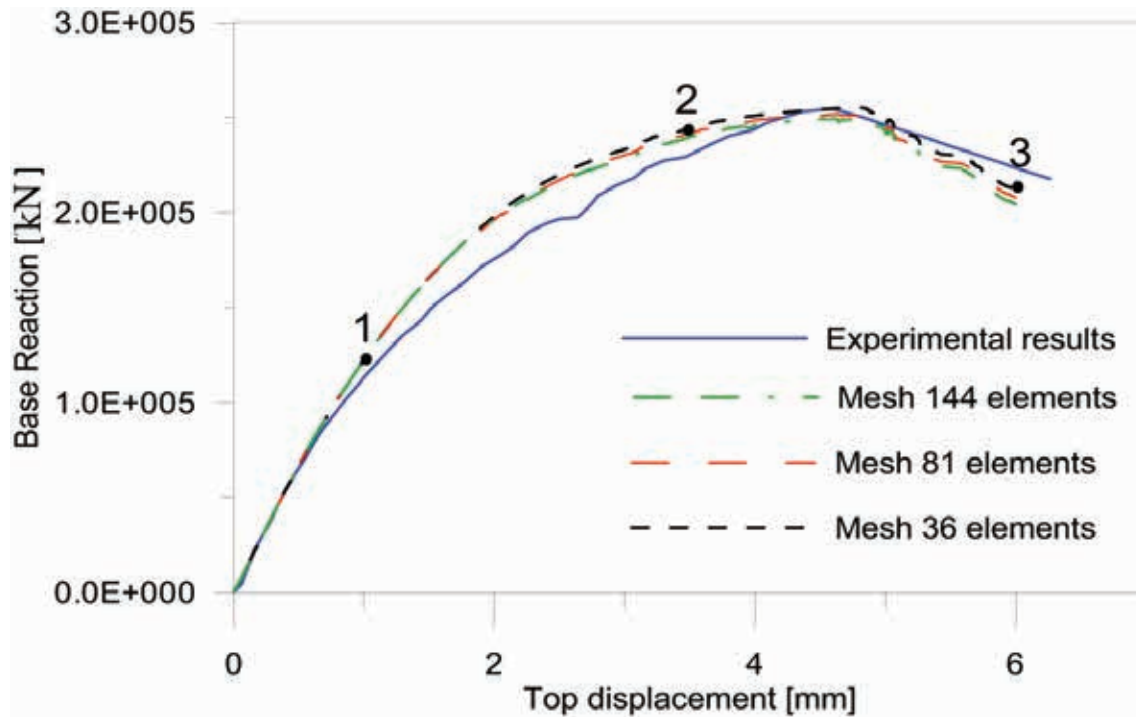

Figure 5.43: Shearing masonry panel: global response curves obtained experimentally by Magenes (1992) and numerically by the proposed procedure.

between experimental and numerical results: the initial stiffness is reproduced well together with the peak value and the post-peak softening trend. Even using a rough macro-level mesh (36 elements) it is possible to capture the dominant evolving mechanisms which characterize the global structural response. In Figures 5.44, 5.45 and 5.46 the vertical stress distribution in the panel, Σ_Y, is plotted (first row), the vertical stress σ_y (second row) and the damage distribution (third row) in three RVEs located at the top left (A), center (B) and bottom left (C) of the panel, corresponding to the points 1, 2 and 3 of the global curve (Figure 5.43), respectively.

Despite the lack of accuracy, due to the rough discretization of the macro-level, it is possible to observe the presence of typical and expected mechanisms. In fact, a diagonal compressive strut appears and grows. A pure symmetric-shear deformation mode appears in the RVE located at point B, while the ones placed at points A and C show coupled shear and bending deformation modes, as expected.
Different types of damage mechanisms are evident at points A, B and C. At point B, only the vertical and horizontal mortar joints are damaged following staircase patterns, while at points A and C, the bricks also start to damage. The RVE located at point C is the most severely damaged due to the combined effect of shear and flexure.

Figure 5.44: Shearing masonry panel: vertical stress distribution at macro-level (first row), vertical stress distributions in the RVEs (second row), damage distribution in the RVEs (third row).

Figure 5.45: Shearing masonry panel: vertical stress distribution at macro-level (first row), vertical stress distributions in the RVEs (second row), damage distribution in the RVEs (third row).
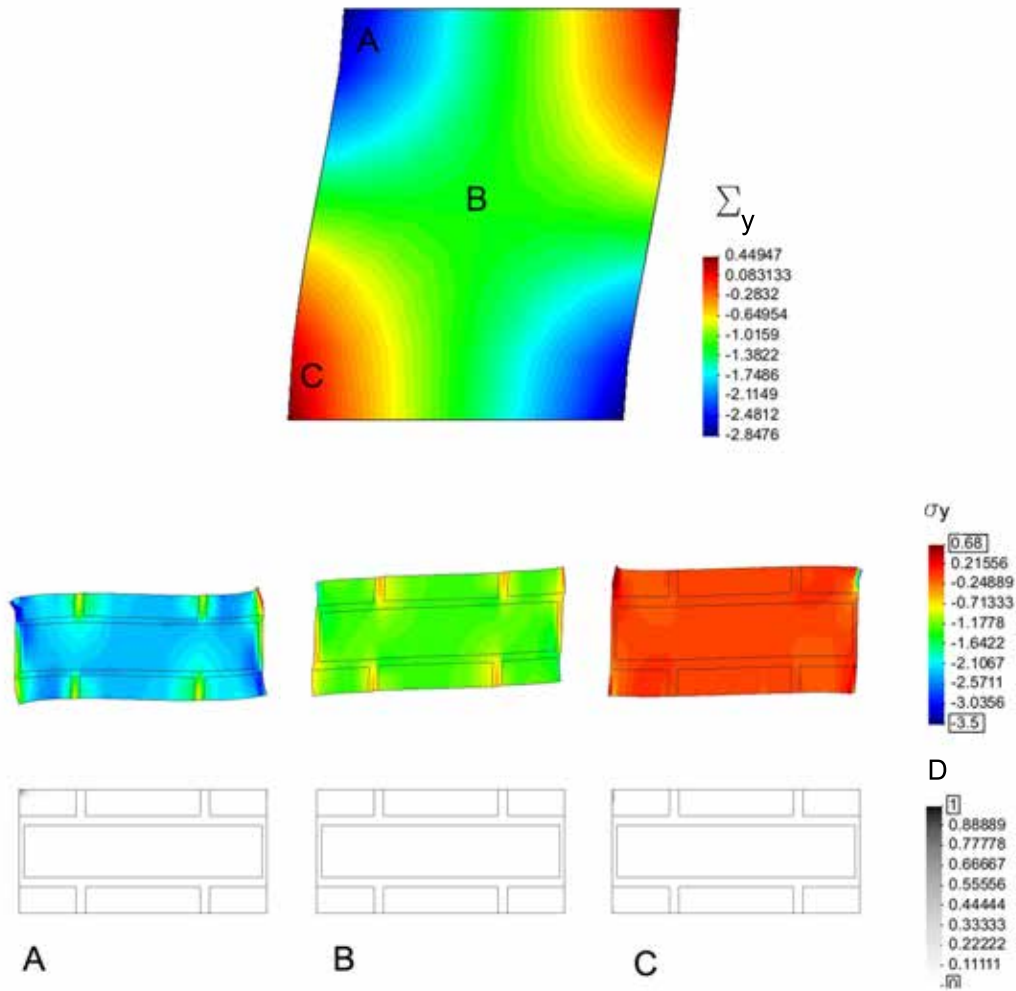
Figure 5.46: Shearing masonry panel: vertical stress distribution at macro-level (first row), vertical stress distributions in the RVEs (second row), damage distribution in the RVEs (third row)
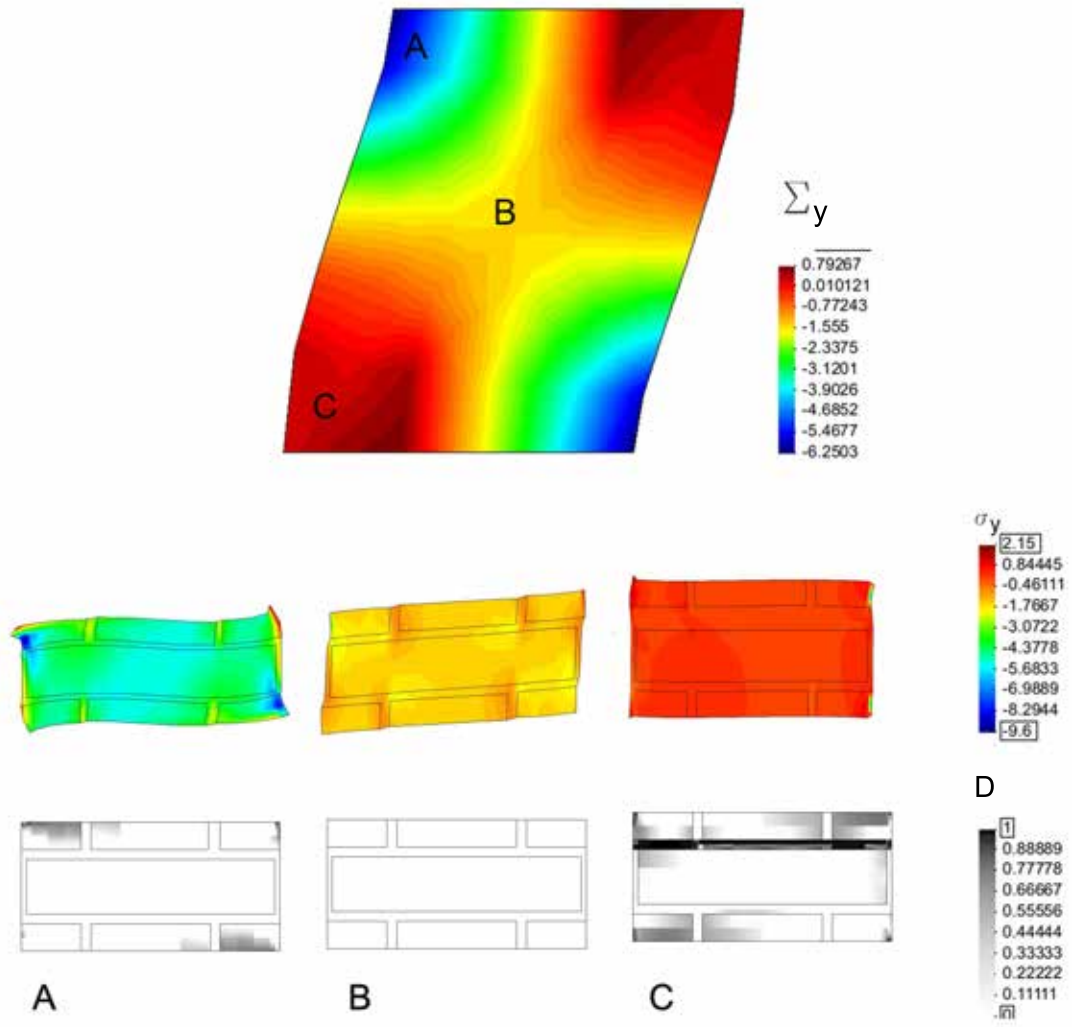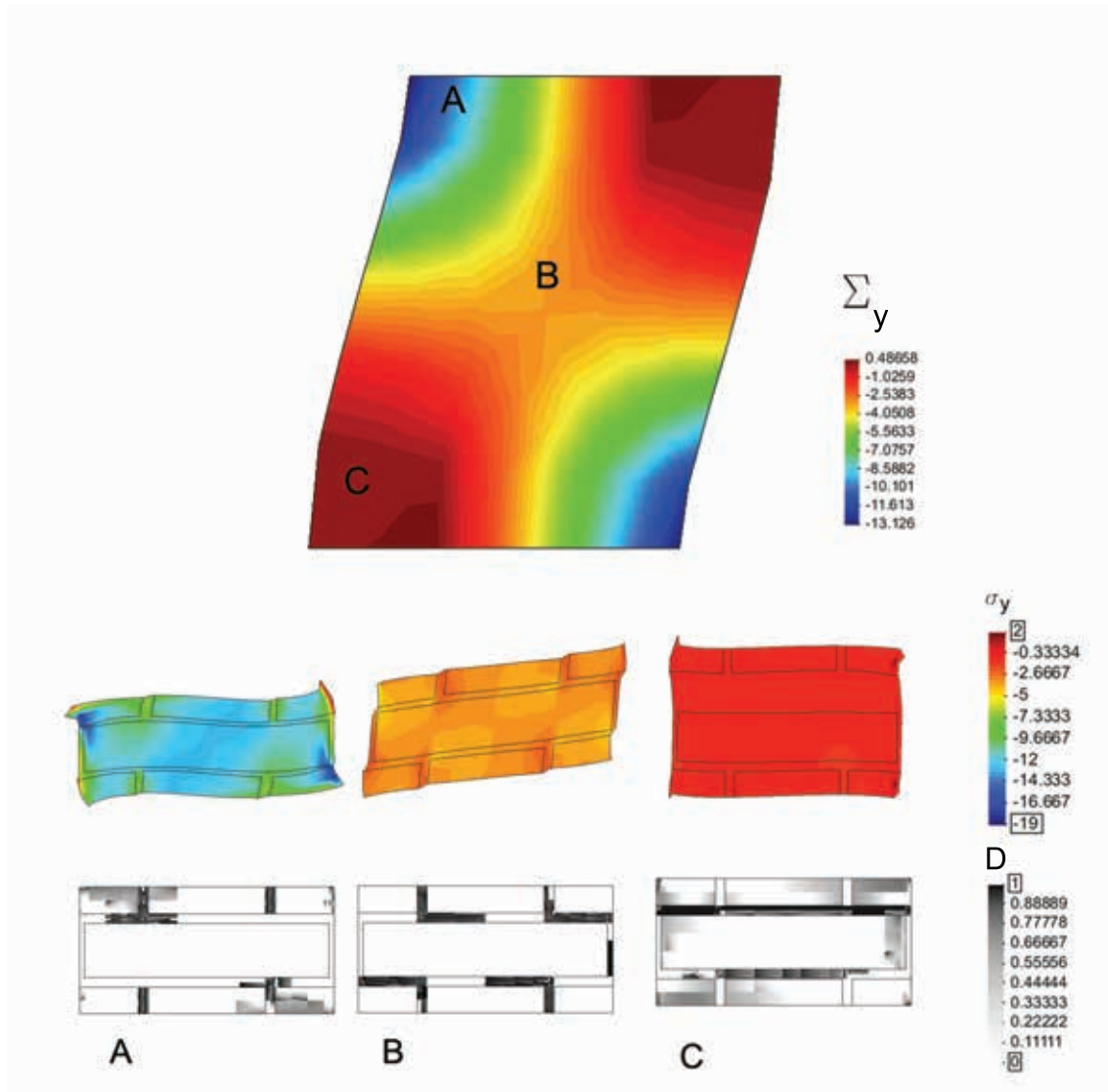
5.6.4 *Comparison between standard first order and enhanced first order computational homogenization*

This section is devoted to exploit the advantages of the Cosserat-Cauchy homogenization with respect to the Cauchy-Cauchy in order to better reproduce the masonry behavior. Thanks to the split of the shear strain and stress tensors into two non-symmetric components E_{xy} and E_{yx}, Σ_{xy} and Σ_{yx} respectively, it is possible to take into account typical effects evidenced by micro-mechanical analyses.

Different examples are presented in the sequel: a first linear elastic test, reported in Casolo (2006), is reproduced with the aim of emphasizing the important role played by the Cosserat additional rotation degrees of freedom in capturing the effective global behavior of a square running bond masonry panel undergoing a vertical load distributed on a square area; the same test is executed also in the non-linear range, by imposing damaging material laws both to the blocks and mortar joints; finally a non-linear test executed by Page (1978) on a deep masonry beam is performed. In the last two examples, global curves and damage maps obtained with the two homogenization techniques are compared.

Linear elastic square masonry wall subjected to vertical loading

A test executed by Casolo (2006) on a square masonry panel is here performed. The geometrical data of the specimen together with the boundary and loading conditions are reported in Figure 5.47. The thickness of the panel is 120 mm. The vertical load is distributed on a shaded square area.
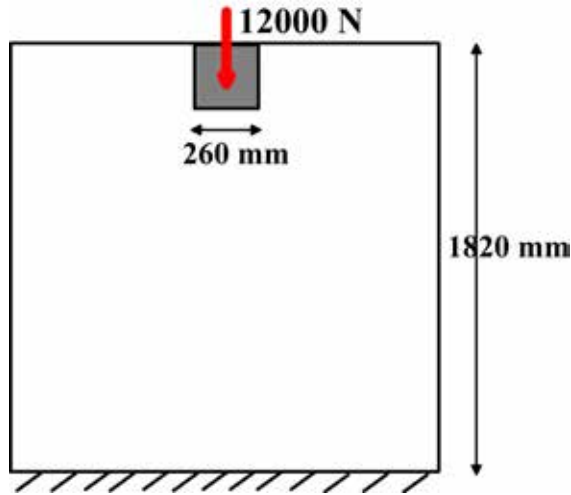
Figure 5.47: Square masonry wall: geometry and boundary conditions.

The bricks of dimension 250x55 mm^2 are arranged in running bond patterns and the thickness of all the mortar joints is 10 mm. In the Table 5.7 the elastic material parameters adopted in the analysis are reported. Different elastic modula have been considered for horizontal and vertical joints, being the former notoriously stiffer than the latter ones.

Bricks	Horizontal joints	Vertical joints
$E = 10000 N/m^2$	$E = 1000 N/m^2$	$E = 100 N/m^2$
$\nu = 0.1$	$\nu = 0.1$	$\nu = 0.1$

Table 5.7: Elastic parameters of bricks, horizontal and vertical mortar joints [MPa]

The test has been performed by adopting three different finite element models. Plane stress conditions have been assumed. Due to the symmetry of the structure only one-half has been considered in the

numerical simulations.

A micro-mechanical analysis has been firstly executed using a standard finite element code: the adopted refined mesh (4218 4-nodes 4-integration points elements), where the different materials are reproduced separately, is considered as reference.

Cauchy-Cauchy and finally Cosserat-Cauchy computational homogenization have been, then, executed by using the same macro-level (120 4-nodes 4-integration points elements) and micro-level (416 4-nodes 4-integration points elements) discretizations. In Figures 5.48 and 5.49 the selected meshes are shown.

Figure 5.48: Micro-model mesh.

Figure 5.49: Macro-level multi-scale mesh (left); RVE (right). The meshes are used both for Cauchy-Cauchy and for Cosserat-Cauchy homogenization.
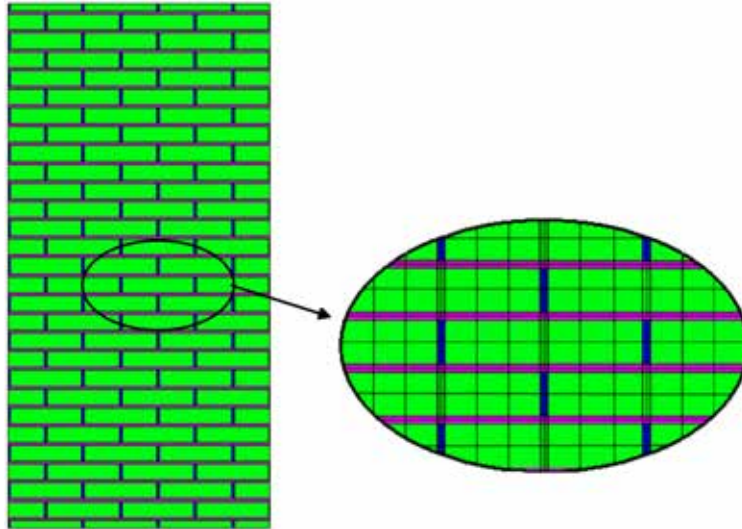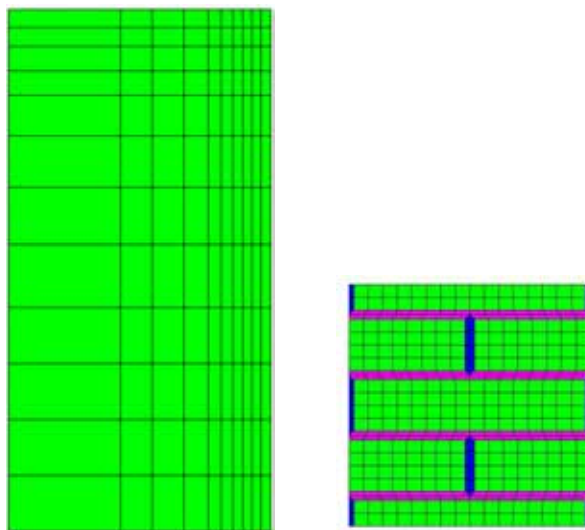
In the Figure 5.50, the deformed shape of the structure obtained with the micro-mechanical model is shown. The maximum vertical displacement, corresponding to the top middle point of the panel is equal to 0.270829 mm.

The global vertical reaction of the structure obtained with the Cosserat -Cauchy model, for the fixed value of the maximum top middle point vertical displacement of 0.270829 mm is the 20% higher than the one obtained with Cauchy-Cauchy homogenization.
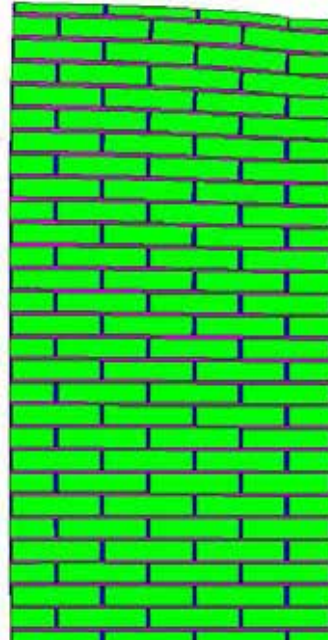

Figure 5.50: Micro-model deformed shape.

In the sequel a direct comparison in terms of stress and strain components is performed between the obtained results of the three aforementioned models.

By observing the micro-mechanical model results, it is evident that the texture effects are predominant. Strain localizations clearly appear into the weakest zones of the structure, i.e. into the vertical and horizontal mortar joints. In particular the shear strain involves preferentially the horizontal joints and it finds its way toward the mortar, following staircase patterns. This non-symmetric effect is very important in order to justify the need of a strain tensor, as in the Cosserat model, able to distinguish between E_{xy} and E_{yx} in the macroscopic homogenized description.

By taking into account the stress distributions, it is possible to notice that the values provided by the homogenized models represent a satisfactory estimate of the averaged values corresponding to blocks and mortar joints obtained with the micro-mechanical model.

A more detailed response, reproducing separately the material behaviors, is clearly achievable if the *RVEs* are examined.

The stress values distributions obtained with Cauchy-Cauchy and Cosserat-Cauchy homogenization models are very close together and both the models are able to reproduce the shape of the area of diffusion of the load.

The advantages of the Cosserat-Cauchy homogenization with respect to the Cauchy-Cauchy one emerge markedly if the strain distributions are considered. By comparing the E_{xx} and E_{yy} components, obtained with the homogenized models, no evident differences arises, while an important difference appears in the shear components for which in the Cosserat model the split into the two non-symmetric parts is evident.

In the Cosserat-Cauchy homogenization model, the values of E_{xy} are flatly higher than the values of E_{yx}. As proved by Casolo (2006), E_{xy} can be related to the shear deformation of the horizontal joints of the composite texture, while E_{yx} accounts for the the shear deformation of the vertical joints. This
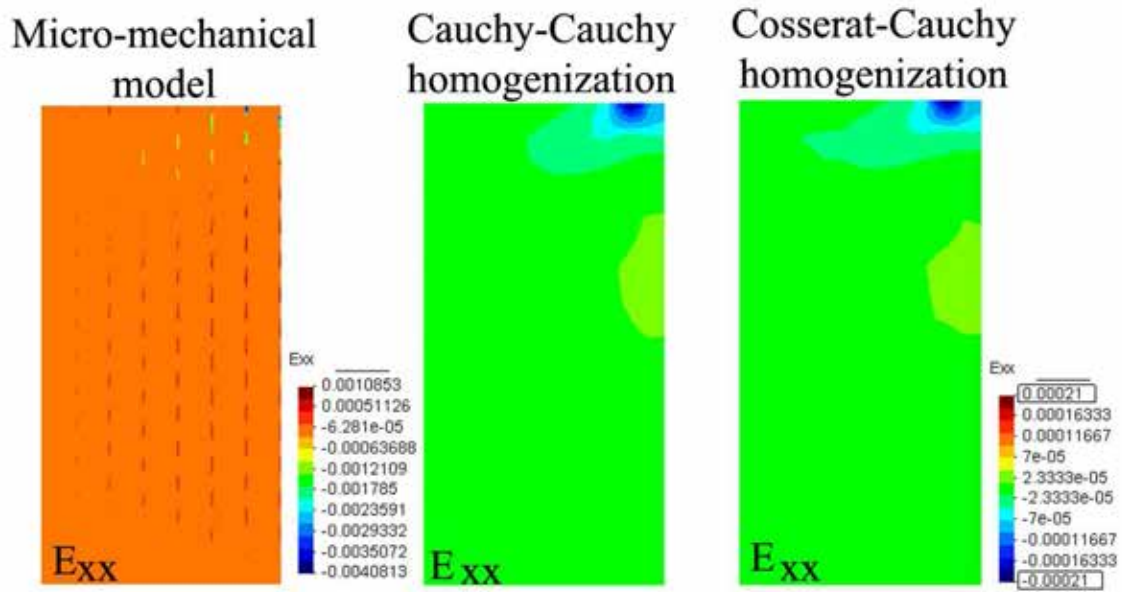
Figure 5.51: Comparison of the E_{xx} strain component maps.
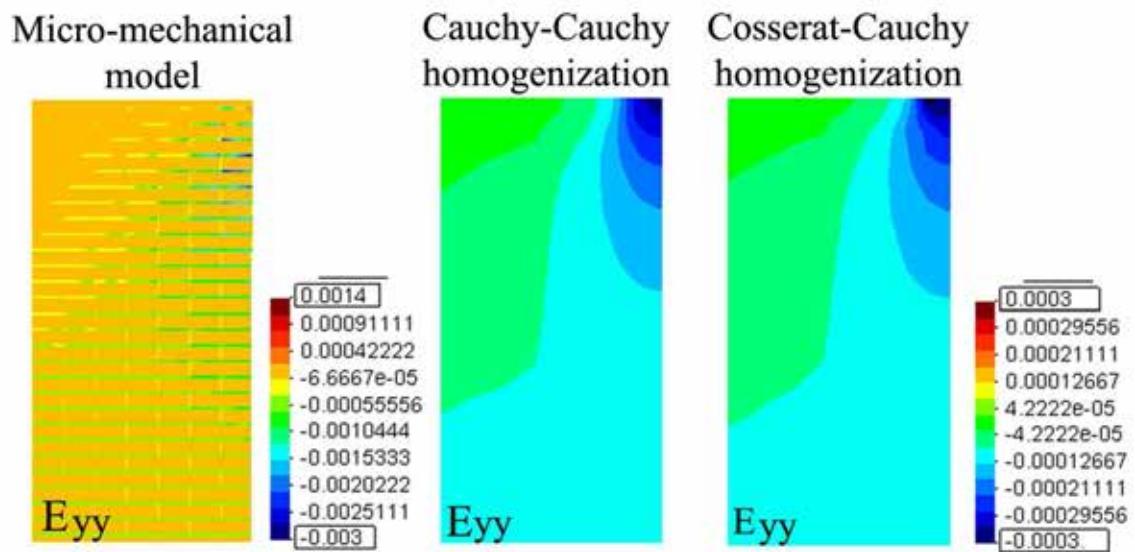
Figure 5.52: Comparison of the E_{yy} strain component maps.

consideration is in accordance with the results of the micro-mechanical model where the prevalence of shear deformation into the horizontal joints is observable. The Cosserat model is, thus, more adequate in the description of the effective response than the Cauchy model.

Figure 5.53: Comparison of the E_{xy} strain component maps.

Figure 5.54: Comparison of the Σ_{xx} stress component maps.

Figure 5.55: Comparison of the Σ_{yy} stress component maps.

Figure 5.56: Comparison of the Σ_{xy} stress component maps.

Linear elastic rectangular masonry wall subjected to uniform horizontal loading

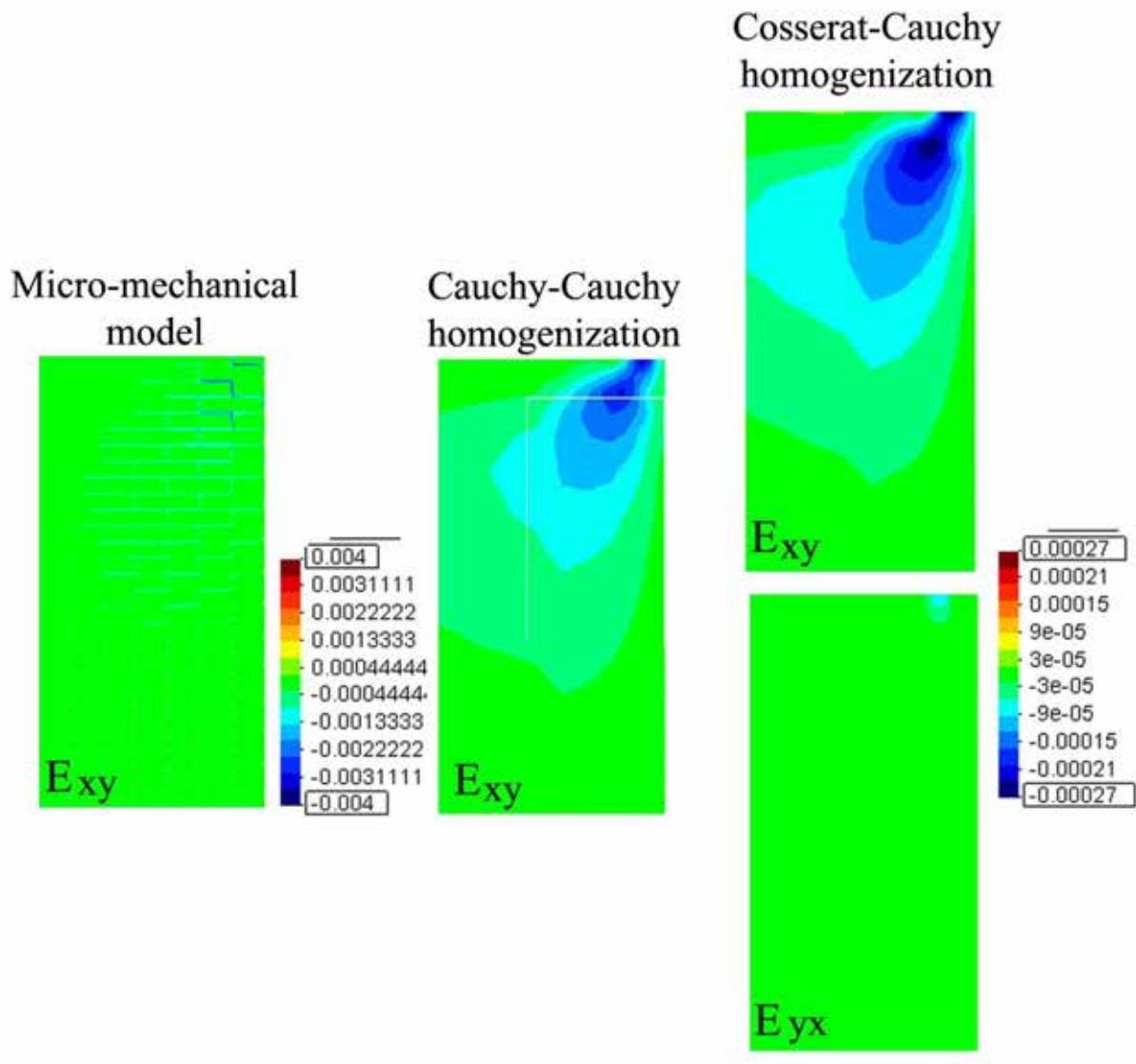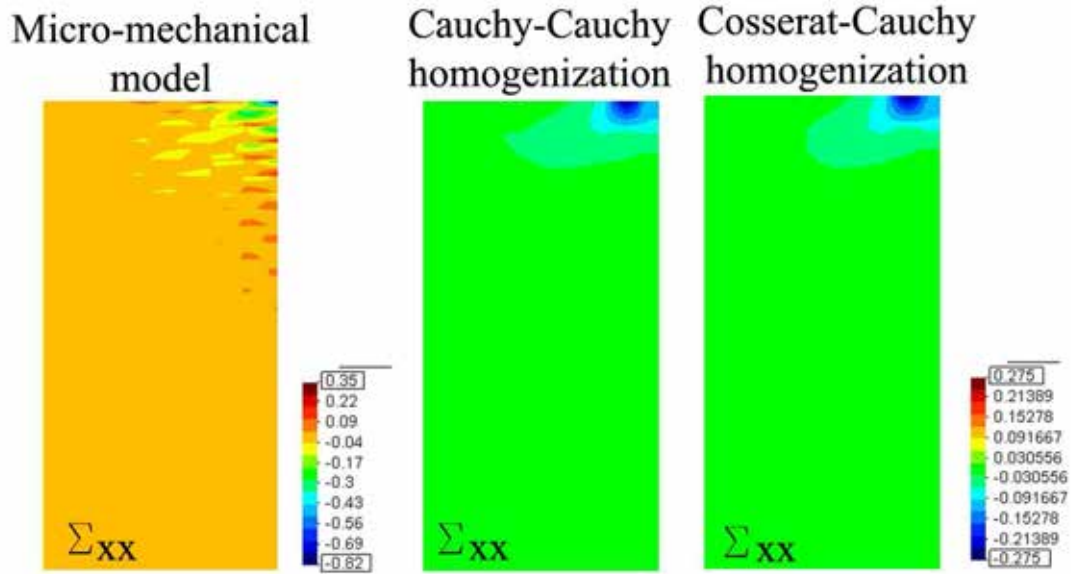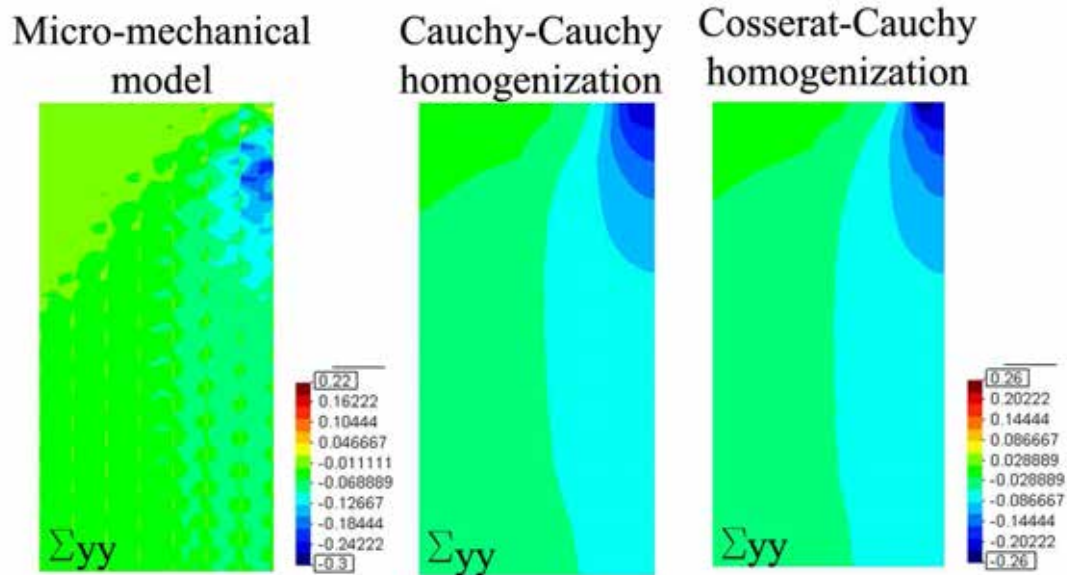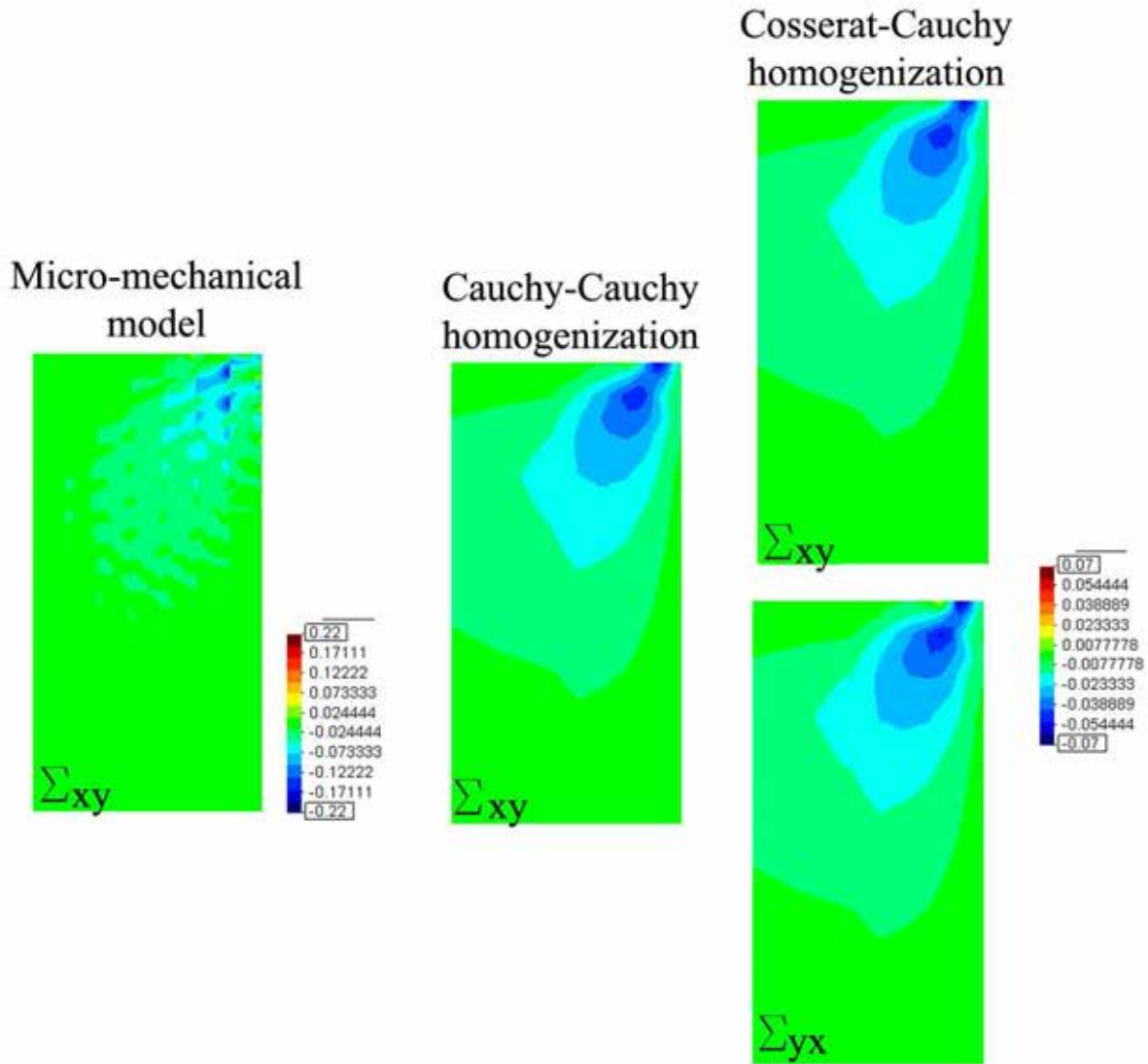At first a simple benchmark example is examined, with the aim of emphasizing the important role played by the Cosserat additional rotational degrees of freedom in order to capture the effective global behavior of a masonry structural panel. In particular, the numerical example presented in Salerno and De Felice (2009) is considered, the geometrical properties and boundary conditions of which are shown in Figure 5.57 (a). It should be noted, on the other hand, that in Salerno and De Felice (2009) a discrete lattice model is considered at the micro-level. The model is made of rigid blocks, normal and tangential deformable springs in order to model the mortar joints.
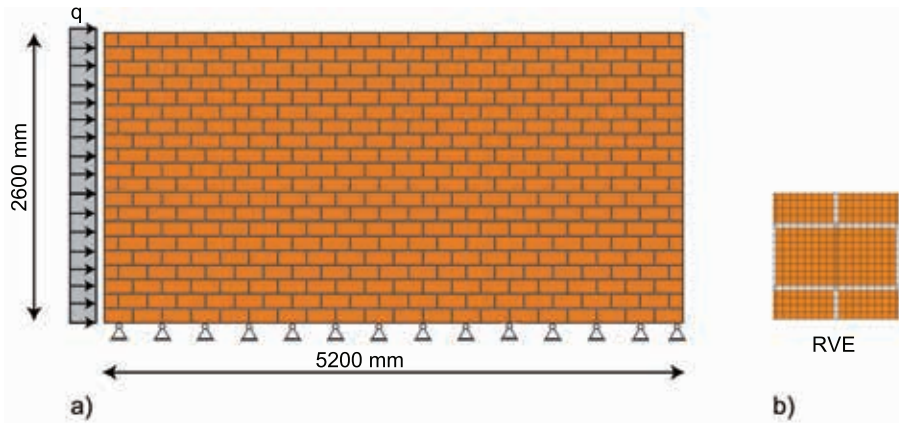
Figure 5.57: Rectangular masonry wall: geometry and boundary conditions at structural level (a); RVE (b).

Bricks whose in-plane dimensions are $250 \times 120 \, mm^2$ are arranged in running bond patterns and the thickness of all mortar joints is equal to $10 \, mm$. The uniformly distributed horizontal load $q = 10 \, N/mm$ is applied along the left edge. The elastic parameters for bricks are Young's modulus $E_b = 30000 \, MPa$ and Poisson ratio $\nu_b = 0.15$ and for mortar joints are Young's modulus $E_m = 2000 \, MPa$ and Poisson ratio $\nu_m = 0.15$.

First, a micromechanical analysis is performed adopting a refined mesh of 7560 FE, where the different materials are modeled separately. The micromechanical solution is used as a point of reference. Subsequently, the multi-scale procedure is adopted to determine the solution, based on a Cauchy-Cauchy and on the proposed Cosserat-Cauchy homogenization. At the macro-level 64 elements are used for the discretization, while at the micro-level a 441-element mesh is employed to discretize the RVE (see Figure 5.57 (b)).

The deformed shapes of the masonry panel obtained with the three different models adopted are shown in Figure 5.58. As clearly seen a good match arises between the shaded area (micromechanical model) and the blue curve (Cosserat-Cauchy homogenization model), while the red curve (Cauchy-Cauchy homogenization model) provides an overestimation of the displacement fields. Moreover, a direct comparison in terms of displacement degrees of freedom is performed. With regard to the horizontal displacement field (Figure 5.59 left column), the results are consistent with those of Salerno and De Felice (2009). It stands to reason that the reference values (micromechanical models) are bounded above by the Cauchy-Cauchy model and below by the Cosserat-Cauchy model. It should be noted that the results obtained with the Cosserat-Cauchy model fit the micromechanical ones better than the Cauchy-Cauchy model. On the right column of the same figure, a comparison in terms of rotations is shown. The rigid rotations w for the micromechanical model and W for the Cauchy-Cauchy model are both plotted, however for the Cosserat-Cauchy model the rotational degree of freedom, Φ, is plotted (Figure 5.59 right column). It should be noted that the maximum value of the rotation obtained by the micromechanical analysis is much higher than the ones evaluated with the two homogenization techniques, this is due to local
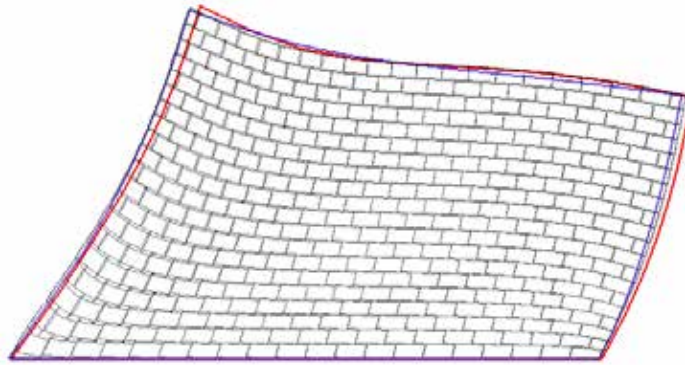
Figure 5.58: Rectangular masonry wall deformed shape: micromechanical model (shaded area); Cosserat-Cauchy homogenization (blue curve); Cauchy-Cauchy homogenization (red curve).

concentrated distributions of the rotation field.
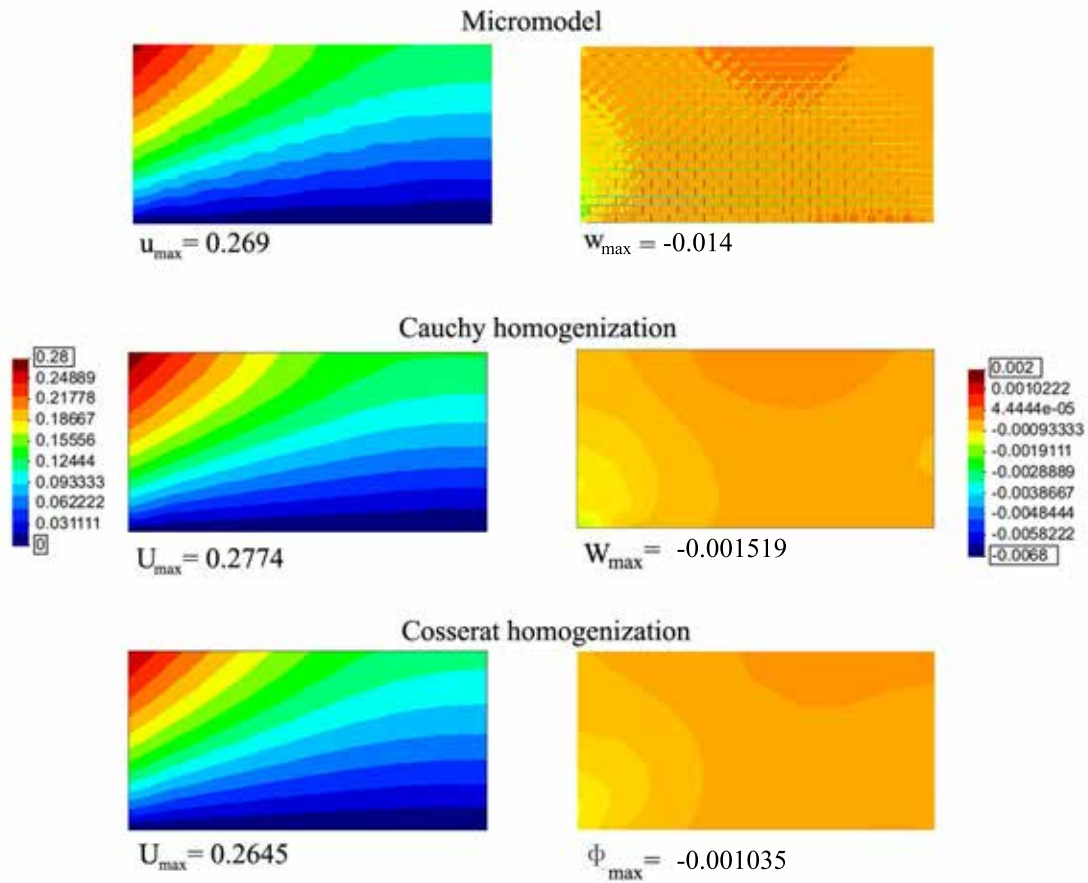
Figure 5.59: Rectangular masonry wall: horizontal displacement(left column) and rotation (right column) fields.

Finally size effects are investigated. In Figure 5.60 the normalized expended work versus the number

of blocks along the height is plotted for the three models considered. As expected, the response obtained by the Cauchy-Cauchy model is insensitive to the microstructural sizes, while both micromechanical and Cosserat-Cauchy model are affected by size. As the microstructural sizes decrease, the expended work tends to increase and to move closer to the Cauchy-Cauchy limit value.
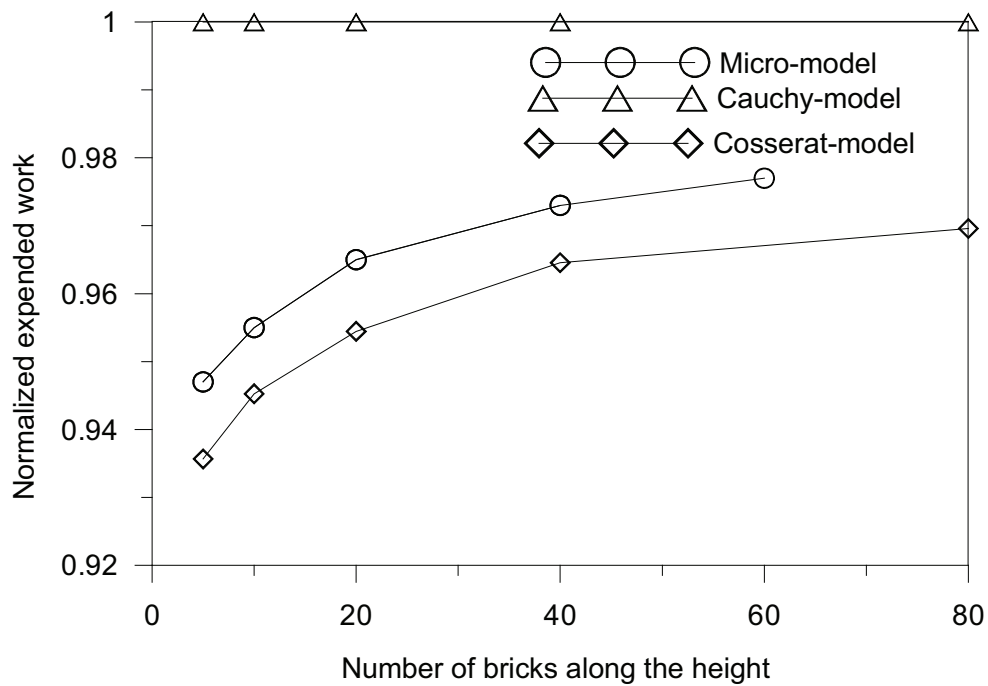
Figure 5.60: Rectangular masonry wall: variation of the expended work with the microstructural size.

Chapter 6

Conclusions

The principal objective of the research reported in this dissertation has been the development of a multi-scale computational tool for the representation of damage effects in 2D masonry structures undergoing seismic like loading conditions.

The exhaustive reproduction of evolving mechanisms appearing in masonry panels, subjected to lateral loads, when the linear range of behavior is overcome, in fact, is a very challenging task due to the inner complexity of the local and global behavior.

Two scales of interest in masonry structures can be recognized: a *macro-scale*, the structural one, on the order of meters, is identified as the typical size of masonry structures and a *micro-scale*, on the order of centimeters, that is the characteristic size of the basic constituents of the masonry texture, namely bricks and mortar joints.

When periodic brickwork is considered, a marked anisotropic behavior is noticed. An important macroscopic feature of masonry in the non-linear range is, indeed, the stiffness degradation caused by cracking of its quasi-brittle constituents, mainly the mortar.

Due to the periodic arrangement of the two phases, preferential cracking orientations appear in the microstructure. This may result in a second type of anisotropy, which is induced by the cracking and which is also closely connected to the micro-structure of the material.

It stands to reason that a detailed description of the dominant phenomena occurring at the micro-level, is essential since the global response is strongly driven by the lower scale behavior.

Several efforts have been done, in the framework of numerical analyses, in order to attempt to solve the problem, with the aim of capturing and reproducing its main features.

A very important strand of research has been focused on the so-called *continuum approach*, based on the extrapolation of closed-form constitutive laws, founded either on phenomenological bases or micro-modeling of the local structure, to be used at the macroscopic scale. With such approaches it is however very difficult to obtain a global response actually aware of the micro-level evolving phenomena, since strong simplifications are often required.

A promising alternative approach for the study of masonry materials response is the so-called computational homogenization method, which has been the main topic of this work.

This technique is essentially based on the solution of nested boundary value problems, one for each scale. A fully-coupling between scales is outlined and a continuous reciprocal exchange of information is guaranteed.

The main advantages assured by such techniques are hereafter enumerated:

1. no closed-form constitutive laws are required at the macro-level;

2. different phases in the microstructure can be modeled (in this case bricks and mortar joints) with

arbitrary non-linear constitutive models. Moreover, only the characteristics of each single phase are to be described;

The standard first order computational homogenization, presented in Chapter 4, is based on coupling two classical Cauchy continua at both macro and micro-levels.

A *strain driven formulation* is chosen, therefore, the homogenized strain vector $\mathbf{E}$ is evaluated at the macro-level for all the local points of the equivalent homogeneous continuum. At this level the direct evaluation of related stresses $\mathbf{\Sigma}$ is not possible, due to the lack of macro-level closed form constitutive laws. This is the reason why a proper formulated *BVP* at the micro-level has to be solved. To this end $\mathbf{E}$ is used as input data for the imposition of local boundary conditions on the *RVE*, using a properly conceived *kinematic map*.

The quasi-static boundary value problem on the *RVE* is solved and the homogenized stress tensor $\mathbf{\Sigma}$, as volume average of the local computed stress field, is calculated.

The obtained value is sent back to the macrostructure.

Based on the initial periodicity of the material, periodic boundary conditions are applied on the *RVE* to determine the macroscopic material response through the multi-scale transition.

In the present work the finite element method has been used as solution technique at both levels and a finite element program, based on parallel calculations, has been implemented in order to bring down the computational effort and to enable the solution of different local problems at the same time.

Different applications have been carried out.

A first step of analyses has been focused on the check of the correct formulation and implementation of the homogenization procedure embedded in the multi-scale program. Different *RVEs* have been considered and the obtained homogenized elastic constitutive tensors have been compared with respective values available in literature.

The second step has been the testing of correct working of the fully-coupled multi-scale program and a series of simple elastic two-scales examples has been performed.

Finally an experimental test has been reproduced, characterized by non-linear behavior of constituents. Both for bricks and mortar joints isotropic damage laws, with a distinct threshold under traction and compression, are considered.

Due to the typically exhibited softening behavior of masonry structures under lateral loading conditions, regularization techniques are required in order to avoid spurious mesh dependencies when a numerical solution is sought in the framework of finite element method.

A regularization based on the imposition of the macroscopical length scale at the micro-level, in the framework of the fracture energy regularization, is proposed.

Further investigations are, however, required with the aim of better verify the capabilities of the method.

Unfortunately there are severe limitations in the application of the first-order scheme, directly related to the underlying assumption of locality at the macro-level.

These limitations can be explained as follows:

1. the Principle of local action fully holds, i.e. the formulation is valid only if the microstructure is very small with respect to the characteristic size at the macro-level; the characteristic wave length of the macroscopic loading must be large compared to the size of the microstructure, so that over the corresponding *RVE* uniform macroscopic (stress-strain) fields are applied ;

2. the method can account for the volume fraction, distribution and morphology of the constituents, but cannot consider the absolute size of the microstructure and consequently fail to account for geometrical size effects;

3. if a macroscopic material point exhibits softening behavior, the solution obtained from the first-order computational homogenization approach fully localizes according to the size of the elements used in the macro-level mesh.

In the light of the aforementioned consideration, for the current case of masonry structures, the applicability of the standard first order computational homogenization technique seems to be highly advised against (unless enhanced strategies are applied).

In fact experimentally it is recognized that, in masonry, the microstructural typical size are comparable with the macrostructural one and, moreover, high deformation gradients can appear due to the constitutive material behavior with damage. This objection is in contraddiction with the first aforementioned limitation . Thus a formulation in which only first-order deformation modes (tension, compression, shear or combinations thereof) of the microstructure can be imposed is inappropriate since it is not capable to describe high deformation gradients.

With regard to the second limitation, it is proved that not only shape and arrangement of the constituents, but also the size, strongly affect the mechanical global response of masonry structures.

Finally, as for the third observation, due to the typical softening behavior experimentally exhibited by masonry panels undergoing seismic like loading conditions, localization phenomena frequently occur and it is necessary to employ a suitable regularization technique, in the numerical approach, in order to avoid spurious mesh dependencies.

The requirement of an enhanced formulation with the aim of overcoming the limits of the standard first order one appears, at this point, evident.

A decisive choice in this direction is the adoption of generalized continua in order to account for a material length scale in a natural manner which is directly related to the size of the microstructural domain in which the basic microstructural deformation mechanisms occur.

Several strategies have been proposed in the two-scale computational homogenization framework.

In this work the proposed strategy is to couple two different continua as for the description of the macro-level and micro-level. At the macro-level a Cosserat continuum is adopted while the Cauchy medium is preserved at the micro-level.

To the knowledge of the author, this work is the first example of adoption of Cosserat-Cauchy computational homogenization applied to localization problems related to the study of masonry structures.

This choice has been turned out to be very suitable for approaching the study of masonry structures. Substantially the first reason is that it allows the introduction of a material length scale so that the overall response of the composite material is spontaneously bound to the the absolute size of the constituents.

The effect of considering a Cosserat continuum at the macro-level, in fact, is to enrich the displacement, strain and stress descriptions and, thus, to pass additional information to the micro-level: apart from the standard Cauchy three deformation modes (two axial and one shear symmetric deformation), three additional deformation modes are considered (a skew-symmetric shear and two bending deformations). This means that, at least for shear and bending behaviors, with this formulation is possible to account for size effects (directly related to the *RVE* dimensions).

The adoption of a Cauchy continuum at the micro-level enables the employment of several non-linear models available and well established in this framework.

The nodal point of the strategy is the coupling between scales, because a one to one correspondence between strain and stress variables defined at two levels not longer arises and, therefore, an *ad hoc* kinematic map has to be formulated in order to manage the communications from the higher to the lower level.

Moreover a properly stated rule to obtain averaged stresses has to be obtained as an extension of the Hill-Mandel principle.

The conceptual scheme remains the same as for the first order computational homogenization; the fundamental difference is the increased number of deformation modes that have to be imposed to the *RVE* as boundary conditions and the higher number of homogenized stress components that have to be evaluated as output variables, by averaging the micro-level stress fields.

The *BVP* formulated at the micro-level on the basis of the new kinematic map accounts, not only for

periodic conditions between couples of periodic points, but also for additional integral conditions, to be imposed on the edges of the *RVE*, that guarantee that the local displacement fluctuation fields produce zero averaged strains.

The Cosserat-Cauchy enhanced computational homogenization is presented in Chapter 5. The theoretical bases and the finite element implementation are outlined. An extension of the finite element code developed in the framework of first order computational homogenization has been obtained.

Also in this case various analyses have been executed.

A preliminary analysis on the influence of the additional integral boundary conditions has been carried out and it appears that they have a low relevance in terms of homogenized parameters extracted from the *RVE*.

A *RVE* has been considered and the obtained homogenized elastic constitutive tensor has been compared with respective values available in literature.

In order to test the correct formulation and implementation of the enhanced multi-scale procedure, a patch test, properly conceived for Cosserat continuum has been satisfactorily performed.

Apart from another linear elastic test, still executed with the aim of testing the correct working of the implemented finite element code, two non-linear examples are performed.

In both cases the response of masonry panels undergoing lateral loading conditions has been investigated. Isotropic damage laws have been considered for the modeling of both bricks and mortar joints.

The regularization demand at both the analysis levels, due to the softening material behavior, is answered by rely upon the inner regularization effects exhibited by the Cosserat medium, at least for dominant shear and bending failure mechanisms, at the macro-level and upon the standard fracture energy technique at the micro-level.

The response obtained by the aforementioned non-linear analyses are very encouraging. The procedure is capable to capture both local phenomena, as the onset and growing of damaging, and global curves.

An ad hoc procedure for the homogenization of the damage variable is proposed.

A direct comparison with experimental response demonstrates a very good agreement: the initial stiffness is well reproduced together with the peak value and the post-peak trend as for the global behavior and despite the lack of accurateness, due to the rough discretization adopted at the macro-level, it is possible to notice the presence of typical expected structural mechanisms.

The main objection against the use of coupled micro-macro computational homogenization strategies for practical problems is related to the significantly larger computation time compared to the solution time of a macroscopic problem with closed-form homogenized constitutive equations. It is, however, recalled that in some cases the complexity of the micro-level phenomena, due to the interaction between constituents, prevent to find the solution in closed form and, moreover, the calculation time required for a coupled numerical analysis may be substantially reduced by the use of parallel computations.

Undoubtedly, many aspects, especially those related to the newly faced Cosserat-Cauchy computational homogenization for the study of masonry structures, still need to be explored. An in-depth examination of the regularization properties of the proposed strategy has to be carried out, anyway very promising results have been found.

The study of quasi-static response of masonry structures, undergoing seismic like loading conditions, is of great interest in civil engineering essentially due to the increasing interest in the preservation and restoration of historical and artistic building heritage.

Masonry is a heterogeneous material with periodic microstructure, whose constituents, bricks and mortar, exhibit a brittle-like mechanical behavior caused by the damaging process. Two scales of interest are recognized: a *macro-scale*, the structural one, is identified as the typical size of masonry structures and a *micro-scale*, that is the characteristic size of the basic constituents of the masonry texture (bricks and mortar).
Among several approaches, proposed in literature, a promising alternative for the study of masonry materials response is the computational homogenization method in which a two-scale approach is adopted. This technique is based on the solution of nested boundary value problems, one for each scale. A fully-coupling between scales is outlined and a continuous reciprocal exchange of information is guaranteed.

The aim of this work is to propose a computational homogenization technique, which adopts a Cosserat medium, at the macro level, and a Cauchy model, at the micro level, specialized for the study of masonry panels, in order to overcome the inner limits of the standard first order computational homogenization based on coupling two Cauchy continua at both levels.

The finite element method has been used as solution technique at both levels and a finite element program, based on parallel calculations, has been implemented in order to bring down the computational effort and to enable the solution of different local problems at the same time.
Different nonlinear constitutive laws with damage are adopted for the masonry constituents and a proper conceived regularization technique is defined in order to avoid spurious mesh dependencies due to softening behavior. Different structural applications have been carried out.

Appendix A

Damage model

A.1 Model formulation

In this appendix the damage model chosen to reproduce the quasi-brittle behavior of masonry is presented. Among several formulations able to reproduce the stiffness and strength degradation connected to damage growth, the isotropic models are relatively simple and widely used. In this work the model proposed by Oliver et al. (1990); Oller (1988) is discussed.
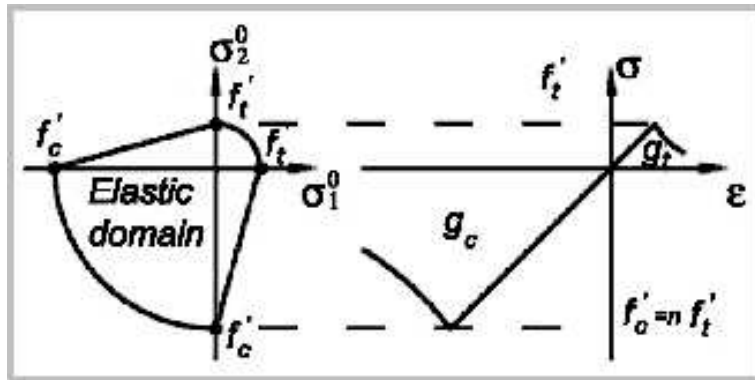
Figure A.1: Damage constitutive law.

It is supposed that the virgin material (before the load history imposition) is isotropic perfectly elastic. As the load increases, a threshold is reached where the degradation starts to appear. Beyond the threshold the material continues to degrade and to lose stiffness. A scalar internal variable d is adopted to simulate this behavior: this variable measures the loss of stiffness and its range is between 0 and 1.

The isotropic damage model constitutive equation is expressed as:

$$\underline{\sigma} = (1 - d)\underline{\mathbf{C}}\underline{\epsilon}; \tag{A.1}$$

where $\underline{\sigma}$ and $\underline{\epsilon}$ are the stress and strain tensors respectively, d is the damage variable and $\underline{\mathbf{C}}$ is the elastic constitutive tensor of the virgin material.
As a consequence, it is possible to state that:
1. the material isotropy is not affected by the damage process (as the damage variable is scalar);
2. it is possible to explicitly integrate the constitutive law as the actual values of stress and strain tensor are considered;

3. the constitutive law belongs to the standard stress decomposition models: the stress is decomposed into an elastic and an inelastic part, as follows:

(A.2) $$\underline{\boldsymbol{\sigma}} = \underline{\mathbf{C}}\,\underline{\boldsymbol{\epsilon}} - d\,\underline{\mathbf{C}}\,\underline{\boldsymbol{\epsilon}} = \underline{\boldsymbol{\sigma}}^0 - \underline{\boldsymbol{\sigma}}^d;$$

It is clear that the model is completely defined if the value of the damage internal variable d is established for every step of the degradation process.

The required ingredients for the considered damage model are:

1. Definition of the variables involved in the problem:

    • free variable $\boldsymbol{\epsilon}$;

    • internal variable d;

2. Definition of free energy:

    (A.3) $$\Psi(\underline{\boldsymbol{\epsilon}}, d) = (1 - d)\Psi^0(\underline{\boldsymbol{\epsilon}}); \quad \Psi^0(\underline{\boldsymbol{\epsilon}}) = \frac{1}{2}\underline{\boldsymbol{\epsilon}}^T\,\underline{\mathbf{C}}\,\underline{\boldsymbol{\epsilon}}$$

3. Fulfillment of thermodynamic laws, in particular for the Clausius-Planck inequality:

    (A.4) $$D = (\underline{\boldsymbol{\sigma}} - \frac{\partial\Psi}{\partial\underline{\boldsymbol{\sigma}}})^T\dot{\underline{\boldsymbol{\epsilon}}} - \frac{\partial\Psi}{\partial d}\dot{d} \geq 0$$

    where D is the dissipation;
    using the Coleman method it follows:

    (A.5) $$\underline{\boldsymbol{\sigma}} = \frac{\partial\Psi}{\partial\underline{\boldsymbol{\epsilon}}} = (1 - d)\,\underline{\mathbf{C}\boldsymbol{\epsilon}}$$

    and

    (A.6) $$D = -\frac{\partial\Psi}{\partial d}\dot{d} \geq 0$$

    and, assuming that $\frac{\partial\Psi}{\partial d} = -\Psi^0$, the dissipation is:

    (A.7) $$D = \Psi^0\dot{d} \geq 0$$

4. Definition the norm $\boldsymbol{\tau}$ of the strain tensor $\boldsymbol{\epsilon}$ (or alternatively of the elastic stress tensor $\boldsymbol{\sigma}^0$); this norm is named *equivalent deformation*. It is used to compare different material states (for example loading and unloading processes).

    Non-Symmetric model. This model is suitable for materials characterized by different elastic domains in traction and compression (masonry is a typical example of such a material). The function used is:

    (A.8) $$\tau = \left(\zeta + \frac{1 - \zeta}{n}\right)\sqrt{\underline{\boldsymbol{\sigma}}\,\underline{\boldsymbol{\epsilon}}}$$

where ζ is the weight factor depending on the stress state σ^0 defined as:

$$\zeta = \frac{\sum_{i=1}^{3} \langle \sigma_i \rangle}{|\sigma_i|} \tag{A.9}$$

and n is the ratio between the tensile and compression strength:

$$n = \frac{f_c'}{f_t'} \tag{A.10}$$

5. Damage criterion. A function F is defined: it splits the admissible stress space between the elastic domain (when $F < 0$) and the damage domain (when $F = 0$). This stress space depends on the norm τ and on a damage threshold r. Thus it is possible to define this space as:

$$F(\tau, r) = G(\tau^t) - G(r^t) \le 0 \quad \forall t \ge 0 \tag{A.11}$$

where $G(\cdot)$ is a monotonic scalar function. This function $F(\tau, r) \le 0$ is defined in the non-damaged strain or stress space. The simplest form for this criterion is:

$$F(\tau, r) = \tau^t - r^t \le 0 \quad \forall t \ge 0 \tag{A.12}$$

where τ^t is the aforementioned norm and r^t is the damage threshold in time. If r^* is the initial threshold (material property), the following statement has to be fulfilled $r^t \ge r^0 = r^*$. Damage appears when the norm τ exceeds the actual threshold value;

6. Evolution laws. The following evolution laws have been defined as for the damage threshold and for the degradation variable.

$$\dot{r} = \dot{\mu} \tag{A.13}$$

$$\dot{d} = \dot{\mu} \frac{\partial F(\tau, r)}{\partial \tau} = \dot{\mu} \frac{dG(\tau)}{d\tau} \tag{A.14}$$

where $\dot{\mu}$ is the damage consistency parameter used in order to define the loading-unloading conditions, respecting the Kuhn-Tucker conditions:

$$F(\tau, r) \le 0; \quad \dot{\mu} \ge 0; \quad \dot{\mu} \, F(\tau, r) = 0 \tag{A.15}$$

The consistency condition states that if $F(\tau, r) = 0$, thus

$$\dot{\mu} \dot{F}(\tau, r) = 0 \tag{A.16}$$

The final expression of dissipation is, according to Simo and Hu (1987):

$$D = \Psi^0 \dot{d} = \Psi^0 G'(\tau) \dot{\tau} \tag{A.17}$$

It is possible to directly integrate the evolution of the internal variables by taking:

$$r = max\{r^0, max\{\tau^s\}\}; \quad 0 \le s \le t \tag{A.18}$$

$$d = G(r); \tag{A.19}$$

that describes the complete evolution of the internal variables during loading-unloading conditions. The function $G(r)$ defining the damage evolution (between 0 and 1) is (Oliver et al. (1990)):

$$G(r) = 1 - \frac{r^*}{r} exp\left[A\left(1 - \frac{r}{r^*}\right)\right]; \quad 0 < r^* \le r \tag{A.20}$$

where

(A.21)
$$r^* = \frac{f_t^{'}}{\sqrt{E^0}};$$

where E^0 is the Elastic modulus. The total dissipation of specific energy (for unit volume) in a generic process is:

(A.22)
$$g = \int_0^\infty D dt = \int_0^\infty \Psi^0 G^{'}(\tau)\dot{\tau} dt$$

in particular, as for a model with damage in traction and compression it is:

(A.23)
$$\tau^2 = 2\Psi^0 \quad for \quad uniaxial \quad tension$$

(A.24)
$$\tau^2 = \frac{2}{n^2}\Psi^0 \quad for \quad uniaxial \quad compression$$

by substituting (A.23) and (A.24) into (A.22) and by using the function $G(\cdot)$ defined in (A.20) and finally by integrating, it results:

(A.25)
$$g_t = \left(\frac{1}{2} + \frac{1}{A}\right)(r^*)^2 \quad for \quad uniaxial \quad tension$$

(A.26)
$$g_c = \left(\frac{1}{2} + \frac{1}{A}\right)(nr^*)^2 \quad for \quad uniaxial \quad compression$$

where g_t and g_c are the specific energies wasted during the traction and compression processes, respectively.

The tangent constitutive tensor $\underline{\mathbf{C}}$ can be obtained explicitly, on the basis of the elastic constitutive tensor $\underline{\mathbf{C}}^0$:

(A.27)
$$\begin{aligned}
\dot{\underline{\sigma}} &= \underline{\mathbf{C}}^d \, \underline{\epsilon} \\
&= (1-d) \, \underline{\mathbf{C}}^0 \, \dot{\underline{\epsilon}} - \dot{d} \, \underline{\mathbf{C}}^0 \, \underline{\epsilon} \\
&= (1-d) \, \underline{\mathbf{C}}^0 \, \dot{\underline{\epsilon}} - \dot{d} \, \underline{\sigma}
\end{aligned}$$

when, during unloading and reloading phases, the elastic threshold is not overcome;

(A.28)
$$\dot{\underline{\sigma}} = (1-d) \, \underline{\mathbf{C}}^0 \, \dot{\underline{\epsilon}}; \quad \dot{d} = 0$$

while during the loading phase:

(A.29)
$$\dot{d} = \dot{G}(r)\dot{r}; \quad \dot{r} = \dot{\tau}$$

thus the tension increasing

(A.30)
$$\dot{\sigma} = (1-d)\underline{\mathbf{C}}^0 \, \dot{\underline{\epsilon}} - \frac{\dot{G}(r)}{\tau}\underline{\sigma} \otimes \underline{\sigma}\dot{\underline{\epsilon}}$$

(A.31)
$$\dot{\underline{\sigma}} = \left[(1-d)\underline{\mathbf{C}}^0 - \frac{\dot{G}(r)}{\tau}\underline{\sigma} \otimes \underline{\sigma}\right] \dot{\underline{\epsilon}}$$

(A.32)
$$C^d = \left[(1-d)\underline{\mathbf{C}}^0 - \frac{\dot{G}(r)}{\tau}\underline{\sigma} \otimes \underline{\sigma}\right]$$

where $\otimes$ is the vector product.

A.2   Damage evolution algorithm

By taking into account the non-symmetric model, in the following table the algorithm is shown:

INPUT DATA   *(time $t + \Delta t$)*
      Material properties: $f'_t, \; n, \; E^0, \; \mu, \; G_f$
      Actual values: $\varepsilon^{t+\Delta t}, \quad d^t, \quad r^t$

---

1) NORM DEFINITION IN THE UNDAMAGED STATE

If $t = 0$, the starting value is $r^0 = r^*$

Determination of parameter A:
$$A = \left(\frac{G_f E^0}{l^* (f'_t)^2} - \frac{1}{2} \right)^{-1};$$

Stress tensor in the undamaged state:
$$\underline{\sigma}^{t+\Delta t} = \underline{\mathbf{C}}^0 \; \underline{\epsilon}^{t+\Delta t}$$

Evaluation of the norm $\tau^{t+\Delta t}$ $(in \; the \; non - symmetric \; model)$:
$$\tau = \left(\zeta + \frac{1-\zeta}{n} \right) \sqrt{\underline{\sigma}^{t+\Delta t} \, \underline{\epsilon}^{t+\Delta t}}$$

where ζ is: $\zeta = \frac{\sum_{i=1}^{3} \langle \sigma_i^{t+\Delta t} \rangle}{|\sigma_i^{t+\Delta t}|}$

2) IN THE ELASTIC CASE *(If $\tau^{t+\Delta t} < \tau^t$)*
      Damage threshold:
$$r^{t+\Delta t} = r^t \qquad \dot{r} = 0$$

Degradation value:
$$d^{t+\Delta t} = d^t = G(r^{t+\Delta t}) \qquad \dot{d} = 0$$

Stress tensor evaluation:
$$\underline{\sigma}^{t+\Delta t} = (1 - d^{t+\Delta t}) \, \underline{\mathbf{C}}^0 \; \underline{\epsilon}^{t+\Delta t}$$
$$END.$$

2) IF DAMAGE OCCOURS *($\tau^{t+\Delta t} \geq \tau^t$)*
      Damage threshold:
$$r^{t+\Delta t} = \tau^{t+\Delta t} \qquad \dot{r} = \dot{\tau}$$

Degradation value:
$$d^{t+\Delta t} = G(r^{t+\Delta t}) \qquad \dot{d} = 0$$

Stress tensor evaluation:
$$\underline{\sigma}^{t+\Delta t} = (1 - d^{t+\Delta t}) \, \underline{\mathbf{C}}^0 \; \underline{\epsilon}^{t+\Delta t}$$

Tangent constitutive tensor :
$$\underline{\mathbf{C}} = (1 - d) \, \underline{\mathbf{C}}^0 - \frac{\dot{G}(r^{t+\Delta t})}{\tau} \, \underline{\sigma}^{t+\Delta t} \otimes \underline{\sigma}^{t+\Delta t}$$

Bibliography

Anthoine, A. (1995). Derivation of the in-plane elastic characteristics of masonry through homogenization theory. *International Journal of Solids and Structures 32*(2), 137–163.

Anthoine, A. (1997). Homogenization of periodic masonry: plane stress, generalized plane strain or 3d modelling? *Communications in numerical methods in engineering 13*, 319–326.

Backes H.P. (1985). *On the behavior of masonry under tension in the direction of the bed joints.* Backes H.P.: Dissertation, Aachen University of Technology, Aachen, Germany.

Baggio, C. and P. Trovalusci (1993). Discrete models for jointed block masonry walls. In *Proc. 6th North American Masonry Conf., Philadelphia, Pennsylvania*, pp. 939–949.

Bathe, K. J. (1995). *Finite Element Procedures.* Prentice-Hall, Englewood Cliffs.

Bendsoe, M. and N. Kikuchi (1998). Generating optimal topologies in structural designusing a homogenization method. *Computer Methods in Applied Mechanics & Engineering 71*, 197–224.

Bensoussan, A., J. L. Lions, and P. G. (1978). *Asymptotic Analysisfix Periodic Structures.*

Berto, L., A. Saetta, R. Scotta, , and R. Vitaliani (2002). An orthotropic damage model for masonry structures. *International Journal for Numerical Methods in Engineering 55*, 127–157.

Berto, L., A. Saetta, R. Scotta, and R. Vitaliani (2004). Shear behavior of masonry panel: parametric fe analysis. *International Journal of Solids and Structures 41*, 4383–4405.

Bertsekas, D. P. (1996). *Constrained Optimization and Lagrange Multiplier Methods.* Athena Scientifics.

Besdo, D. (1985). Inelastic behavior of plane frictionless block-systems described as cosserat media. *Archives of Mechanics 37*(6), 603–619.

Besdo, D. and H.-U. Dorau (1988). Zur modellierung von verbundmaterialien als homogenes cosseart-kontinuum. *Z. Angew. Math. u. Mech. 68*, T153–T155.

Brasile, S., R. Casciaro, and F. G. (2007a). Multilevel approach for brick masonry walls part i : A numerical strategy for the nonlinear analysis. *Computer Methods in Applied Mechanics and Engineering 196*, 4934–4951.

Brasile, S., R. Casciaro, and F. G. (2007b). Multilevel approach for brick masonry walls part ii: On the use of equivalent continua. *Computer Methods in Applied Mechanics and Engineering 196*, 4801–4810.

Calderini, C. and S. Lagomarsino (2006). A micromechanical inelastic model for historical masonry. *Journal of Earthquake Engineering 10*(4), 453–479.

Casolo, S. (2006). Macroscopic modelling of structured materials: Relationship between orthotropic cosserat continuum and rigid elements. *International Journal of Solids and Structures Macroscopic modelling of structured materials: Relationship between orthotropic Cosserat continuum and rigid elements 43*, 475–496.

Cecchi, A. and R. Di Marco (2000). Homogenization of masonry walls with a computational oriented procedure. rigid or elastic block? *Eur. J. Mech. A/Solids 19*, 535–546.

Cecchi, A. and N. Rizzi (2001). Heterogeneous elastic solids: a mixed homogenization- rigidification technique. *International Journal of Solids and Structures 38*, 29–36.

Cecchi, A. and K. Sab (2002). A multi-parameter homogeneization study for modelling elastic masonry. *European Journal of Mechanics A/Solids 21*, 249–268.

Christensen, R. (1979). *Mechanics of Composite Materials*. New Yok: Wiley.

Crisfield, M. A. (1997a). *Non-linear Finite Element Analysis of Solids and Structures, Vol. 1: Essentials.* J. Wiley & Sons, New York.

Crisfield, M. A. (1997b). *Non-linear Finite Element Analysis of Solids and Structures, Vol. 2: Advanced Topics.* J. Wiley & Sons, New York.

Cristescu, N. D., E. M. Craciun, and E. Sos (2004). *Mechanics of Elastic Composites*. CRC Press.

De Borst, R. (1991). Simulation of strain localization:a reappraisal of the cosserat continuum. *Engineering Computation 8*, 317–332.

De Buhan, P. and G. De Felice (1997). A homogenisation approach to the ultimate strength of brick masonry. *J. Mech. Phys. Solids 45*(7), 1085–1104.

Del Piero, G. (1989). Constitutive equation and compatibility of the external loads for linear elastic masonry-like materials. *Meccanica 24*, 150–162.

Dhanasekar, M., A. W. Page, and P. W. Kleeman (1982). The elastic properties of brick masonry. *International Journal of Masonry Construction 2*(4), 155–160.

Drugan, W. J. and J. R. Willis (1996). A micromechanics-based nonlocal constitutive equation and estimates of representative volume element size for elastic composites. *J. Mech. Phys. Solids 44*(4), 497–524.

Eshelby, J. D. (1958). The determination of the elastic field of an ellipsoidal inclusion and related problems. *Proceedings of the Royal Society of London 241*, 376–396.

Feyel, F. (2001). Multiscale non linear fe2 analysis of composite structures: fiber size effects. *Journal de Physique 11*, 195–202.

Fish, J., Q. Yu, and K. Shek (1999). Computational damage mechanics for composite materials based on mathematical homogenization. *International Journal For Numerical Methods In Engineering 45*, 1657–1679.

Forest, S. (1998). Mechanics of generalized continua. In *J. Phys. IV France 8*.

Forest, S. (1999). Homogenization methods and the mechanics of generalized continua. *Geometry, continua and microstructure, Travaux en Cours 60*, 35–48.

Forest, S., R. Dendievel, and G. Canova (1999). Estimating the overall properties of heterogeneous cosserat materials. *Modelling Simul. Mater. Sci. Eng. 7*, 829–840.

Forest, S. and K. Sab (1998). Cosserat overall modelling of heterogeneous materials. *Mechanics Research Communications in numerical methods in engineering 4*, 449–454.

Geymonat, G., F. Krasucki, and J. J. Marigo (1987). Sur la commutativite des passages a la hmite en theorie asymptotique des poutres composites. *C. R. Acad. Sci. Paris, 305*, 225–228.

Ghosh, S., K. Lee, and S. Moorthy (1995). Multiple scale analysis of heterogeneous elastic structures using homogenisation theory and voronoi cell finite element method. *International Journal for Solids and Structures 32*, 27–62.

Ghosh, S., K. Lee, and S. Moorthy (1996). Two scale analysis of heterogeneous elasticplastic materials with asymptotic homogenisation and voronoi cell finite element model. *Computer Methods in Applied Mechanics & Engineering 132*, 63–116.

Ghosh, S., K. Lee, and P. Raghavan (2001). A multi-level computation model for multi-scale damage analysis in composite and porous media. *International Journal for Solids and Structures 38*, 2335–2385.

Giambanco, G., S. Rizzo, and R. Spallino (2001). Numerical analysis of masonry structures via interface models. *Computational Methods in Applied Mechanics and Engineering 190*, 6493–6511.

Giaquinta, M. and E. Giusti (1985). Researches on the equilibrium of masonry structures. *Arch. Rat. Mech. Anal. 88*, 359–392.

Guedes, J. and N. Kikuchi (1990). Preprocessing and postprocessing for materials based on the homogeneization method with adaptative finite element method. *Computer Methods in Applied Mechanics & Engineering 83*, 143–198.

Hashin, Z. (1962). The elastic moduli of heterogeneous materials. *Journal of Applied Mechanics 29*, 143–150.

Hill, R. (1963). Elastic properties of reinforced solids: some theoretical principles. *Journal Mech. Phys. Solids 11*, 357–372.

Hill, R. (1965). A self-consistent mechanics of composite materials. *J. Mech. Phys. Solids 13*, 213.

Hill, R. (1967). The essential structure of constitutive laws for metal composites and polycristal. *J. Mech. Phys. Solid 15*, 79–95.

Hinton, E. and D. R. J. Owen (1977). *Finite Element Programming.* Academic Press, London.

Hughes, T. J. R. (2000). *Finite Element Method - Linear Static and Dynamic Finite Element Analysis.* Prentice-Hall, Englewood Cliffs.

Hughes, T. J. R. and K. S. Pister (1978). Consistent linearization in mechanics of solids and structures. *T. J. R. Hughes and K. S. Pister, 'Consistent linearization in mechanics of solids and structures', Comp. Struct., 8, 391 8*, 391–397.

Jiang, M., K. Alzebdeh, I. Jasiuk, and M. Ostoja-Starzewski (2001). Scale and boundary conditions effects in elastic properties of random composites. *Acta Mechanica 148*, 63–78.

Kazufumi, I. and K. Kunisch (2004). *Lagrange Multiplier Approach to Variational Problems and Applications.* Society for Industrial and Applied Mathematics.

Kouznetsova, V., Brekelmans, W. A. M., and F. P. T. Baaijens (2001). An approach to micro-macro modeling of heterogeneous materials. *Comput. Mech. 27*, 37–48.

Kouznetsova, V., M. Geers, and W. Brekelmans (2004). Size of a representative volume element in a second-order computational homogenization framework. *International Journal for Multiscale Computational Engineering 2*, 575–598.

Kouznetsova, V. G. (2002). *Computational homogenization for the multi-scale analysis of multi-phase materials.* Ph. D. thesis, Technische Universiteit Eindhoven.

Larsson, R. and S. Diebels (2007). A second-order homogenization procedure for multi-scale analysis based on micropolar kinematics. *International Journal for Numerical Methods in Engineering 69*, 2485–2512.

Lene, F. (1986). Damage constitutive relations for composite materials. *Engineering Fracture Mechanics 25*, 713–728.

Lene, F. and D. Leguillon (1982). Homogenize constitutive law for a partially cohesive composite. *International Journal of Solid and Structures 18*, 443–458.

Lofti, H. and P. Shing (1994). Interface model applied to fracture of masonry structures. *Journal of Structural Engineering ASCE 120*(1), 63–80.

Lopez, J., S. Oller, E. Oate, and J. Lubliner (1999). A homogeneous constitutive model for masonry. *International Journal For Numerical Methods In Engineering 46*, 1651–1671.

Loureno, P. B. (1996). *Computational Strategies for Masonry Structures*. Ph. D. thesis, Delft University of Technology.

Loureno, P. B., R. De Borst, and J. G. Rots (1997). A plane stress softening plasticity model for orthotropic materials. *International Journal for Numerical Methods in Engineering 40*, 4033–4057.

Loureno, P. B. and J. G. Rots (1997). Multisurface interface model for analysis of masonry structures. *Journal of Engineering Mechanics 123*(7), 660–668.

Luciano, R. and E. Sacco (1995). *A micromechanical approach to the damage of the masonry material*. Computational Mechanics Publications.

Luciano, R. and E. Sacco (1997a). Homogenization technique and damage model for old masonry material. *International Journal of Solids and Structures 32*(24), 3191–3208.

Luciano, R. and E. Sacco (1997b). Un modello di danno per le murature. *IGF 13*.

Luciano, R. and E. Sacco (1998). A damage model for masonry structures. *European Journal of Mechanics A/Solids 17*(2), 285–303.

Macchi, G. and G. Magenes (2002). *Teoria e tecnica delle costruzioni a cura di E. Giangreco*, Volume 3, Chapter XIII Le strutture in muratura. Utet.

Magenes, G. (1992). *Comportamento sismico di murature di mattoni: resistenza e meccanismi di rottura di maschi murari*. Ph. D. thesis, Politecnico di Milano - Universit degli studi di Pavia.

Maier, G., A. Nappi, and E. Papa (1991). *Damage models for masonry as a composite material : a numerical and experimental analysis. In Constitutiue Laws for Engineering Materials*. ASME, New York.

Mandel, J. (1972). *CISM lecture Notes*, Chapter Number 97. Springer Verlag.

Mann, W. and Mller, H., (1982). *Failure of shear-stressed masonry - an enlarged theory, tests and application to shear walls*. Mann, W. and Mller, H.,: British Ceramic Society.

Masiani, R., R. Rizzi, and P. P. Trovalusci (1995). Masonry as structured continuum. *Meccanica 30*(6), 673–683.

Massart, T., P. Bouillard, M. Geers, and R. Peerlings (2001). A 2 d anisotropic damage model for masonry walls. In *2 nd European Conference on Computational Mechanics*.

Massart, T., R. Peerlings, and M. Geers (2007). An enhanced multi-scale approach for masonry wall computations with localization of damage. *International Journal for Numerical Methods in Engineering 69*(5), 1022–1059.

Massart, T. J. (2003). *Multiscale modelling of damage in masonry structures*. Ph. D. thesis, Technische Universiteit Eindhoven.

Mazars, J. (1986). A description of micro- and macroscale damage of concrete structures. *Eng. Fract. Mech., 25*, 729–737.

Mhlhaus, H. B. (1989). Application of cosserat theory in numerical solutions of limit load problems. *Ingenieur Archive 59*, 124–137.

Miehe, C. (1996). Numerical computation of algorithmic (consistent) tangent moduli in large-strain computational inelasticity. *Computer Methods in Applied Mechanics & Engineering 134*, 223–240.

Miehe, C., J. Schrder, and J. Schotte (1999). Computational homogenization analysis in finite plasticity. simulation of texture development in polycrystalline materials. *Computer Methods in Applied Mechanics and Engineering 171*, 387–418.

Mori, M. (1986). *The Finite Element Method and Its Applications*. Macmillan Press, New York.

Mori, T. and T. K. (1973). Average stress in matrix and average elastic energy of materials with misfitting inclusions. *Acta Metall 21*, 571–574.

Moulinec, H. and P. Suquet (1998). A numerical method for computing the overall response of non-linear composites with complex microstructure. *Computer Methods in Applied Mechanics & Engineering 157*, 69–94.

Nappi, A. and F. Tin-Loi (2001). A numerical model for masonry implemented in the framework of a discrete formulation. *Structural Engineering and Mechanics (South Korea) 11*(2), 171–184.

Oliver, J., M. Cervera, S. Oller, and J. Lubliner (1990). Isotropic damage models and smeared crack analysis of concrete. In *Second International Conference on Analysis and design of concrete structures*.

Oller, S. (1988). *Un modelo de dao continuo para materiales friccionales*. Ph. D. thesis, Universidad Politecnica de Catalua.

Oller, S., L. Neamtu, and E. Oate (1995). Una generalizacin de la teora de mezclas clsica para el tratamiento de compuestos en serie/paralelo. In *Congreso Nacional de Materiales Compuestos*.

Ortiz, M. and E. P. Popov (1982). *Mech of materials*, Chapter Plain Concrete as a Composite Material. North Holland Publishing Company.

Page, A. (1983). The strength of brick masonry under biaxial compression-tension. *Int. J. Masonry Constr. 3(1)*, 26–31.

Page, A. W. (1978). Finite element model for masonry. *Journal of the Structural Division, New York: ASCE, 104*, 1267–1285.

Pande, G. N.and Liang, J. X. and J. Middleton (1989). Equivalent elastic moduli for brick masonry. *Computers Geotechnical 8*(5), 243–265.

Papa, E. and A. Nappi (1997). Numerical modelling of masonry: a material model accounting for damage effects and plastic strains. *Applied Mathematics Modelling 21*, 319–335.

Pegon, P. and A. Anthoine (1997). Numerical strategies for solving continuum damage problems with softening: application to the homogenization of masonry. *Computers and Structures 64*, 623–642.

Petrangeli, M. and V. Ciampi (1997). Equilibrium based iterative solutions for the non-linear beam problem. *International journal for numerical methods in engineering 40*, 423–437.

Pietruszczak, S. and X. Niu (1992). A mathematical description of macroscopic behaviour of brick masonry. *International Journal of Solids and Structures 29*(5), 531–546.

Providas, E. and M. Kattis (2002). Finite element method in plane cosserat elasticity. *Computers & Structures 80*, 2059–2069.

Raijmakers, T. M. J. and A. T. Vermeltfoort (1992). Deformation controlled tests in masonry shear walls (in dutch). Technical Report B-92-1156, TNO - Bouw, Delft, The Netherlands.

Reddy, J. N. (1984, 1993, 2005). *An Introduction to the Finite Element Method.* McGraw-Hill Book Co., New York.

Reddy, J. N. (2004). *An Introduction to Nonlinear Finite Element Analysis.* Oxford University Press, Oxford.

Romano, G. and E. Sacco (1984). Sul calcolo di strutture non resistenti a trazione. In *Atti del VII Congresso AIMETA*.

Saada, A. S. (1974). *Elasticity: Theory and Applications.*

Salerno, G. and G. De Felice (2009). Continuum modeling of periodic brickwork. *International Journal of Solids and Structures 46*, 1251–1267.

Sanchez-Palencia, E. (1980). *Non homogeneous media and vibration theory. Lecture Notes in Physics*, Volume 127. Springer-Verlag, Berlin.

Sanchez-Palencia, E. (1987). *Homogenization Techniques for Composite Media*, Chapter Boundary Layers And Edge Effects In Composites, pp. 121–192. Springer Verlag, Berlin.

Simo, J. and J. Hu (1987). Stain-and-stress based continuum damage models-ii. computationa aspects. *International Journal of Solids ans Structures 23*, 821–840.

Smit, R. J. M., W. A. M. Brekelmans, and H. E. H. Meijer (1998). Prediction of the mechanical behaviour of nonlinear heterogeneous systems by multi-level finite element modeling. *Computer Methods in Applied Mechanics and Engineering 155*, 181–192.

Stefanou, I., J. Sulem, and I. Vardoulakis (2008). Three-dimensional cosserat homogenization of masonry structures: elasticity. *Acta Geotechnica 3*, 71–83.

Sulem, J. and H.-B. Muhlhaus (1997). A continuum model for periodic two-dimensional block structures. *Mechanics of Cohesive- Frictional Materials 2*, 31–46.

Suquet, P. (1982). *Plasticit et Homognisation.* Ph. D. thesis, Universit Pierre et Marie Curie, Paris.

Suquet, P. M. (1985). *Plasticity today: modelling, methods and applications*, Chapter Local and global aspects in the mathematical theory of plasticity, pp. 279–310. London. Elsevier Applied Science Publishers.

Terada, K., M. Hori, T. Kyoya, and N. Kikuchi (2000). Simulation of the multi-scale convergence in computational homogenization approach. *International Journal of Solids and Structures 37*, 2285–2311.

Terada, K. and N. Kikuchi (2001). A class of general algorithms for multi-scale analyses of heterogeneous media. *Computer Methods in Applied Mechanics and Engineering 190*, 5427–5464.

Trovalusci, P. and R. Masiani (1996). Cosserat and cauchy materials as continuum models of brick masonry. *Meccanica 31*, 421–432.

Trovalusci, P. and R. Masiani (2005). A multifield model for blocky materials based on multiscale description. *International Journal of Solids and Structures 42*, 5778–5794.

Trusdell, C. and R. Toupin (1960). *The classical field theory*. Springer Verlag.

van der Pluijm, R. (1999). *Out-of-Plane Bending of Masonry- behavior and strength*. Ph. D. thesis, Eindhoven University of Technology.

van der Sluis, O., P. J. G. Schreurs, W. A. M. Brekelmans, , and H. E. H. Meijer (2000). Overall behaviour of heterogeneous elastoviscoplastic materials: effect of microstructural modelling. *Mech. Mater. 32*, 449–462.

Whittaker, E. T. and G. Robinson (1967). *The Newton-Raphson Method*. New York: Dover.

Zalamea, F. (2001). *Tratamiento numrico de materiales compuestos mediante la teoria de homogeneizacin*. Ph. D. thesis, Universitad Politecnica de Catalua.

Zaoui, A. (2002). Continuum micromechanics: Survey. *J. Engrg. Mech.-ASCE 128*, 808–816.

Zienkiewicz, O. C. and R. L. Taylor (1989). *Finite Element Method- Basic Formulation and Linear Problems*, Volume 1. McGraw-Hill Publ., New York.

Zienkiewicz, O. C. and R. L. Taylor (2000). *Finite Element Method: Volume 1- The Basis*. Butterworth Heinemann, London.

Zucchini, A. and P. Loureno (2007). Mechanics of masonry in compression: Results from a homogenisation approach. *Computers & Structures 85*, 193–204.

Zucchini, A. and P. B. Loureno (2002). A micro-mechanical model for the homogenization of masonry. *International Journal of Solids and Structures 39*, 3233–3255.

Zucchini, A. and P. B. Loureno (2004). A coupled homogenisation-damage model for masonry cracking. *Computers and Structures 82*, 917–929.

Zucchini, A. and P. B. Loureno (2009). A micro-mechanical homogenisation model for masonry: Application to shear wall. *International Journal of Solids and Structures 46*, 871–886.